STEM CELL BASED NERVE TISSUE ENGINEERING
ON GUIDED CONSTRUCTS

A THESIS SUBMITTED TO
THE GRADUATE SCHOOL OF NATURAL AND APPLIED SCIENCES
OF
MIDDLE EAST TECHNICAL UNIVERSITY

BY

DENİZ YÜCEL

IN PARTIAL FULFILLMENT OF THE REQUIREMENTS
FOR
THE DEGREE OF DOCTOR OF PHILOSOPHY
IN
BIOTECHNOLOGY

JANUARY 2009

Approval of the thesis:

**STEM CELL BASED NERVE TISSUE ENGINEERING
ON GUIDED CONSTRUCTS**

submitted by **DENİZ YÜCEL** in partial fulfillment of the requirements for the degree of **Doctor of Philosophy in Department of Biotechnology, Middle East Technical University** by,

Prof. Dr. Canan Özgen   _____
Dean, Graduate School of **Natural and Applied Sciences**

Prof. Dr. Gülay Özcengiz   _____
Head of Department, **Biotechnology**

Prof. Dr. Vasıf Hasırcı   _____
Supervisor, **Biological Sciences Dept., METU**

Assoc. Prof. Dr. Gamze Torun Köse   _____
Co-Supervisor, **Genetics and Bioengineering Dept.,
Yeditepe Univ.**

Examining Committee Members:

Prof. Dr. Meral Yücel   _____
Biological Sciences Dept., METU

Prof. Dr. Vasıf Hasırcı   _____
Biological Sciences Dept., METU

Prof. Dr. Mesude İşcan   _____
Biological Sciences Dept., METU

Prof. Dr. Aykut Özkul   _____
Virology Dept., Vet. Med. Fac., Ankara Univ.

Prof. Dr. Tülin Güray   _____
Biological Sciences Dept., METU

Date: 26.01.2009

I hereby declare that all information in this document has been obtained and presented in accordance with academic rules and ethical conduct. I also declare that, as required by these rules and conduct, I have fully cited and referenced all material and results that are not original to this work.

Name, Last name: Deniz Yücel

Signature:

ABSTRACT

STEM CELL BASED NERVE TISSUE ENGINEERING ON GUIDED CONSTRUCTS

Yücel, Deniz

Ph.D., Department of Biotechnology

Supervisor: Prof. Dr. Vasıf Hasırcı

Co-Supervisor: Assoc.Prof. Dr. Gamze Torun Köse

January 2009, 161 pages

Nerve injury is a serious clinical problem that has a direct impact on the quality of life. Nerve tissue engineering (NTE) is one of the most promising methods in human health care to restore the function of damaged neural tissues. The current state of the art involves the construction of a tissue engineered, nano or micropatterned 3-D nerve tube that has fibers or channels in the inside.

The scope of this study is to construct a 3-D, biodegradable nerve tube which consists of an aligned, electrospun mat seeded with stem cells that is wrapped in a porous micropatterned film which contains support cells. In two separate approaches human mesenchymal stem cells (MSCs) and mouse neural stem cells (NSCs) were used. In the design with the MSCs, the micropatterned exterior part of the nerve tube contained undifferentiated MSCs as support cells and this was wrapped around the fibers seeded with MSCs which were induced to neural differentiation. In the other case, NSCs differentiated into astrocytes were used as support cells seeded on the micropatterned film and the mat was loaded with undifferentiated NSCs. Differentiation into neural cells and astrocytes were shown

with immunocytochemistry and RT-PCR. The neuron-like MSCs and NSCs were shown to express neural marker β-Tubulin III whereas astrocytes expressed glial fibrillary acidic protein (GFAP), an astrocyte marker. RT-PCR showed that early neural markers, nestin and Nurr 1, were expressed at passage 4 by undifferentiated MSCs and by MSCs induced to neural differentiation, while these markers were not expressed in undifferentiated MSCs at passages 2 and 3. The cells aligned along the axis of the micropattern of the film and along the axis of the fiber on the fibrous mat. This behavior was also maintained after construct formation. MTS and confocal microscopy revealed that the cells were viable and homogeneously distributed over the two parts of the scaffold. This indicates that the construct has a potential to be tested *in vivo* for nerve tissue engineering purposes.

Keywords: Nerve Tissue Engineering, Stem Cell, Guided Nerve Tube, Aligned Fibrous Mat, Micropatterned Film.

ÖZ

YÖNLENDİRİLMİŞ YAPILAR ÜZERİNDE KÖK HÜCRE TEMELLİ SİNİR DOKU MÜHENDİSLİĞİ

Yücel, Deniz

Doktora, Biyoteknoloji Bölümü

Tez Yöneticisi: Prof. Dr. Vasıf Hasırcı

Ortak Tez Yöneticisi: Doç. Dr. Gamze Torun Köse

Ocak 2009, 161 sayfa

Hasar görmüş sinir dokuları yaşam kalitesini etkileyen ciddi bir klinik sorundur. Sinir doku mühendisliği hasar görmüş dokunun yenilenmesi ve işlevselliğini tekrar kazanmasını sağlamak açısından umut veren bir yöntemdir. Günümüzde en güncel yöntem doku mühendisliği metotları kullanılarak içerisinde lifler ve kanallı nano ve mikro desenlerlerle yönlendirilmiş üç boyutlu nöral tüpler oluşturmaktır.

Bu çalışmada amaç destek hücreleri içeren gözenekli mikrodesenli filmin, kök hücreleri içeren elektroeğirme yöntemi ile elde edilmiş paralel lifsi bir yapıya sarılması ile oluşan üç boyutlu, vücutta eriyebilen bir nöral tüp oluşturmaktır. İki değişik yaklaşımda hücre kaynağı olarak insan mezenkimal kök hücreleri ile fare sinir kök hücreleri kullanılmıştır. Mezenkimal kök hücreleri kullanılarak farklılaşmamış kök hücre (destek hücre) ekilmiş desenli filmin sinir hücresine farklılaştırılan kök hücrelerinin bulunduğu fiber yapıya sarılması ile 3-

boyutlu tüp elde edilmiştir. Sinir kök hücreleri kullanıldığında ise destek hücre olan astrosit hücrelerini taşıyan desenli yapı sinir kök hücreleri içeren fiber yapıyı sarmıştır. Sinir hücresine farklılaşma immün boyama ve RT-PCR teknikleri ile gösterilmiştir. Sinir hücresine farklılaşan mezenkimal kök hücreleri ve sinir kök hücreleri sinir hücresine özel β-Tubulin III oluştururken, astrosit hücresine dönüşen hücreler ise astrosit hücresine özgü GFAP proteini oluşturmuşlardır. Sinir hücrelerinde erken aşamada ifade edilen nestin ve Nurr 1 genlerinin dördüncü pasajdaki farklılaşmamış mezenkimal kök hücrelerinde ve sinir hücresine farklılaştırılan hücrelerde ifade edildiği görülürken, ikinci ve üçüncü pasajdaki farklılaşmamış mezenkimal kök hücrelerinde görülmemiştir. Hücrelerin desenli filmlerdeki kanallar boyunca ve lifsi yapıdaki lifler boyunca uzandığı görülmüştür. Hücrelerin bu davranışı sinir tüpünü oluşturup kültive ettikten sonra da sürmüştür. MTS ve konfokal mikroskopisi sonuçlarına göre nöral tüp içindeki hücrelerin canlı kalabildiği ve üç boyutlu hücre taşıyıcısının her yerinde dengeli bir şekilde bulundukları gözlenmiştir. Elde edilen sonuçlar tasarlanan bu yapının sinir doku mühendisliği alanında *in vivo* uygulamalarda da kullanılma potansiyeli taşıdığını göstermektedir.

Anahtar Kelimeler: Sinir Doku Mühendisliği, Kök Hücre, Yönlendirilmiş Nöral Tüp, Paralel Lifsi Yapı, Mikrodesenli Film.

Dedicated to my parents…

ACKNOWLEDGEMENTS

TABLE OF CONTENTS

LIST OF TABLES

TABLES

LIST OF FIGURES

FIGURES

xix

LIST OF ABBREVIATIONS

ALP	Alkaline Phosphatase
ATCC	American Type Cell Collection
AT-RA	All Trans-Retinoic Acid
BDNF	Brain-derived Neurotrophic Factor
BM	Bone Marrow
BSA	Bovine Serum Albumin
CDL	Chemically Defined Lipids
CNS	Central Nervous System
CNTF	Ciliary Neurotrophic Factor
DMEM	Dulbecco's Modified Eagle Medium
DMF	N,N-Dimethylformamide
DMSO	Dimethyl Sulfoxide
E	Young's Modulus
ECM	Extracellular Matrix
ESCs	Embryonic Stem Cells
EAB	Elongation at Break
EGF	Epidermal Growth Factor
FCS	Fetal Calf Serum
FGF	Fibroblast Growth Factor
Fnc	Fibronectin
Fng	Fibrinogen
GFAP	Glial Fibrillary Acidic Protein
HES1	Hairy and Enhancer of Split 1
Lmn	Laminin
MAP2	Microtubule-associated protein2
MP	Micropatterned

MSCs	Mesenchymal Stem Cells
Mw	Molecular Weight
NeuroD1	Neurogenic Differentiation 1
NGF	Nerve Growth Factor
Ngn1	Neurogenin1
NS	Nervous System
NSCs	Neural Stem Cells
Nurr1	Nuclear Receptor Related Factor1
Pax6	Paired Box Gene 6
PBS	Phosphate Buffer Saline
PCR	Polymerase Chain Reaction
PDMS	Polydimethyl Siloxane
Pen/Strep	Penicillin/Streptomycin
PEG	Polyethylene Glycol
PFA	Paraformaldehyde
PHBV	Poly(3-hydroxybutyrate-co-3-hydroxyvalerate)
PI	Preinduction Medium
PLGA	Poly(DL-lactide-co-glycolide)
P(L-D,L)LA	Poly(L-lactide-co-D,L-lactide)
PNS	Peripheral Nervous System
RARA	Retinoic Acid Receptor Type-α
RT-PCR	Reverse Transcription-Polymerase Chain Reaction
SCI	Spinal Cord Injury
Si	Silicone
SEM	Scanning Electron Microscopy
TCPS	Tissue Culture Polystyrene
UCM	Umbilical Cord Matrix
UTS	Ultimate Tensile Strength
WJ	Wharton's Jelly
VA	Valproic Acid

CHAPTER 1

INTRODUCTION

1.1.   Physiology of the Nervous System

1.1.1.   Organization of the Nervous System

The nervous system is mainly composed of the central nervous system (CNS) and the peripheral nervous system (PNS). The CNS includes the brain and the spinal cord, optic, and olfactory and auditory systems. It conducts and interprets signals as well as provides excitatory stimuli to the PNS. The PNS consists of cranial nerves arising from the brain, the spinal nerves arising from the spinal cord, and autonomic nerves that connect to the CNS (Zhang et al., 2005a). Peripheral nerves innervate muscle tissue, transmitting sensory and excitatory input to and from the spinal column.

1.1.2.   Cellular Components of the Nervous System

The nervous system mainly contains two cell types: nerve cells, also called the neurons, and neuroglia. Neurons, the basic structural and functional elements of the nervous system, consist of a nucleated cell body (soma) and its extensions (axons and dendrites) (Figure 1.1). Clusters of sensory nerve soma, known as ganglia, are located just outside the spinal column. Typically, the cell body and the dendrites are input zones, where a neuron receives signals from the surroundings or other neurons. The axons, conducting fibers, transport impulses from the cell body to the axon terminals via propagation of action potentials. At

axon terminals, the arrival of action potentials triggers release of neurotransmitters. These signaling molecules diffuse across chemical synapses, where the neuron forms a junction with the dendrite of another neuron, with a muscle cell or a gland cell. In addition, electrical impulse can also be directly passed from axon to axon, axon to soma, or from dendrite to dendrite among neurons. Glial cells, or neuroglia, include Schwann cells in the PNS and astrocytes and oligodendrocytes in the CNS, are supportive cells that aid the function of neurons (Figure 1.2). The glial cells are more abundant than neurons, and have some capacity for cell division. Unlike glial cells, neurons can not undergo mitosis, they can regenerate a severed portion or sprout new processes under certain conditions.
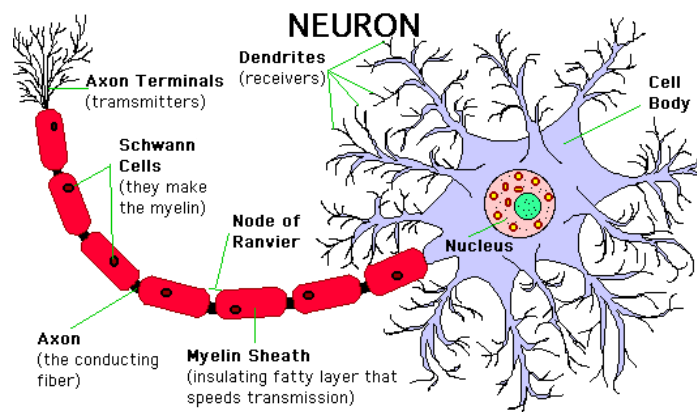
Figure 1.1. Structure of the neuron

(Enchanted Learning, .enchantedlearning.com/subjects/anatomy/brain/Neuron)
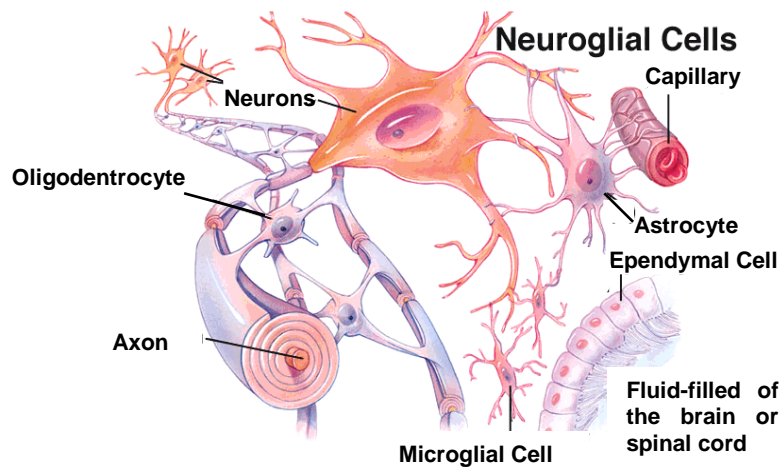
Figure 1.2. Types of glial cells in the CNS

(Owensboro Community & Technical College,
http://www.octc.kctcs.edu/gcaplan/anat/Notes/API%20Notes%20K%20%20Neurons.htm)

In the PNS, sheaths of living Schwann cells maintain myelination by wrapping the axons (Figure 1.3). CNS axons are surrounded by an insulating myelin sheath which is formed from dense layers of successive wrappings of the cell membrane of oligodendrocytes, instead of Schwann cells. Each cell is separated from adjacent ones by a small unsheathed node and the signals jump from node to node and this speeds up the transmission of signal along the axon. The propagation of the velocity of the nerve impulse is particularly important for those axons that extend long distances (up to 1 m).

1.1.3.   Anatomy of the Peripheral Nerve and the Spinal Cord

In many neurons the axons are bundled into cables that provide long-distance communication between brain and spinal cord and the rest of the body. The nerves in PNS are composed of bundled motor and sensory axons in parallel arrays in connective tissue and are called the nerve trunk (Schmidt and Leach, 2003). The

3

individual axons and their Schwann cell sheaths are surrounded by endoneurium which is composed predominantly of oriented collagen fibers (Figures 1.3 and 1.4). Groups of axons are wrapped by the perinerium which is composed of many layers of flattened cells (i.e., fibroblasts) and collagen to form fascicles. An outer sheath of loose fibrocollagenous tissue, the epineurium, assembles individual nerve fascicles into a nerve trunk. The vascularization in these nerves is provided by capillaries within the support tissue of the nerve trunk or by vessels penetrating into the nerve from surrounding arteries and veins.
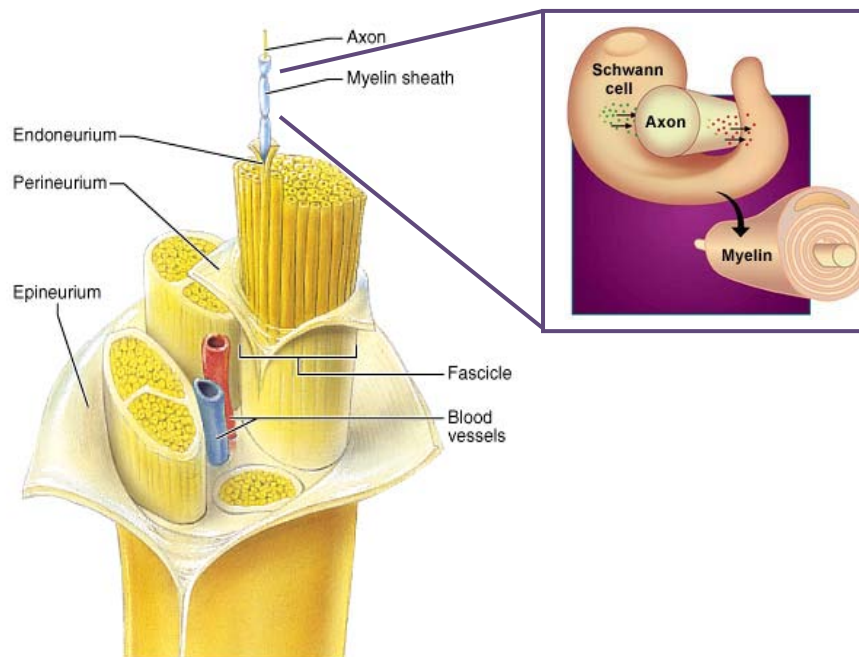
Figure 1.3. Anatomy of the PNS

(Tarleton State University, www.tarleton.edu/~anatomy/nervepix4.html, Muscular Dystrophy Association, www.mda.org/publications/quest/q81cmtds.html)
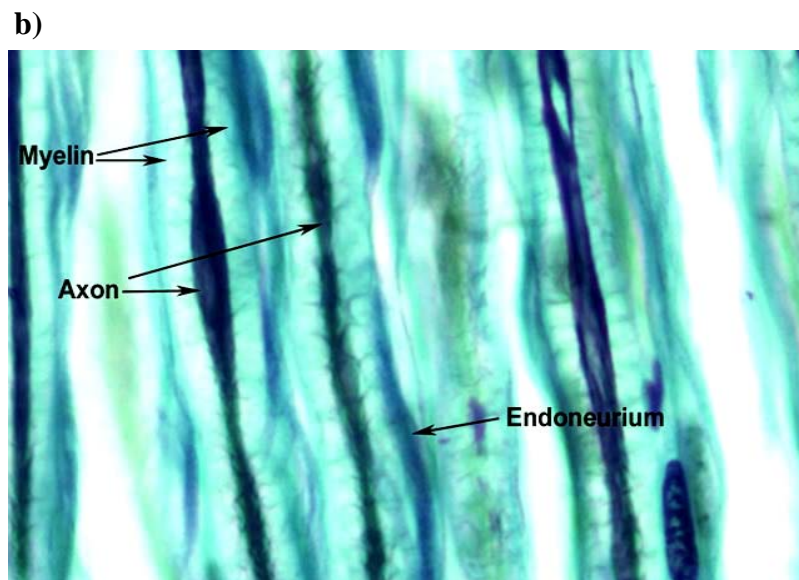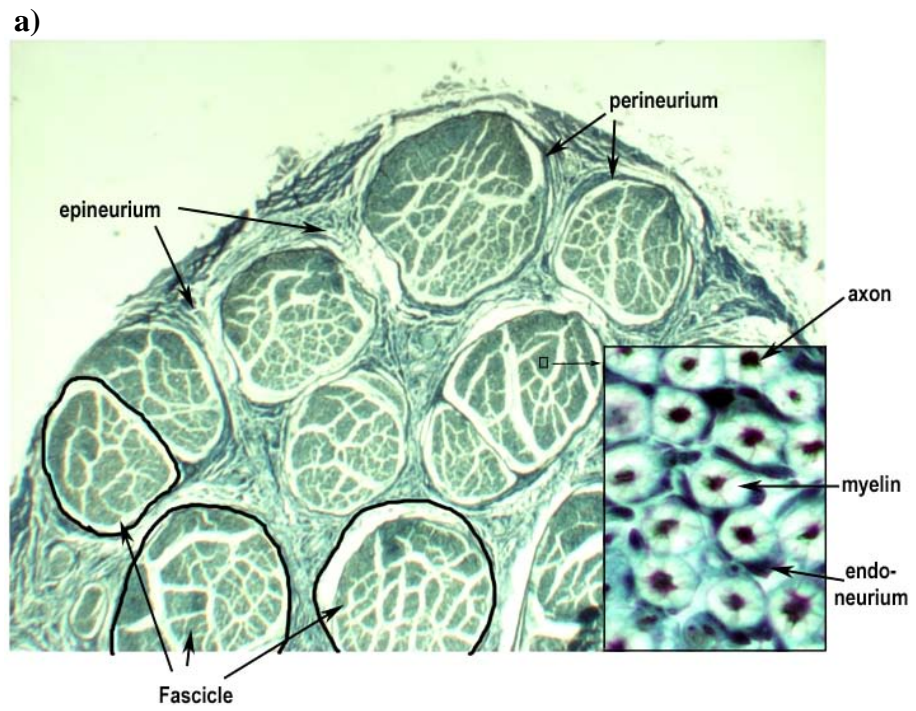
Figure 1.4. Histology of human nerve. a) cross section, and b) longitudinal section.

(UCSF School of Medicine, http://missinglink.ucsf.edu/lm/IDS_101_histo_resource)

Within the brain and spinal cord, such bundled-together axons are called nerve tracts. Typically, the spinal cord consists of dendrites, axons, and cell bodies (Schmidt and Leach, 2003). A gray matter localized in the center of the spinal cord is composed of the cell bodies of excitatory neurons, glial cells and blood vessels. The gray matter is surrounded by white matter, which provides protection and insulation of the spinal cord. White matter consists of axons and glial cells, such as oligodendrocytes, astrocytes, and microglia. Oligodendrocytes myelinate the axons in the CNS, while astrocytes are active in the blood-nerve barrier, separating the CNS from blood proteins and cells. Fascicles, axons in bundles, come out from the white matter and then exit the encasing bone of the spinal column. Following travel through the PNS-CNS transition zone, nerves enter the PNS.

1.2.   Nerve Injury and Regeneration

Nervous system injuries are commonly seen throughout the world. Nerve injuries can occur in the spinal cord, in the central nervous system or, in nerve bundles in the peripheral nervous system. Spinal cord injury (SCI) usually leads to devastating neurological defects and disabilities. The data published by the National Spinal Cord Injury Statistical Center in 2008 showed that the annual incidence of SCI, not including those who die at the scene of the accident, is approximately 40 cases per million in the U. S. or approximately 12 000 new cases each year. It also estimated that the number of patients with SCI in the US was estimated to be 225 000 to 288 000 in 2005 (Ackery et al., 2004). Five percent of all open wounds in the extremities due to sports and road accidents are complicated by peripheral nerve trauma. Moreover, during complicated births, peripheral nerves may be disrupted by traction (Van Dijk et al., 2001), the mean incidence of these lesions are 0.12% of all births (Kay, 1998). Nearly 50 000 peripheral nerve repair procedures were performed in 1995 (National Center for Health Statistics, 1995).

Damage to the nervous system by mechanical, thermal, chemical, or ischemic factors through crush or transection of nerve tracts can impair various nervous system functions such as memory, cognition, language, and voluntary movement (Zhang et al., 2005a). These damages bring about the interruption of

communication between nerve cell bodies and their targets as well as the disruption of the interrelations between neurons and their supporting cells, and the destruction of the blood-brain barrier. Among nerve injuries, the most risky is the one in CNS which may result in death or permanent disability.

A complete nerve transaction is the most severe injury in PNS (Schmidt and Leach, 2003). When a nerve is severed, the distal portion starts to degenerate because of protease activity and separation from the metabolic resources of the nerve cell bodies (Figure 1.5a). The cytoskeleton begins to breakdown, followed by the decomposition of the cell membrane. The proximal end of the nerve stump swells, but experiences only minimal damage via retrograde degradation. In the PNS, support cells help neuronal regeneration (Schmidt and Leach, 2003). Proliferating Schwann cells, macrophages, and monocytes work together. They remove myelin debris, release neurotrophins, and lead axons toward their synaptic targets; as a result they restore neuronal function (Figure 1.5.a). The rate of axon regeneration in humans is about 2-5 mm/day; thus severe injuries can take many months to heal (Jacobsen and Guth, 1965). However, in the CNS, the few neurons that survive axotomy attempt regeneration and subsequently face an impenetrable glial scar of myelin and cellular debris, and support cells as astrocytes, oligodendrocytes, and microglia. The glial scar may also contain fibroblasts, monocytes, and macrophages. Consequently, regenerating neurons in the spinal cord are blocked and are not able to reach their synaptic target (Figure 1.5.b).

a

Nerve cell body

Injury >>>

Muscle fibers

Proliferating Schwann cell   Macrophage   Monocyte

b

Nerve cell body

Injury >>>

Postsynaptic cell

Astrocyte   Oligodendrocyte
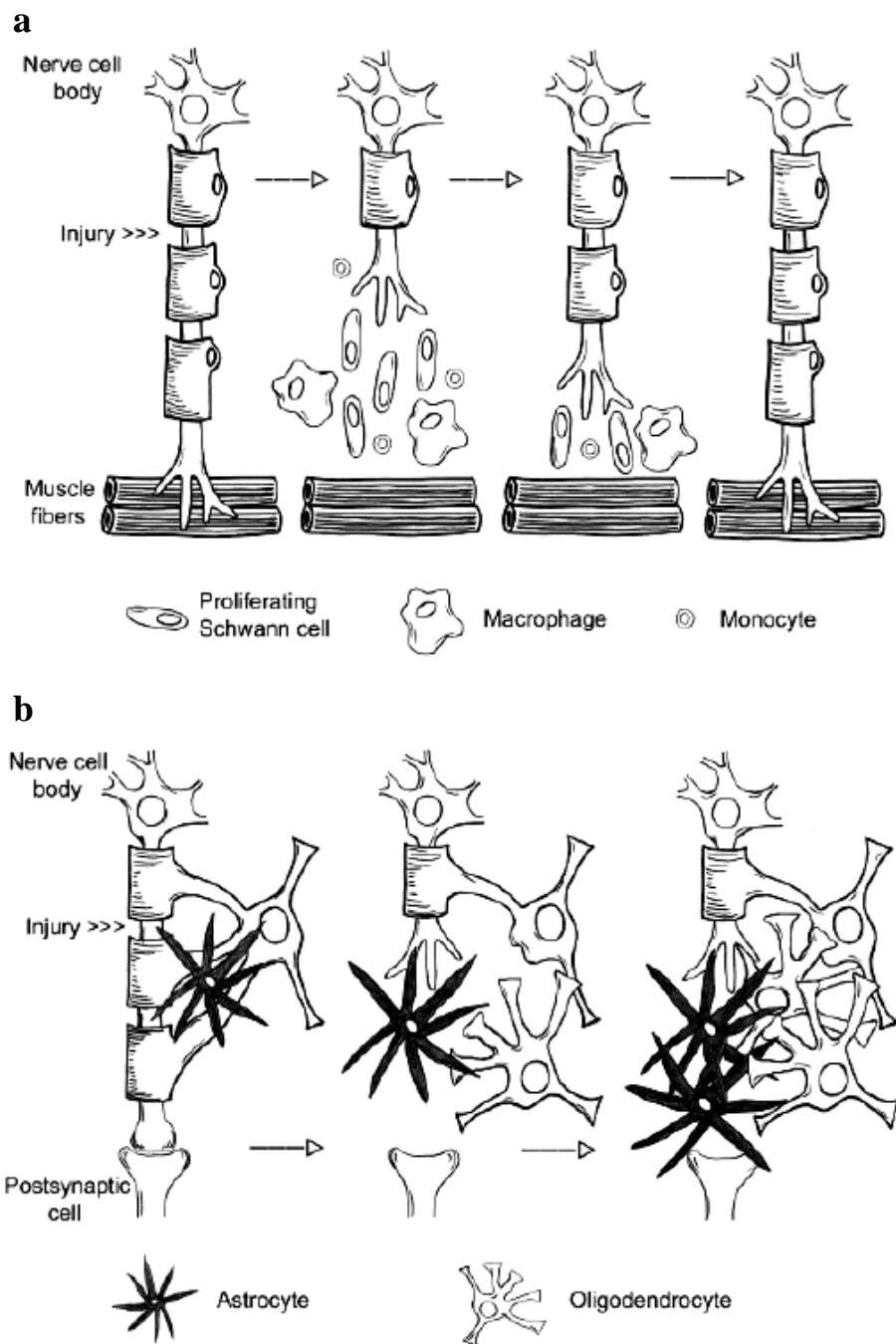
Figure 1.5. Responses to nerve injury in the a) PNS and b) spinal cord (adapted from Bahr and Bonhoeffer, 1994)

8

1.3. Current Clinical Approaches in Nerve Injury Treatment

Self regeneration of nervous tissue is difficult in severe damages of PNS and almost impossible in CNS (Meek et al., 2002, Schmidt and Leach, 2003). End-to-end anastomosis for small gaps, autologous nerve grafts and biological or synthetic conduits are used to bridge the severed nerve ends in PNS injuries (Sanghvi et al., 2004). There are a few devices that are now FDA approved for relatively short nerve defects, including Integra Neurosciences Type I collagen tube (NeuraGen Nerve Guide) and SaluMedica's SaluBridge Nerve Cuff (Lundborg et al., 1997).

The autologous nerve grafts, a segment of nerves removed from another part of the body, has inevitable disadvantages, such as limited supply of available nerve graft materials, permanent loss of the donor nerve function and need for multiple surgeries (Millesi, 1991, Terzis et al, 1997). The other options are to use allografts and xenografts, but these require immunosuppressive therapy and have highly differing success rates (Zalewski and Gulati, 1981, Bain, 2000).

The treatment in CNS injuries is more limited; the common treatment is the fixation of the spine, and restoration of its normal alignment together with surgical decompression in acute spinal cord injury (Samadikuchaksaraei, 2007). It has been shown that embryonic spinal cord grafts and peripheral nerve tissue grafts aid regeneration of fibers in the CNS; however, the fibers often do not successfully grow back across the PNS-CNS transition zone (Carlstedt, 1997).

Most of the current treatments can be useful for small defects (several millimeters), but they do not address larger nerve injuries. Thus, the burgeoning area, the tissue engineering strategies for the nervous system have centered on developing alternative treatments to the nerve graft (e.g., guidance channels for nerves), especially for larger defects. This approach also improves recovery rates and functional outcome. Moreover, tissue engineering efforts are focused on making a permissive environment for renewal and providing an interface between the CNS and PNS without stitches.

1.4.   Nerve Tissue Engineering

1.4.1.   Concept of Tissue Engineering

Organ and tissue loss or failure resulting from an injury or any kind of damage is a major human health problem (Chen et al., 2002). Transplantation of tissue or organ is a standard therapy to treat these patients, but the donor shortage is the main problem. The other approaches are surgical reconstruction, drug therapy, synthetic prostheses, and medical devices. These are not limited by supply, but they have other problems. These problems and limitations have been overcome by the development of new biomaterials and alternative therapies. Tissue engineering as a promising alternative approach is used to treat the loss or malfunction of a tissue without the limitations of current therapies.

The fundamental aim of tissue engineering is to replace or restore the anatomic structure and function of the damaged, injured, or missing tissue by combining biomaterials, cells, biologically active molecules, and/or stimulating mechanical forces of the tissue microenvironment (Zhang et al., 2005a). Two pioneers of the field, Langer and Vacanti (1993) have defined it as "an interdisciplinary field that applies the principles of engineering and the life sciences toward the development of biological substitutes that restore, maintain, or improve tissue function." It actually is the process of creating living, physiological, three-dimensional tissues and organs utilizing specific combinations of cells, cell carriers, and a variety of chemical and biological signals (Hasirci and Yucel, 2007). At this point extracellular matrix (ECM) needs to be studied, for it is the natural material that carries the cells, and that is what a biodegradable carrier needs to mimic. ECM consists of proteins (collagen, laminin, fibronectin, etc.) and glycosaminoglycans (hyaluronic acid, chondroitin sulfate, heparan sulfate, etc.), is a shelter for cells, and forms the scaffold of the tissues. The ECM is not only a surface on which cells reside but is an active source of physical and chemical signals influencing cell behavior.

In tissue engineering approaches 3-D ECMs called scaffolds are designed to provide mechanical support, and environmental information, and they

guide the cells to form new functional tissues (Kim and Mooney, 1998). The scaffolds have to be porous to allow the growth of cells, and to facilitate the infiltration and formation of large numbers of blood vessels for nutrient supply of the transplanted cells and the removal of waste products. Of a large number of scaffolds fabricated from various kinds of materials, a very large fraction is of polymeric origin because of their similarity to natural tissues in chemistry and physical properties along with their biodegradability, and suitability for functionalization and attachment of biosignal molecules. Researchers, therefore, incorporate a variety of factors such as the Arg-Gly-Asp (RGD) sequences, a minimal sequence required to mediate cell adhesion, the growth factors and the surface designs on biodegradable polymeric films and foams. The cell carrier, the scaffold, should confer the physical, mechanical, and functional properties of the tissue. Overall signals from the substrate and the surrounding environment govern the response of the cells and their assembly into desired structures. Consequently, the scaffolds are designed to form an appropriate 3D microenvironment for the desired cell types, and also to provide mechanical support for new, structurally stabilized tissue formation and specific signals to guide the gene expression of tissue forming cells.

The cell sources used in tissue engineering are: autologous cells (from the same individual), allogeneic cells (from a different individual), and xenogeneic cells (from another species) (Hasirci and Yucel, 2007). The best cell source for tissue engineering is obviously the patient's own cells, in other words, autologous cells, especially because it eliminates the risk of rejection or adverse tissue reactions. The problem associated with autologous cells is the questionable state of health of these cells and also the limitation in the quantity of cells that could be harvested from a patient who probably himself is in need of extra healthy cells. Besides, these cells are at an advanced stage of development, and therefore, do not have so many cell divisions to go through. The most promising cell source in tissue engineering is the stem cells which have a great potential for proliferation and differentiation into various cell types. Until recently, it was thought that tissues of an adult would not have any stem cells and existence of such cells was only known

in embryos and newborn animals. However, stem cell populations were found in many adult tissues and even amongst the nerve cells in the mammalian brain.

1.4.2.   Ideal Scaffold in Nerve Tissue Engineering

A typical result of degenerative disease or injury in the nervous system is the disruption of the native unidirectional aligned architecture that directs and guides developing axons toward their targets (Zhang et al., 2005a). Loss of this well designed architecture leads to the disorganization of the axons. The only way to restore that architecture is to build a bridge that replaces the lesion gap and has all the morphological, chemical, and biological cues needed to mimic the native tissue microenvironment.

Few axons successfully pass through the lesion site; therefore, patterning of guidance cues is an important point to be considered in the design of the bridge. Guidance cues include short range cues that reside in cell membranes or ECM, and long range cues in soluble form provided by molecules that communicate with the growth cones, as neuronal adhesion molecules, and the molecules that are known to specifically attract or repel axons, such as netrins, semaphorins, and ephrins (Zhang et al., 2005a). The growth cones of the regenerating axons transform attractive and repulsive cues into signals which modulate cytoskeletal organization and thus determine the rate and direction of axon outgrowth. At the end, the regenerating axons reach the targets, and the guidance molecules receive stop signals. The elongation is terminated, and then synapses are formed. The functional recovery is accomplished by the rearrangement of the synaptic connections into topography similar to the preinjury condition.

Prior to the emergence of tissue engineering, the bridges for nerve regeneration were heavily relied on the use of biomaterials alone (Griffith, 2002). The general approach was to shape the bridges into guidance channels with tubular structures in order to protect the regenerating axons in the lumen from the external environment. These structures were constructed from polymeric materials, both from nondegradable polymers such as silicone, polyvinyl chloride, polyethylene, expanded polytetrafluroethylene, polyvinylidenefluoride, and biodegradable

polymers including poly(glycolic acid) (PGA), poly(lactic acid) (PLA), and collagen. The advantage of biodegradable materials is their disappearance from the implant site once regeneration has been completed, eliminating the risk of the foreign body response and the long-term possibility of infection-related complications. The tubular sleeve of a guidance channel can reduce the infiltration of fibrous tissue; provide a conduit for the diffusion of neurotrophic factors. Moreover, it can lead to increase in the concentration of endogenous proteins inside the channel, and serve as a barrier to selectively permit or inhibit the diffusion of macromolecules between the device and the surroundings. Conventional strategies on the uses of either biomaterials or cells alone have proven inadequate to ensure a significant regenerative response from severed CNS axons of the mature nervous system. As a result, utilizing tissue engineering approach is a promising one to restore the structure and functionality of the damaged nerve. A number of engineered substrates accompanied with oriented ECM, cells, or channels have displayed potential of supporting axonal regeneration and functional recovery. Current attempts are focused on seeking new biomaterials, new cell sources, and novel designs of tissue engineered neuronal bridging devices to produce a safer and a more efficient nervous tissue repair.

The desired physical properties of a nerve conduit are to be biodegradable and porous; to have the ability to deliver bioactive factors, such as growth factors; to be able to incorporate support cells; to carry an internal oriented matrix for cell migration and intraluminal channels to mimic the native nerve fascicles; and finally to maintain an electrical activity (Figure1.6).
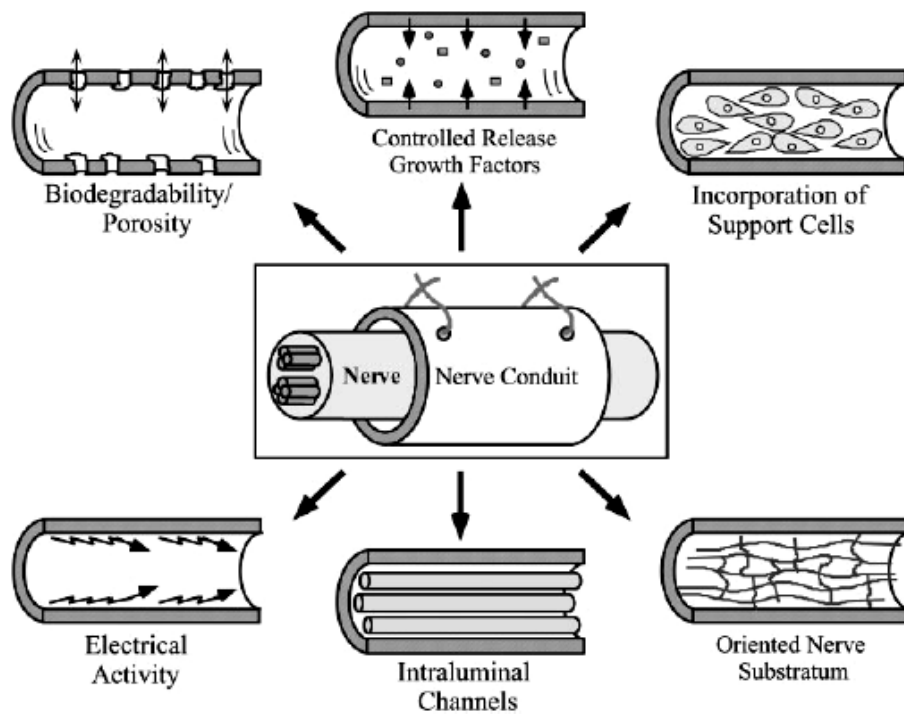
Figure 1.6. Properties of the ideal nerve conduit (Hudson et al., 1999)

Biodegradability is an important property in tissue engineering which creates space for tissue growth within the construct and eliminates the need for a second surgery to remove the implant (Huang and Huang, 2006). The degradation rates should be tailored to match that of new tissue formation by altering chemistry and components used in the formulation. The scaffold should have adequate porosity to promote cell attachment and tissue growth. Incorporation of support cells enhances the performance of the tissue engineered conduit. It was reported that Schwann cells offer a highly preferred substrate for axon migration and release bioactive factors that enhance nerve migration (Geller and Fawcett, 2002). Recently, stem cells or nerve progenitor cells derived from various regions of the adult or embryonic CNS of mice, rat, and human were tested for nerve regeneration application (Gage et al., 1995, Kocsis et al., 2002). The incorporation of growth

factors in the conduit should be effective at various levels, from molecular interactions to macroscopic tissue responses, results in neural development, survival, outgrowth, and branching (Jones et al., 2001). The physical guiding of axons across a site of injury via oriented substratum and intralumen channels would aid to retain the native organization of regenerating axons and increase the functionality of the construct. In addition application of an electric field stimulates microtubule disassembly locally along the neurite shaft, which results in a polarized rearrangement of the neuronal cytoskeleton (McCaig, 1990).

1.5. Approaches Used in Nerve Guidance

The cellular behaviors as cytoskeletal organization, orientation and migration are affected by ECM topography and its chemical composition (Flemming et al., 1999). ECM proteins, fibronectin, laminin, or collagen form certain protein networks which displays tissue specific variation (Hay, 1991). Cellular response to these networks depends on the composition of ECM. Specific cell–matrix interactions between ECM proteins and cell adhesion receptors such as transmembrane integrins modulate the organization of the actin cytoskeleton (Geiger et al., 2001). Orientation in actin filaments was identified as the preliminary event in contact-guided cell alignment (Oakley and Brunette, 1993). The most important group for cell adhesion is the RGD sequence, a minimal sequence required to mediate cell adhesion to the ECM molecule fibronectin, and has since been found to be present in a wide range of molecules, including the blood circulating fibrinogen (Ruoslahti and Pierschbacher, 1987, Hasirci and Yucel, 2007).

In most tissues cells are well organized by the aid of ECM, especially in the nervous system the cells are either unidirectionally aligned or form networks. Thus, the scaffold used in nerve tissue engineering should facilitate the directional orientation of cells by topographical or chemical cues as in native tissue.

1.5.1.   Patterning with Chemical Cues

Chemical patterning is achieved by immobilization of biological molecules mimicking the organization of cells in target native tissue. These biological molecules can be ECM proteins such as fibronectin, vitronectin, laminin, and collagen or their constitutional motifs such as RGD peptides (Lim and Donahue, 2007). Besides biological molecules, patterned nonbiological molecules or altered surface chemistry can be effective on cell behavior. Chemical cues, whether biological or nonbiological, are biomimetic due to the direct receptor-ligand binding. The most common chemical cues for nerve guidance involve the specific peptide sequence Ile-Lys-Val-Ala-Val (IKVAV) (Wei et al., 2007), poly(D-lysine) (Nam et al., 2007), and laminin (Thompson and Buettner, 2004, Schmalenberg and Uhrich, 2005, Song and Uhrich , 2007). Fibronectin can be an alternative chemical cue since it enhances attachment, proliferation, and nerve regeneration (Vleggeert-Lankamp et al., 2004). In the presence of chemical cues cells sense signals from these patterned molecules that induce specific integrin binding (for example, fibronectin-integrin $\alpha5\beta1$) (Hynes, 2002). Thus cells synthesize focal adhesion proteins (vinculin, paxillin, talin, etc.) that connect to cytoskeletons and focal contacts are formed at the integrin-binding sites (Anselme, 2000).

1.5.2.   Patterning via Topographical Cues

1.5.2.1.   Commonly Used Techniques for Guidance

The knowledge accumulated on the cell-ECM and cell-material interactions is used in tissue engineering approaches to mimic native tissues in architecture and function in the design of the new scaffolds.The scaffolds to be used in nerve tissue engineering should be designed to achieve the guidance of cells. For this purpose, micro and nano structures are formed on material surfaces using various techniques. Such patterned surfaces could be obtained by lithography and subsequent transfer methods, or by other methods such as molding, surface grafting,

ink jet printing, surface etching, and etc. (Hasirci and Kenar, 2006). Fibrillar scaffolds, on the other hand, are generated by pressure-assisted microsyringe, self-assembling, and electrospinning techniques.

1.5.2.2.   Contact Guidance via Micropatterning

Substratum topography is a nonbiological method of regulating cell behavior; however, topography could provide a biomimetic cell-stimulating cue (Lim and Donahue, 2007). Cell response to topography is still not clear but it has been proposed that cells adapt to physical topographic substrates by conditioning growth environments through secretion and modulation of ECM proteins (Chou et al., 1995). Synthetic substrates with various desired topographies can be created by microfabrication techniques. The most common technique to produce features with controlled dimensions and specific shapes is the photolithography (Flemming et al., 1999) (Figure 1.7). A substrate with a resist, a thin light sensitive polymeric film, is exposed to light through a patterned mask. Following this, the irradiated regions are either more soluble or less soluble in a developer solvent depending on resist chemistry and produce a negative or positive image of the mask. To transfer this image in the resist to the substrate, regions which are free of resist are etched with KOH to obtain V-shaped grooves, whereas square grooves are produced by reactive ion etching. The groove structures with V-shape are used in most of the studies related to the interactions between substrate topography and cells such as capillary endothelial cells, epithelial cells and gingival fibroblasts (Oakley and Brunette, 1993 and 1995, Chou et al., 1995, Mrksich et al., 1996). Use of patterned substrates is prominent and common in the control of neural cells orientation (Rajnicek et al., 1997, Mahoney et al., 2005, Goldner et al., 2006, Song and Uhrich, 2007).
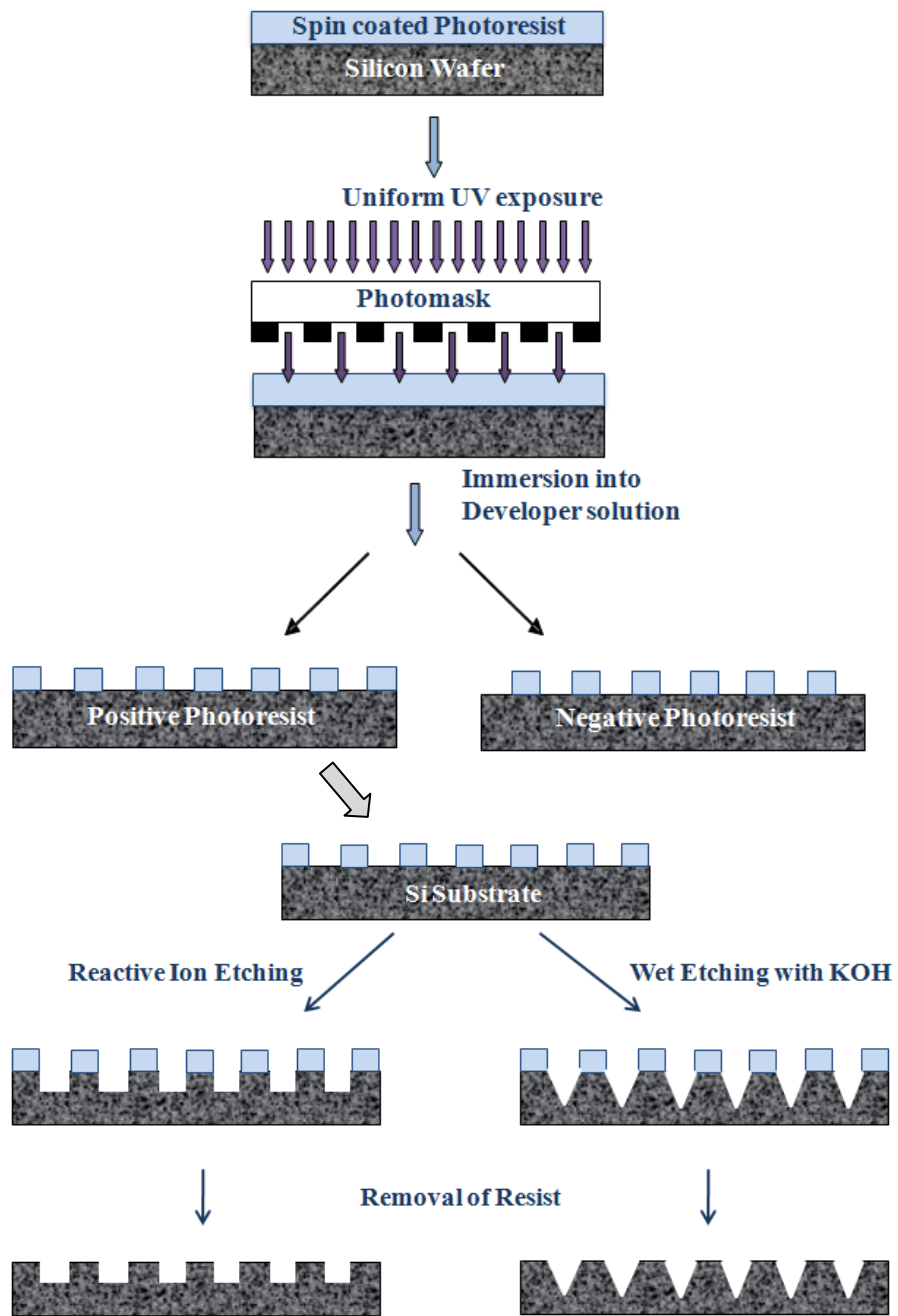
Figure 1.7. Schematic diagram of the phololithography and the pattern transfer

Many groups have used the photolithography and microfabrication techniques to create microchannels or microgrooves. Mahoney et al. (2005) used photolithography to deposite polyimide walls (11 µm in height and 20–60 µm in width) onto a planar glass substrate. It was revealed that neurites grown from NGF-stimulated PC12 cells were strongly oriented parallel to channel walls. In another study, silicone microchannels (60 µm wide, 50 µm deep, spaced 60 µm apart) were produced to study the morphology of dorsal root ganglion cells on these grooved substrates (Goldner et al., 2006). A subpopulation of cells unexpectedly developed neurites that bridged the channels, spanning 60 µm with no underlying solid support. The explanation for this behavior was the formation of bridges as neurites extended from a neuron in a groove. The neurites could first contact the wall and then continue to extend vertically up the wall, and then the cell body might detach from the substrate and form a bridge across the groove. These unexpected cell responses were currently investigated by researchers to understand the cytoskeletal dynamics of the cells.

The dimensions of the micropatterned substrates had a strong effect on the behavior of cells, varying with the cell type and cell size. Microgrooved substrata of varying dimensions (8 µm groove, 20 µm ridge, and 1 or 2 µm depth) were produced to study the effect of topographical cues on the behavior of neurons derived from chick embryo cerebral hemisphere (Clark et al., 1990). The shallower grooves (1 µm depth) were not effective on the outgrowth of neurites, with the growth cones crossing many grooves and ridges. However, on 2 µm deep patterns neurite outgrowth was significantly aligned along the groove axis with little crossing over the edges. The influence of groove depth on orientation of Schwann cells was seen in the study of Hsu et. al. (2005). By fixing the width/spacing of the grooves at 10/10 µm, the mean percentage of aligned cells was increased from 12% to 26% when the groove depth increased from 0.5 to 1.5 µm. In the same study, with the depth of grooves fixed at 1.5 µm, the percentage of aligned cells increased from 26% for patterns with width/spacing of 10/10 µm to 41% for patterns with 20/20 µm.

Polystyrene substrates were prepared on patterned silicon wafers by solvent casting (Recknor et al, 2004). Like in most of the studies, the effect of

physical cue (micropatterns) on behavior and morphology of cells improved with chemical cue laminin adsorption. The results showed that of the over 85% astrocytes aligned parallel to the groove axis. In later studies Recknor and colleagues showed that the substrate topography, in synergy with chemical (laminin) and biological (astrocytes) guidance cues, resulted in oriented growth of astrocytes, and accelerated the neurite outgrowth and alignment *in vitro* (Recknor et al., 2005). These cues also facilitated the neuronal differentiation and promoted the neurite alignment on topographically distinct regions of the same substrate (Recknor et al., 2006).

The use of biodegradable polymers in creating patterned surfaces makes them suitable for use in tissue engineering as implantable materials (Patel et al., 1998). Biodegradable polymers degrade to low molecular weight biocompatible products and are gradually replaced by the growing tissue to help produce a proper and fast healing tissue (Hasirci and Yucel, 2007). The rate and mode of degradation can be controlled by type and combination of polymers to suite the target tissue.

1.5.2.3. Contact Guidance via Electrospinning

Electrospinning is a simple process that essentially employs electrostatic forces to produce versatile polymeric nano-fibers ranging in diameter from a few microns down to tens of nanometers (Murugan and Ramakrishna, 2007). This top-down approach is also very cost effective. Even though Zelency is the first researcher who introduced this technique in 1914 (Zelency et al., 1914), Formhals developed the technique, and obtained several patents in the 1930s and 1940s (Formhals, 1934, 1939, 1940, 1943, 1944). Recently, electrospinning technique has been widely applied in tissue engineering to produce fibrous scaffolds with most of the structural features required for cell growth and succeeding tissue organization. Compared to conventional scaffold preparation techniques electrospinning offers many advantages such as production of ultra fine fibers with spatial orientation, high surface area, and controlled pore geometry (Murugan and Ramakrishna, 2007). These favorable characteristics directly affect cell adhesion, cell expression, and transport of oxygen and nutrients to the cells, therefore, they could be considered to

achieve better cellular growth functions *in vitro* and *in vivo* (Li et al., 2002). The electrospun fibrous scaffolds serve as a good cell carrier and provide spatial environment for the new tissue growth with appropriate physiological functions.

The electrospinning system is schematically illustrated in Figure 1.8. Three major components of the system are: (i) a syringe containing viscous polymer solution, (ii) a grounded metallic collector, and (iii) a high voltage power supply. The polymer solution can be fed at a constant and controllable flow rate by the aid of a syringe pump. The collector is positioned right below or opposed to the syringe, with an appropriate distance. The principle of electrospinning is to draw polymer solution in an electric field (Ma et al., 2005a). Upon high voltage (10–20 kV) application, a pendent droplet of the polymer solution at the tip of the needle of the syringe is charged. This allows the droplet to deform into a cone shape, known as Taylor's cone (Taylor, 1969) by two electrostatic forces as electrostatic repulsion between the surface charges of the droplet and Columbic force exerted by the strong external electric field (Yarin et al., 2001). Thus, when a sufficient surface charge is generated to overcome the surface tension in a pendant drop of the polymer fluid, a fine charged polymer jet is forced to eject from the tip of the Taylor cone (Murugan and Ramakrishna, 2007). This polymer jet then moves toward the metallic collector, accompanied by rapid evaporation of the solvent of the polymer solution, and collected as a mat composed of fibers, nano or several micron sizes in diameter. In tissue engineering the scaffolds having different fiber diameters are required depending on the tissue. The diameter of the electrospun fiber can be controlled by adjusting certain parameters like polymer concentration, flow rate of the polymer solution, solvent conductivity, the distance between two poles (tip of needle and the collector), applied potential and temperature, and so on.

Different types of fiber collectors are available according to the desired fiber's spatial orientation (aligned and random) (Ma et al., 2005a). The static, plate-type collectors are used to obtain a randomly oriented nonwoven fiber matrix fibers, while for aligned nanofiber matrixes the rotatable cylinder or disc type collector are commonly used (Murugan and Ramakrishna, 2007). The recently used approach to producing aligned electropsun fibers is the use of frame collector or collecting fibers between two parallel electrodes. Li and Xia (2004) produced polymeric and

ceramic nano-fibrous assemblies by the use of a collecting substrate consisting of two pieces of electrically conductive materials separated by an insulating gap whose width could be a few micrometers to centimeters. When the electric field is applied, the charged nanofibers are stretched and align themselves perpendicular to the gap. To obtain aligned fibers is rather complicated and various parameters affect the fiber orientation such as the rotational speed and shape of collector, the concentration of polymer solution, the polymer molecular weight, the surface tension, the conductivity, the dielectric constant of the solvent, the strength of the electric field, as well as the environmental conditions such as relative humidity and temperature.
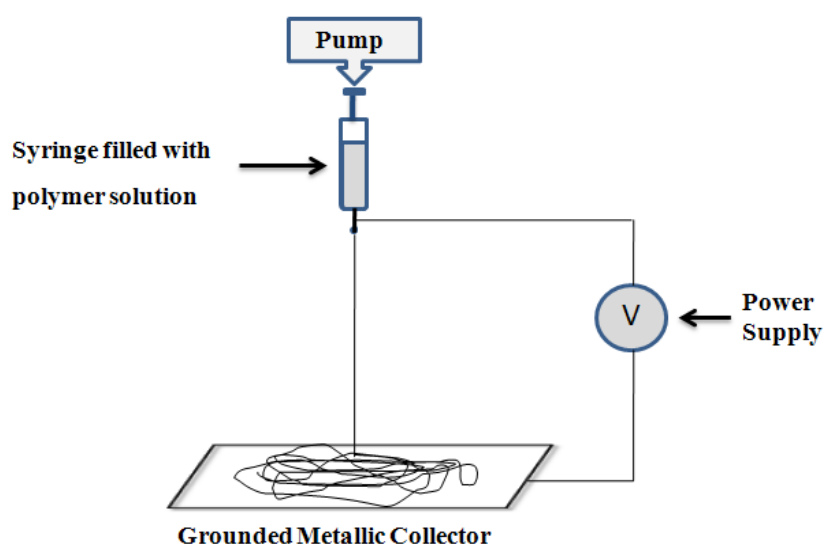
Figure 1.8. A schematic presentation of the electrospinning system

It is challenging to fabricate a scaffold which is composed of precisely uniaxially oriented, electrospun fibers to restore the damaged nerve by mimicking the native architecture of nerve tissue, because directional cell growth is a prerequisite for functional nerve regeneration. Indeed the aligned electrospun fibers

are potentially ideal for neural tissue engineering since the cell orientation, phenotypic expression, and other neuronal cellular behaviors are affected by the fiber orientation of the scaffolds. It was reported by Yang et al. (2005) that, the well-aligned, PLLA nano fiber orientation predominantly controls the directional cell growth. Neural stem cells elongated and their neurites outgrew along the direction of the fiber orientation, which shows the importance of spatial orientation of the fibers for the cellular growth behavior. It was found that the fiber diameter did not show any significant effect on the cell orientation, while it was effective on NSC differentiation. The rate of differentiation was higher on nanofibers compared to microfibers, but independent of the fiber alignment. In another study, it was noticed that aligned poly-caprolactone (PCL) and collagen/PCL (C/PCL) nanofibers, produced by electrospinning, supported oriented neurite outgrowth and glial migration from dorsal root ganglia explants (Schnell et al., 2007). Kim et al. (2008) mentioned that the aligned fiber-based polymer constructs, serving as sub-micron scale topographical cues, facilitated the regeneration of peripheral nerves (both sensory and motor nerve) across long nerve gaps (17 mm) in the absence of exogenous growth promoting proteins. In a recent study, the electrospinning parameters such as collection disk rotation speed, needle size, needle tip shape, and syringe pump flow rate were precisely optimized to obtain highly aligned PLLA electrospun fibers (Wang et al., 2009). It was reported that these aligned PLLA fibers, guided neurite and Schwann cell growth along the axis of fibers. Thus, all studies recommend the highly aligned electrospun fibrous scaffolds as the cell carrier in nerve tissue engineering.

1.6. Cell Sources Used in Nerve Tissue Engineering

1.6.1. Stem Cells

Stem cells have extensive self-renewal capacity and are able to provide additional undifferentiated stem cells (Choumerianou et al., 2008). Stem cells are ideal promising candidates to be used in regenerative medicine, tissue engineering, and cell replacement therapies with their ability to differentiate into one or more

committed descendants, including fully functional mature cells. Stem cells were classified according to their origin, as embryonic, germinal, or somatic (fetal or adult).

1.6.1.1. Embryonic Stem Cells

Embryonic stem cells (ESCs), which are derived from blastocyst stage embryos, have an extensive *in vitro* proliferative capacity in undifferentiated state and have a potential to differentiate into various types of cells from all the three germ layers, endoderm, mesoderm and ectoderm. However, there are ethical and practical issues, like formation of teratoma when implanted into the body in an undifferentiated form, and triggering of immune response, related with their use in humans (Denker, 2006).

ESCs have the intrinsic capacity to form all cell types of the nervous system using the appropriate developmental cues, which points out to the possibility of reconstructing the neural development pathway starting with ESCs *in vitro* (Gottlieb and Huettner, 1999, O'Shea, 1999). In general, the initial step of differentiation is embryoid body (EB) formation. When ESCs are cultured on a nonadhesive substrate in leukemia inhibitory factor (LIF)-free expansion medium, they form small aggregates of cells called EBs in the form of hanging drops. On the 4th day of culture the stem cells differentiate into a complex mixture of ectodermal and mesodermal progenitors, and then further culturing forms a complex mixture of terminally differentiated cells including heart, muscle, blood, and neurons among others. Retinoic acid (RA), a potent form of vitamin A, is effective in cell differentiation and homeostasis, and also is used in directing the early differentiation events in ESCs predominantly toward endodermal and neuroectodermal lineages (Campione-Picardo et al., 1985, Soprano et al., 2007). Spontaneous differentiation of EBs forms only a small fraction of neural lineage cells. To promote neural differentiation, RA is added at the end of 4 days of ESC culture, and then followed by 4 days of additional culture in the presence of RA (Bain et al., 1995 and 1998). It was observed that the great majority of cells differentiate into neural lineage cells. In order to differentiate further into neurons,

astrocytes, and oligodendrocytes, RA-induced EBs are dissociated and then plated on an adhesive substrate (Bain et al., 1995, Finley et al., 1996, Liu et al., 2000).

1.6.1.2.   Mesenchymal Stem Cells

Adult stem cells, either hematopoietic or mesenchymal, have an inherent tendency to differentiate only into the cells of the tissue that they were isolated from. However, the growing number of research present data about their transdifferentiation into tissues different from their origin (Verfallie et al., 2002, Serafini and Verfaillie, 2006). These cells can be isolated not only from bone marrow but also from many other adult tissues such as umbilical cord, adipose tissue, etc. Bone marrow (BM) is considered a common source of autologous adult stem cells, however, its collection from the donor is not simple and it is not practical as a routine method. The umbilical cord blood is a good source for mesenchymal stem cells (MSCs), but it is usually poorer in MSCs compared to bone marrow (Wexler et al., 2003, Yang et al., 2004). Placenta and umbilical cord matrix (Wharton's Jelly), are readily available tissues that house MSCs (Wulf et al., 2004, Portman-Lanz et al., 2006, Weiss et al., 2006), however, isolation of MSCs is easier from Wharton's Jelly (WJ) through explant culture (Mitchell et al., 2003) or by enzymatic digestion (Wang et al., 2004, Weiss et al., 2006). BM and WJ MSCs can differentiate into osteoblasts, chondrocytes and adipocytes (Wang et al., 1997, Romanov et al., 2003, Mauney et al., 2005, Marolt et al., 2006). Their potential to differentiate into neurons, glial cells, cellular lineages that are not their normal destiny, was reported in many studies on their use as a cell source for the treatment of neural malfunctions (Woodbury et al., 2000, Kohyama et al., 2001, Sanchez-Ramos et al., 2001, Kim et al., 2002, Jeong et al., 2004, Cho et al., 2005, Kondo et al., 2005, Tao et al., 2005, Tropel et al., 2006).

MSCs from BM (Kim et al., 2002, Tondreau et al., 2004, Bossolasco et al., 2005, Cho et al., 2005, Tao et al., 2005, Mareschi et al., 2006, Krampera et al., 2007), adipose tissue (Zuk et al., 2002, Kokai et al., 2005), umbilical cord blood (Buzanska et al., 2002, Jeong et al., 2004, Kang et al., 2006, Park et al., 2006), umbilical cord matrix (Mitchell et al., 2003, Ma et al., 2005b, Fu et al., 2006) were

induced to proliferate and differentiate into glia and neurons besides cells of mesodermal origin. Even though the differentiation mechanism of transplanted MSCs in engrafted tissue is not clear, several *in vivo* studies showed that MSCs can migrate and differentiate into astrocytes and neurons depending on the extracellular matrix and signal molecules in their environment (Kopen et al., 1999). MSCs can be differentiated into neuron-like cells under *in vitro* conditions in the presence of some inducing agents such as retinoic acid alone or in combination with growth factors (Sanchez-Ramos et al., 2001, Kim et al., 2002, Kondo et al., 2005, Cho et al., 2005) beta-mercaptoethanol (BME) and/or dimethylsulfoxide (DMSO) (Woodbury et al., 2000, Jeong et al., 2004, Tao et al., 2005), and 5-Aza-C (Kohyama et al., 2001). Some *in vitro* studies claim that the neural induction of MSCs with cytotoxic chemicals, such as BME or DMSO/butylated hydroxy anisole, is a transient event as a cell shrinkage and actin cytoskeleton retraction in response to chemical stress, not a real differentiation (Lu et al., 2004, Neuhuber et al., 2004, Bertani et al., 2005). However, most of the researchers have shown the transdifferentiation of MSCs into neurons and glial cells under *in vitro* conditions, and the recent studies have shown the functionality of these neurons (Cho et al., 2005, Tropel et al., 2006). In order to obtain functional mature neurons or glial cells, the molecular mechanism of neural differentiation of MSCs needs to be clarified. The expression of early neural markers such as nestin, Pax6, Nurr1 supports the differentiation capacity of MSCs into neurons and glial cells (Tondreau et al., 2004, Blondheim et al., 2006). Studies on multipotency of adult MSCs have revealed that undifferentiated MSCs of human, rat and mouse origin express neuroectodermal marker genes (Woodbury et al., 2000, Tondreau et al., 2004, Bossolasco et al., 2005, Kondo et al., 2005, Wislet-Gendebien et al., 2005, Hermann et al., 2006). Moreover, Blondheim and colleagues (2006) revealed a broad selection of neural genes expressed by undifferentiated human MSCs of bone marrow origin, indicating that these cells already possess neural features; or alternatively, stem cells express a wide range of genes at a low and nonfunctional level, and some of them are upregulated upon differentiation to certain cells, while some other (nonspecific) genes are downregulated. Most of the studies indicated

that MSCs have a capability to transdifferentiate into neurons or glials upon induction with appropriate combinations of growth factors and chemical stimulants.

1.6.1.3.   Neural Stem Cells

Undifferentiated, multipotent neural stem cells (NSCs) have an inherent ability for extensive self-renewal, thus under appropriate conditions they can proliferate for a long time in culture and are often cultured as neurospheres (Filippis et al., 2007). Under certain conditions NSCs can give rise to the three cell lineages of the CNS: (i) neurons, (ii) astrocytes, and (iii) oligodendrocytes. Stem cells or nerve progenitor cells have been isolated from various regions of the adult or embryonic CNS of mice, rat, and humans for nerve regeneration applications (Gage et al., 1995, Kocsis et al., 2002). It was reported that stem-cell-like precursors which are capable of driving neurogenesis and gliogenesis are found in the specialized CNS germinal niches, in the ganglionic eminence(s) in the embryo, as well as in the subventricular zone (SVZ) of the lateral ventricles and the subgranular zone (SGZ) of the hippocampal dentate gyrus (DG) in the adult (Gage, 2000, Doetsch, 2003). The maintenance and differentiation of NSCs in brain niches is controlled by their physical contact with the basal lamina (Mercier et al., 2002). The basal lamina modulates cytokines and growth factors derived from local fibroblasts, macrophages and pericytes and also acts as a scaffold. The inherent plasticity of NSCs has suggested replacing them with the cells in the mammalian CNS. Indeed, it was shown in some studies that stem cells implanted into injured spinal cord differentiate into neurons and glial cells (Chow et al., 2000, Cao et al., 2001). Considering their preferential differentiation to neural cell lineages, NSCs and neural progenitor cells also constitute a potential cell source to be used in nerve tissue engineering (Yang et al., 2005, Recknor et al., 2006).

1.6.2.   Mature Cells

The most common cell sources used in nerve guidance studies are Schwann cells (Eguchi et al., 2003, Thompson and Buettner, 2004), astrocytes

(Recknor et al., 2004, Nam et al., 2007), dorsal root ganglion cells (Schnell et al., 2007, Song and Uhrich, 2007) and PC12, a model cell line (Mahoney et al., 2005) in neural cell investigations. Schwann cells produce structural and adhesive ECM molecules such as laminin and collagen, and synthesize neurotrophic molecules (NT-3, NGF, BDNF, CNTF, and FGF) to promote nerve regeneration (Tonge and Golding, 1993, Martini, 1994). They form an endoneurial sheath to direct axonal growth, participate in clearing debris and enable a suitable environment for nerve growth, and myelinate axons (Bunge, 1994). Schwann cells were important in leading peripheral axons to the distal nerve stump and in synapse formation (Son et al., 1996). Many researchers were interested in the ability of Schwann cells to promote nerve regeneration (Cebellos et al., 1999, Jones et al., 2001). Even though there are still some drawbacks of Schwann cell use like immunogenicity, their survival time, donor site morbidity, etc., these cells are the most commonly used cells in nerve tissue engineering applications especially for PNS injuries, and even for CNS nerve tract repair (Thompson and Buettner, 2001, Rutkowski et al, 2004, Novikova et al., 2008). Like Schwann cells, the other support cell, astrocytes are also commonly used as biological cues to provide a permissive environment for the regeneration of axons in nerve tissue engineering. Astrocytes, as neuroglial cells of the CNS, support the proliferation, survival, and maturation of developing neurons, as well as guiding the migration of growing axons (Recknor et al., 2004). They are also involved in the integration of neuronal inputs and modulation of synaptic activity. The mature astrocytes can also participate in the induction of neurogenesis from adult neural stem cells (Song et al., 2002).

1.7. Applications in Nerve Tissue Engineering

The current clinical gold standard in repairing larger nerve defects (20 mm or longer in humans) is to use nerve autografts (Bellamkonda, 2006). However, the disadvantages and the clinical outcomes of autograft use create a critical need for engineered alternatives. Autografts are limited by a shortage of donor nerves, a mismatch of donor nerve size with the recipient site, and occurrences of neuroma formation. Many groups have constructed 3-D nerve guides to enable the nerve

regeneration across the lesion gap, but only some of them were approved by the Food and Drug Administration (FDA) (USA) for surgical use such as GEM Neurotube Nerve Conduit composed of Polyglycolic acid (Synovis Micro Companies Alliance (St. Paul, MN), 1999), SaluBridge Nerve Cuff composed of Polyvinyl alcohol (Salumedica LLC (Atlanta, GA), 2000) and collagen based NeuraGen Nerve Guide (Integra Lifesciences Corp. (Plainsboro, NJ), 2001). Nerve guides derived form synthetic and biological materials without any cell incorporation have exhibited key advances toward functional nerve regeneration. However, a comprehensive knowledge in the dynamic interactions among neurons, their support cells, and their 3D ECM surroundings enable to develop an innovative nerve guide which addresses the requirements to regenerate structural and functional normal nerve. To enhance regeneration across nerve gaps, the growth permissive guided scaffolds should be accompanied with topographical cues via fabrication of patterned or fibrillar structures, chemical cues via immobilization of neurostimulatory ECM proteins or peptides (typically laminin1 or its fragments like IKVAV sequence), addition of trophic factors (bFGF, NGF or BDNF), and biological cues via incorporation of support cells as glial cells and Schwann cells (Bellamkonda, 2006). Moreover, the use of mature neurons or especially the stem cells can improve the healing process of the damaged nerve. These fundamental approaches have been used individually or as a combination of some of them in nerve tissue engineering applications. The synergistic influence of combining some approaches has been found to be more effective than individual cues in nerve guidance, but it is not easy to satisfy all the conditions indicated above.

Among the tissue engineered designs proposed for neuronal bridging devices, the ones using contact guidance via physical cues are among the most promising. In nerve injury the initial response is axonal sprouting which results in either abortive regeneration, misdirection, or in neuroma-like formation upon contact with the scar. This problem can be solved by incorporation of matrices into the lumen of the guidance channel to improve the organization of the regeneration environment. Indeed this approach provides topographic guidance cues with unidirectional aligned textures to facilitate unidirectional outgrowth of the

regenerating axons. Thus, an entubulation configuration of bridging device is one practical application of the contact guidance concept.

The construction of minichannel entubulation device was the pioneering study in nerve tissue engineering area (Winn et al., 1989). A random copolymer of acrylonitrile and vinylchloride (PAN–PVC) based semipermeable, nondegradable, hollow fiber membranes were seeded with Schwann cells. Both myelinated and nonmyelinated regenerating axons were found in the midpoint of the channel. Some of the regenerating axons were able to pass across the bridge-host interface and reach the host CNS environment.

The guidance potential of a nerve entubulation bridging device was enhanced by fabricating hollow fiber membranes (HFM) with aligned texture on the inner surface (Zhang et al., 2005b). *In vitro* studies of dorsal root ganglion cells showed that both the alignment and outgrowth rate of regenerating axons improved significantly on HFMs with aligned textures compared to those on HFMs with a smooth inner surface.

In one study, a porous tubular scaffold with desired mechanical properties and controllable inner structure was obtained by a novel method (Wang et al., 2006). Chitosan fiber-based hollow tubes, which served as the outer wall of the scaffolds, were produced through an industrial knitting process. On the other hand, the inner matrices with multiple axially oriented macrochannels and radially interconnected micropores were developed by an innovative molding technique. *In vitro* studies showed that differentiated Neuro-2a neuroblastoma cells grew along the oriented macrochannels and the presence of interconnected micropores provided the nutrient diffusion and cell ingrowth to the inside of the scaffold. The other chitosan based scaffold was fabricated by novel molds and a thermally induced phase-separation technique to obtain multimicrotubule conduits (Ao et al., 2006). *In vitro* studies showed that these conduits have a suitable mechanical strength, microtubule diameter distribution, porosity, swelling, biodegradability, and nerve cell affinity (to mouse neuroblastoma cell line).

Valmikinathan et al. (2008) constructed a poly(lactide-co-glycolide) (PLGA) microsphere-based spiral scaffold with a nanofibrous surface obtained by electrospinning. According to *in vitro* studies carried out with Schwann cells

showed that the nanofibrous spiral scaffolds enhanced cell attachment and proliferation compared to contemporary tubular scaffolds or nanofiber-based tubular scaffolds.

A hydrogel scaffold of well-defined geometry with peptide modified longitudinal channels was constructed to enhance cell adhesion and neurite outgrowth (Yu and Shoichet, 2005). By incorporation of laminin-derived oligopeptides, CDPGYIGSR and CQAASIKVAV, as the chemical cue, the scaffold enhanced neural cell adhesion and guided neurite outgrowth of dorsal root ganglia neurons relative to non-peptide modified controls.

A resorbable, semipermeable nerve guide conduit with microstructured internal polymer filaments was constructed to mimic the bands of Büngner, which function as guides for regrowing axons (Lietz et al., 2006). Schwann cell orientation and the growth of dorsal root ganglia axons were directed with longitudinal microgrooves. Incorporation of Schwann cells was also seen in the study of Hadlock et al. (2000) in an attempt to design an efficient neural guidance conduit. A biodegradable polymer conduit was composed of longitudinally aligned channels which facilitated the adherence of Schwann cells through the increase in available surface area in comparison to a simple hollow conduit. *In vivo* studies demonstrated the presence of neural regeneration in each of the longitudinally-aligned channels. The effect of biological cue was clearly shown in the study carried out by Novikova et al. (2008). A biodegradable poly(β-hydroxybutyrate) (PHB) tubular conduit was used as a scaffold. When plain PHB conduit was transplanted into the injured spinal cord, it was well-integrated into posttraumatic cavity and induced modest astroglial reaction. Moreover, the axon regeneration was seen mainly outside the PHB with only single fibers crossing the host-graft interface. However, in the scaffolds supplemented with Schwann cells, neurofilament-positive axons filled the conduit and became associated with the implanted cells.

For the treatment of CNS, NSCs and a biologically derived polymer, collagen, were combined (Ma et al., 2004). The collagen-entrapped NSCs expanded and efficiently generated functional, excitable, polar neurons. This study is very important as being the first demonstration of CNS stem cell-derived functional synapse and neuronal network formation in a 3D scaffold.

Since they are closer to the natural tissue the development of 3D scaffolds is required to replace or restore the nerve gap. However, the ideal constructs involve distributing 2D-like substrates/surfaces in 3D space because the neurite extension on 2D surfaces is generally better than the cells embedded in 3D substrates (Bellamkonda, 2006). Gomez and Letourneau (1994) demonstrated the preference of the growth cones to follow 2D substrates. The peripheral and central primary neurons (DRGs, retinal ganglia) as well as cell lines (PC 12 cells) sink to the bottom of the well and always extend the longest processes upon culturing in 3D scaffolds such as collagen, agarose, agarose derivatized with Laminin-1, and etc.(unpublished data) (Bellamkonda, 2006). As a result, distributing micron- or nano-sized growth permissive structures like fibers or films in 3D scaffolds by providing a 2D surface for regenerating axons was suggested. However, while maximizing the guidance cues with the use of fibers, maximizing the total cross-sectional area that is physically available to the regenerating nerve without obstruction by the thick embedded fibers should be considered in the design of ideal 3D scaffold.

1.8. Aim and the Approach of the Study

1.8.1. Aim

The ultimate aim of this study was to develop a porous and tubular nerve guide from a biodegradable polymer to facilitate the regeneration of nerves across long nerve gaps formed upon injury. For this purpose, a 3D nerve tube composed of aligned stem cells on an oriented electrospun fibrous mat wrapped in a porous, micropatterned film was constructed. Human MSCs and mouse NSCs were used as the cell source.

1.8.2. The Approach of the Study

The present study has a unique approach in its experimental design. In literature most groups constructed an integral 3D scaffolds as porous hollow tubes

or tubes with intraluminal channels. In this study the final scaffold is composed of two 2D surfaces to enhance cell attachment and growth. Thus, the difficulty in cell seeding and growing in 3D scaffolds was overcome by seeding cells on the exterior and interior of the scaffold separately as a 2D surface. Thus, the whole structure has a guiding property with aligned fibers and patterned film as suggested by Bellamkonda (2006) to maximize the guiding cues. The tubular structure was constructed after culturing cells on these surfaces for a while to maintain cell growth and differentiation. This idea is important in differentiation step. The stem cells on one of the surfaces had to stay in undifferentiated form while the cell on the other surface had to differentiate, as a result the applied differentiation protocol should not affect the cells which had to stay in undifferentiated form. In the current studies, most groups try to maintain guided neurite outgrowth in the presence of support cells, however, in this study stem cells were used besides support cells. The stem cells in the interior part of the scaffold are induced to grow and differentiate by the help of aligned support cells which face the inside of the tube wrapping the nanofibers. The other important characteristic of this study is that in one application the whole construct is populated with stem cells. Neural stem cells or progenitor cells were used in 3D nerve constructs (Ma et al., 2004) but the use of isolated human MSCs in 3D nerve constructs is unique. Hence, the tissue engineered construct designed in this study could alleviate some drawbacks or deficiencies in current nerve constructs and will potentially be used in nerve regeneration.

In this study, human MSCs were seeded separately on each the components of the construct. The support cells on the patterned films were cultured with expansion medium without any differentiation, while MSCs on the aligned fibers were induced with neurological stimulants. After separate culturing for 7 days, the patterned film with MSCs on it was wrapped around the electrospun mats which were loaded with MSCs induced to neuron differentiation. It was aimed that the aligned support cells would aid the alignment, growth and the complete differentiation of the cells on the electrospun fibers.

The other cell source, mouse NSCs, were seeded separately. In this case, NSCs seeded on the patterned films were differentiated into astrocytes as support cells, whereas the NSCs on the electrospun mats were kept as undifferentiated

NSCs. Following 9 days of culture, tubular structure was formed by rolling the patterned film containing astrocytes over NSCs on the electrospun mats. In this design, it was aimed that the aligned astrocytes on the film would serve as a growth and differentiation factor supply for NSCs besides enhancing their alignment on the electrospun mats.

The synergistic effects of combination of the topographical cues (macropatterned film and electrospun fibers), the chemical cues (laminin or fibronectin coating), and the biological cues (support cells on the exterior part of the tube) was expected to make this construct an ideal 3-D scaffold to be used in nerve tissue engineering.

CHAPTER 2

MATERIALS AND METHODS

2.1.   Materials

Poly(3-hydroxybutyrate-co-3-hydroxyvalerate) (PHBV5 containing 5% by mole of 3-hydroxyvalerate) was purchased from Aldrich Chem. Co. (UK). Poly(L-lactide-co-D,L-lactide) (P(L-D,L)LA) (70:30) and poly(DL-lactide-co-glycolide) (PLGA) (50:50) were obtained from AppliChem (Germany) and Boehringer Ingelheim Pharma KG (Germany), respectively. The cell source was mouse Balb C strain neural stem cell line (CRL-9392) and was purchased from American Type Cell Collection (ATCC). Dulbecco's Modified Eagle Medium:F12 (DMEM:F12), chemically defined lipids (CDL) and trypsin inhibitor were purchased from Gibco. DMEM Low and DMEM High Glucose, α-MEM, F12 Nutrient Mixture media, Fetal Calf Serum (FCS), Penicillin/Streptomycin (Pen/Strep) solution were the products of HQClone. Trypsin-EDTA (0.25%), glutaraldehyde, cacodylic acid (sodium salt), human transferrin, sodium selenite, bovine insulin, laminin1, all trans-retinoic acid (AT-RA), valproic acid (VA), forskolin were obtained from Sigma (USA). Epidermal growth factor (EGF) and fibronectin were the products of Roche (Germany). MTS kit was obtained from Promega Corporation (USA). Alexa Fluor 488 phalloidin and DAPI were obtained from Chemicon (USA). All primary antibodies for flow cytometry analysis were purchased from BD Biosciences except anti-CD105 (Serotec, USA) and anti-CD133 (Miltenyi Biotech, USA).

2.2. Methods

2.2.1. Polymeric Scaffolds

2.2.1.1. Preparation of Micropatterned Films

Micropatterned (MP) silicon (Si) templates (angle of inclined walls: 54.7^o (A4) or perpendicular walls: 90° (B1)) were produced by photolithography and subsequent chemical wet etching and reactive ion etching techniques to produce V-shaped and square grooves, respectively (kindly provided by Prof. A. Aydınlı and A. Kocabaş, Bilkent University, Ankara).

The pattern on the wafer was designed by Wavemaker Mask Drawing Editor. The obtained GDS II electronic file was transferred to mask producer and then the mask was produced on chrome coated quartz plates. As a wafer platform, generally single crystal pieces were used and in case gallium arsenide pieces were used. Thin films of SiNx and SiOx were deposited on the wafers by Plasma Enhanced Chemical Vapor Deposition (PECVD) technique. Following chemical cleaning, UV sensitive photo-resist films were coated on the wafers. The pattern on the mask was transferred onto the photoresist film on the wafers upon exposure to UV. The Si wafers with its photoresist film were placed in KOH solution and the bare Si parts were etched by chemical wet etching technique down to the desired depth. Lastly the remaining photoresist film was removed by acetone and the template having V-shaped grooves (A4) were ready to use. The Si wafers with square grooves (B1) were obtained by reactive ion ething instead of the KOH etching.

In order to investigate the effect of topography of polymeric films on the cell behavior, templates with different wall angles and ridge widths were used. The representative cross-section of the templates is shown in Figure 2.1 and the dimensions of the produced templates are given in Table 2.1. The original design was in the dimensions of ridge width: 2 and 10 µm, groove width: 2 and 10 µm, and groove depth: 30 and 5 µm for A4 and B1, respectively, but experimentally could not be exactly matched.

36
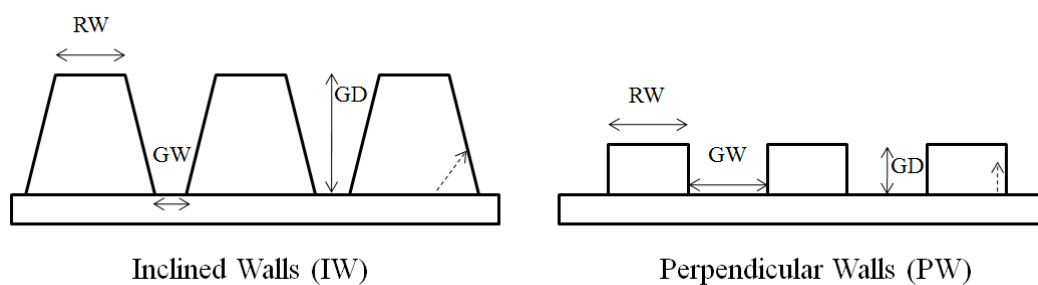
RW: Ridge Width, GW: Groove Width, GD: Groove Depth

Figure 2.1. The representative cross-section view of the templates

Table 2.1. The dimensions of the patterns on the wafers

Walls	Code	Wall Angle (^{0})	Ridge Width (µm)	Groove Width (µm)	Groove Depth (µm)
IW	A4	54.7^0	2	1	30
PW	B1	90.0^0	5	14	5

Besides these Si templates, negative polydimethyl siloxane (PDMS) replica of the B1 pattern was used to obtain patterned polymeric films. PDMS replica was prepared by pouring the PDMS prepolymer-catalyst mixture on the Si template and following polymerization at 70°C. The PDMS replica was removed from the Si template.

The patterns on the Si templates and PDMS replica were transferred to biodegradable polymeric films by solvent casting (Figure 2.2). The blend of PHBV5, P(L-D,L)LA and PLGA (2:2:1, w/w) was prepared in chloroform with a concentration of 5% (w/v). The solution of PHBV5-P(L-D,L)LA (4%, w/v; 1:1,

37

w/w) was prepared by mixing the equal amounts of PHBV5 and P(L-D,L)LA, which were dissolved separately. Subsequently PLGA (1%, w/v) and PEG (polyethylene glycol) (10%, w/v) were added into polymer solution and mixed. Polymer solutions were poured on MP Si templates and on PDMS replica. Following air drying or solvent evaporation, the films were peeled off the surfaces. In order to obtain the porous micropatterned film, the PEG in the film was extracted by washing the films in distilled water.

In the preliminary studies, the blend of PHBV and P(L-D,L)LA (1:1, w/w) was prepared in dichloromethane or chloroform with a concentration of 4% (w/v) in the absence of PLGA and PEG in order to study the effect of polymer type on neural and mesenchymal stem cell behavior.
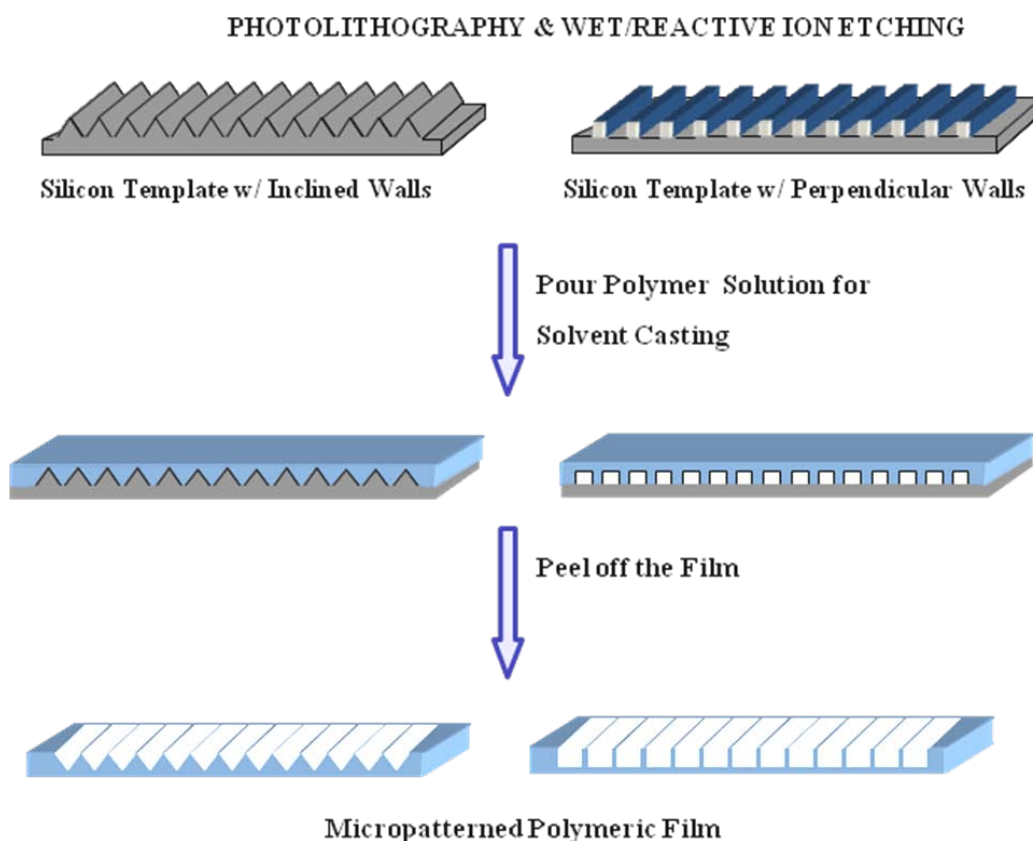
Figure 2.2. Schematic presentation of the preparation of micropatterned polymeric films by solvent casting,

2.2.1.2.   Preparation of Electrospun Fibrous Mats

Microfibers were obtained by electrospinning. The experience on electrospinning was obtained at Prof. C. Migliaresi's laboratory at Trento University (Italy) using various polymers. Then the system was set up in our laboratory at METU. The electrospinning system was consisted of a high voltage supply (Gamma High Voltage Research, USA), a 10 mL syringe capped with a 30 Ga needle, syringe pump (New Era Pump Systems, USA) and a metal, grounded collector (Figure 2.3). In order to obtain aligned fibers the collector used had two metal rods and the fibers were collected between them to form a parallel aligned fibrous mat. Polymer solution of PHBV5-PLGA (50:50) in chloroform:DMF was placed into a syringe mounted on a syringe pump.The positive electrode was connected to the metallic needle of the syringe. When the potential was applied the repulsive electrostatic forces overcame the surface tension of the solution, and thus Taylor cone shaped polymer solution at the needle tip was ejected in the form of a microfiber while the solvent evaporated. In order to obtain reproducible and defect-free fibers with certain diameters a number of parameters need to be adjusted and optimized. During the optimization process, concentrations of polymer solution (5%, 10% and 15%, w/v), the distance between the two poles (15-25 cm), the flow rate of the syringe pump to deliver the polymer solution (10-30 µL/min) and the applied potential (15-25 kV) were varied.

In order to study PLGA and PHBV5 mixing and their distribution in mat, a solvent that dissolves one of the components of the blend but not the other were chosen. The resultant fiber mat was treated with acetone for 2 h to dissolve out one component (PLGA) leaving behind the other (PHBV).
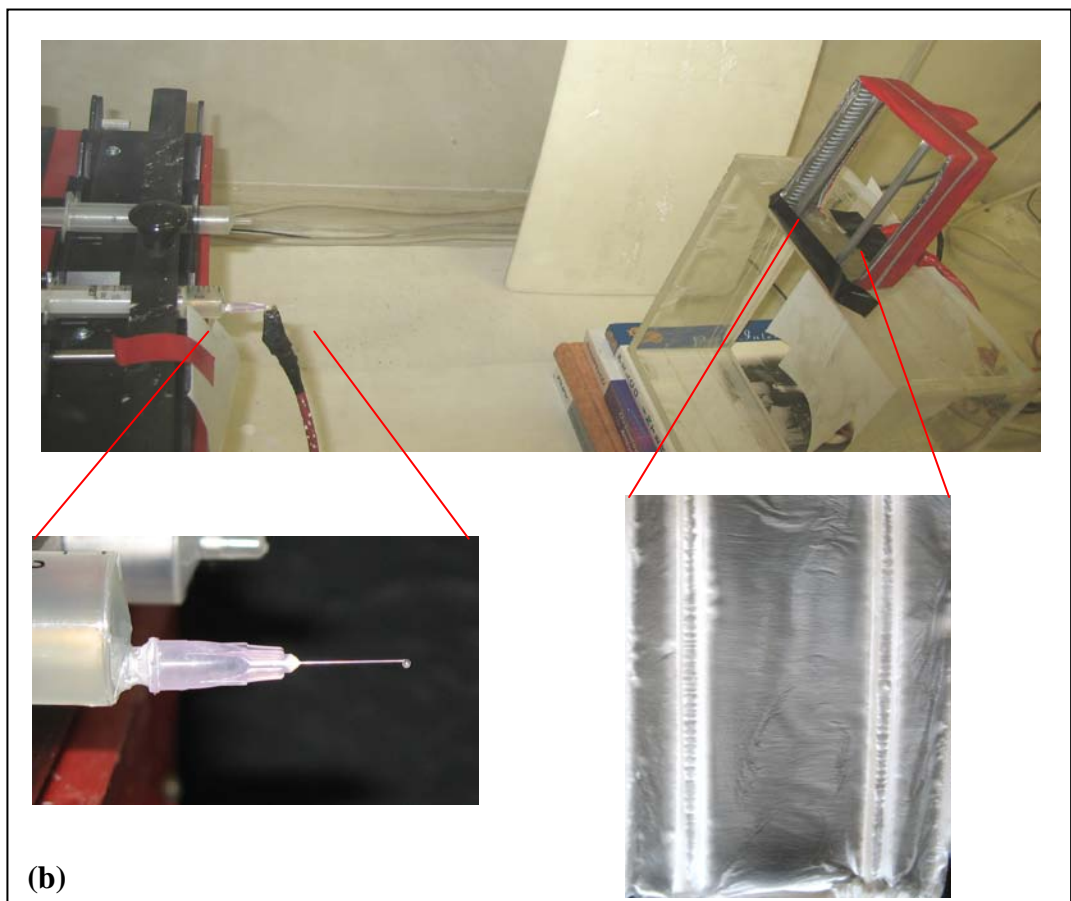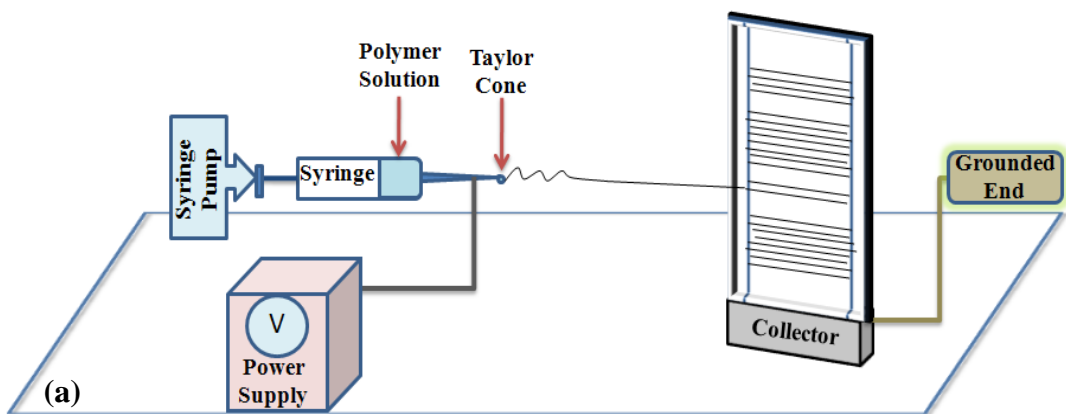
Figure 2.3. Electrospinning system. a) the schematic presentation of the system, and b) the photos from the original system

2.2.1.3. Characterization of Polymeric Scaffolds

2.2.1.3.1. Scanning Electron Microscopy

Surfaces of the micropatterned polymeric films and the electrospun fibrous mats were all coated with Ag-Pd under vacuum. Scanning electron microscopy (SEM) was carried out by a QUANTA 400F Field Emission SEM at METU Central Lab and at Bilkent University UNAM, and by a Carl Zeiss EVO 40 SEM at Yeditepe University (Istanbul) to observe the surface characteristics and to determine micropattern dimensions of the polymeric films and fiber diameter of the electrospun mats.

2.2.1.3.2. Measurement of Porosity of the Polymeric Films

The porous PHBV-P(L-D,L)LA-PLGA films obtained after leaching out the PEG was stained with Nile Red, and then was examined using the confocal microscopy (Leica-DM 2500, Germany) and the images of three different regions of two separate micropatterned films was taken from layers (1 µm) in z-direction. The porosity of the micropatterned films was assessed using NIH Scion Image program.

2.2.1.3.3. Mechanical Analysis of the Polymeric Films

Mechanical properties of polymeric films were studied in a wet state at room temperature by Lloyd LRX 5K Mechanical Tester, controlled by a computer running program (WindapR). Polymeric films, PHBV-P(L-D,L)LA, PHBV-P(L-D,L)LA-PLGA, porous PHBV-P(L-D,L)LA-PLGA (thickness 0.028 ± 0.006 mm, 0.072 ± 0.007 mm, 0.113 ± 0.012 mm, respectively) were 10.0 mm in width and 40.0 mm in length, were attached to the holders (gauge length: 10 mm) of the instrument. The samples were tested under a 10 mm/min test speed. The load deformation curve was obtained for each sample. Using an equation $\rho = F/A$, where ρ is the tensile strength (MPa), F is the maximum load applied (N) before rapture, and A is the initial area (m^2) of the sample, the tensile strength was calculated. The

load deformation curve was converted to stress–strain curve, where stress is the load applied per unit area (F/A) and strain is the deformation per unit length. The Young's modulus of the sample was determined from the slope of straight line (elastic region of the stress-strain curve).

2.2.1.3.4. Erosion of Micropatterned Films and Electrospun Mats

For study the erosion, PHBV5-P(L-D,L)LA, PHBV5-P(L-D,L)LA-PLGA films (porous and nonporous) and PHBV5-PLGA mats (1 x 3 cm^2) were dried completely and then weighed. The samples were placed into 50 mL Corning flasks containing phosphate buffer (PBS, 30 mL, pH 7.4, 10 mM) and incubated at 37^{0}C for 90 days by continuous shaking at 50 rpm. Samples were removed from the medium every 10 days, dried completely under vacuum at room temperature for 2-3 days, weighed and then placed again into the same medium to continue the erosion study.

2.2.2. *In Vitro* Studies

2.2.2.1. *In Vitro* Studies of Human MSCs

The characterization and comparison of human MSCs derived from bone marrow and Wharton's Jelly were carried out at Mass. General Hospital (MGH), Harvard Medical School, Shriners Burn Hospital for Children and Tufts University all in Boston (USA). The rest of the studies with isolated Wharton's Jelly human MSCs were carried out at METU. The characterization studies of MSCs were carried out jointly with Halime Kenar.

2.2.2.1.1. Isolation and Culture of Human MSCs

Human bone marrow MSCs (BM MSCs) were obtained from bone marrow aspirates (Clonetics-Poietics, Walkersville, USA) as described by Chen et al. (2003). Whole bone marrow aspirates were plated on tissue culture polystyrene

(TCPS) flasks and cultivated until confluency in an expansion medium consisting of Dulbecco's Modified Eagle Medium (DMEM) supplemented with 10% fetal calf serum (FCS), 100 U/mL penicillin - 100 μg/mL streptomycin (Pen/Strep), 0.1 mM nonessential amino acids, and 1 ng/mL of basic fibroblast growth factor (bFGF). After 5 days culture in a 5% CO_2 incubator at 37^0C, the medium was replaced to remove the non-adherent hematopoietic cells, and the medium was changed twice per week thereafter. Human BM MSCs were kindly provided from Prof. Dr. David Kaplan's laboratory, TERC, Tufts University, Boston (USA). Human Wharton's Jelly MSCs (WJ MSCs) obtained from umbilical cord matrix (UCM) were kindly provided by Dr. Hans Klingemann, Tufts New England Medical Center, Boston (USA). Both BM and WJ MSCs were provided at passage 1 and then cultured in the expansion medium described above. Human BM and WJ MSCs at passage 2, 3 and 4 were used for the characterization studies to investigate surface antigen and gene expression by flow cytometry and RT-PCR analysis, respectively (Boston, USA). The rest of the studies with human MSCs (hMSCs) isolated from Wharton's Jelly were carried out at METU.

Wharton's Jelly MSCs were isolated from umbilical cord matrix according to the protocol adapted from that in Ludwig Boltzman Institute, Linz (Austria). The umbilical cords from two different donors (28 and 32 years old mothers, with their consent (Appendix A)) were supplied in PBS (containing Pen/Strep (100 units/mL-100 mg/mL)), and were stored at 4^0C. The cells had to be isolated within 24 h of the delivery of the baby. The umbilical cord tissue was cut into 2-3 cm pieces and transferred into Pen/Strep containing PBS to wash out blood. One piece at a time was transferred to a large sterile petri plate and the arteries and the vein were pulled out with a tweezer (Figure 2.4). UCM was cut into smaller pieces and transferred into a well of a 6-well plate. Then the complex expansion medium (1 mL) was added on each piece and tissue pieces in plates were put into a humidified 5% CO_2 incubator at 37^0C. Four different complex expansion media (#1: DMEM supplemented with 20% FCS, 100 units/mL-100 mg/mL of Pen/Strep, 1 ng/mL of bFGF, and 0.1 mM nonessential amino acids; #2: DMEM low glucose:HAMF12 (1:1) with 10% FCS, 100 units/mL-100 mg/mL of Pen/Strep, 1 ng/mL of bFGF; #3: RPMI with 10% FCS, 100 units/mL-100 mg/mL of Pen/Strep;

#4: α-MEM: HAMF12 (1:1) with 2% FCS, 100 units/mL-100 mg/mL of Pen/Strep) were used. After 2 days, the medium was changed. The medium was refreshed 3 times a week. After 2 weeks, the tissue was removed from the well and put into a new well for further isolation of MSCs. For further culturing the isolated cells that formed a confluent monolayer on 6 well plates were detached with 0.1% Trypsin-EDTA, passaged and frozen in 10% DMSO. These cells were used in characterization and differentiation studies, and also in the studies of cell culture on the scaffolds.
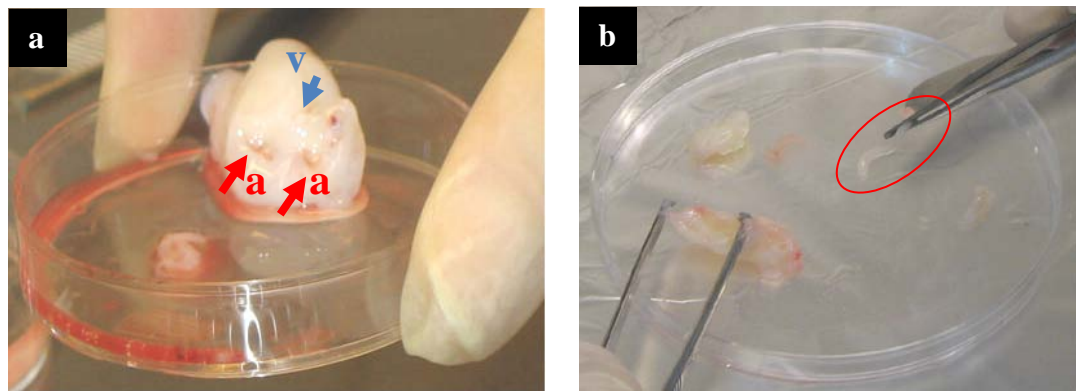
Figure 2.4. Isolation of human MSCs from umbilical cord matrix. Two arteries (labeled as a) and one vein (labeled as v) shown in (a) were pulled out with tweezers (b).

2.2.2.1.2. Characterization and Comparison of Bone Marrow and Wharton's Jelly-derived MSCs

2.2.2.1.2.1. Flow Cytometric Analysis

Specific surface antigens of BM and WJ MSCs at passage 2, 3 and 4 were analyzed by flow cytometry (FACSCalibur, Becton Dickinson, USA). Cell surface markers included hematopoietic lineage markers (CD34, CD45), adhesion

integrins (CD49d, CD106), and MSC markers like SH2 (CD105), SH3 (CD73), CD44 and CD90, CD29, immunogenic antigens (HLA-ABC (MHC class I), HLA-DR (MHC class II)), and early endothelial progenitor cell marker CD133. To stain the MSCs, the cells were detached via trypsinization, pelleted (ca. 10^5 cells), and resuspended in 1% bovine serum albumin (BSA) in PBS before addition of fluorochrome conjugated monoclonal antibodies. After incubation for 45 minutes at 4^0C with fluorochrome conjugated monoclonal antibodies, the cells were centrifuged, fixed with 1% paraformaldehyde (PFA) in PBS, and analyzed on a FACSCalibur flow cytometer (BD Biosciences), using CellQuest software (BD Pharmingen). An isotype control was included in each experiment; specific staining was measured from the cross point of the isotype graph with the particular antibody graph, and positive cells were counted.

2.2.2.1.2.2.   Morphology of Human MSCs

To investigate the morphology and cytoskeletal organization of cells MSCs derived from both sources were stained with Phalloidin for actin filaments and with Hoechst 33342 for their nuclei, and examined via fluorescence microscopy for morphological analysis.

The cells were fixed with 4% PFA for 15 min at room temperature and then washed two times with PBS (10 mM, pH 7.4). The cells were permeabilized by incubation in 0.1% Triton X-100 (in PBS) for 5 min at room temperature. Following the wash with PBS, the cells were incubated in 1% BSA, a blocking solution, for 30 min at 37^0C to prevent nonspecific binding. After incubation, the cells were incubated in Alexa Fluor 546 labeled Phalloidin (1:40 in 0.1% BSA) for 1 h at 37^0C. After washing with PBS, the cells were stained with Hoechst 33342 for 5 min. The cells were washed and then examined under fluorescence microscope.

2.2.2.1.2.3.   Osteogenic Differentiation of Human MSCs

In order to differentiate hMSCs into osteoblasts, MSCs from both sources at P2 were seeded at $5x10^3$ cells/well into 24 well plates in the expansion

medium. After 1 day of incubation, the MSCs were cultured in expansion medium DMEM containing 10% FCS, Pen/Strep (100 units/mL-100 mg/mL), 0.1 mM nonessential amino acids (without bFGF) supplemented with 10 nM dexamethasone, 50 µg/mL ascorbic acid, and 10 mM β-glycerophosphate for 21 days in CO_2 incubator at 37^oC, and the medium was changed twice a week. The control samples were cultured under the same conditions in the absence of osteogenic supplements. After 21 days of culture, differentiation into osteoblasts was assessed based on alkaline phosphatase (ALP) activity by UV spectroscopy.

The cells on each well of 24 well plate were lysed with 0.2% (v/v) Triton X-100 (in 10 mM, pH7.5 Tris-HCl buffer) and the samples were centrifuged at 12 000 rpm for 10 min at 4^0C. The lysate, present in the supernatant part, was combined with 2% (v/v) Triton X-100, and then incubated with the 2-amino-2-methyl-1propanol (AMP) buffer and the substrate p-nitrophenyl phosphate at 37^oC for 1 h to carry out the reaction given in Equation 2.1. The reaction was stopped with 0.2 M NaOH and then the concentration of p-nitrophenol, the yellow product of ALP activity, was measured spectrophotometrically at 405 nm. The activity was expressed as µmol of substrate converted to product/min/ 250 µL of cell lysate (taken from a single well of 24 well plate), considering the calibration curve for the enzymatic product (Appendix B.1a). The solution of 0.2% (v/v) Triton X-100 in the absence of lysate (in the absence of ALP) was used as a blank.

<div align="center">

ALP

P-Nitrophenyl Phosphate $\longrightarrow$ **P-Nitrophenol + Phosphate**

Substrate   Yellow Product   **(2.1)**

</div>
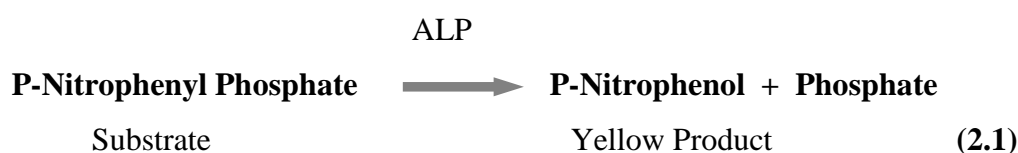
2.2.2.1.2.4. Adipogenic Differentiation of Human MSCs

Human MSCs at P2 were plated at 5×10^3 cells/well in 24 well plates, and cultured in expansion medium for 1 day. To induce adipogenic differentiation,

the MSCs were grown for 21 days in the expansion medium DMEM containing 10% FCS, Pen/Strep (100 units/mL-100 mg/mL), 0.1 mM nonessential amino acids (without bFGF) supplemented with adipogenic stimulants: 0.5 mM 3-isobutyl-1-methylxanthine (IBMX), 1 µM dexamethasone, 5 µg/mL insulin, and 50 µM indomethacin (Mauney et al., 2005). MSC control cultures were maintained similarly in parallel in the absence of adipogenic stimulants. All MSC cultures were maintained in CO_2 incubator at 37^oC and medium was changed twice a week.

To detect fat deposition, cells were fixed and stained for 45 min with a filtered 60% Oil Red-O solution in PBS, prepared from a stock solution of 0.07 g Oil Red-O powder in 20 ml of isopropanol (Stewart et al., 2004). The background due to Oil Red-O staining was removed by washing with PBS and the photomicrographs of cells were obtained under a light microscope.

2.2.2.1.2.5.   Neural Gene Expression of Undifferentiated MSCs

Total RNA was isolated from human MSCs (BM and WJ at P2, P3 and P4) using NucleoSpin RNA II kit and stored at -80°C. The cDNA was synthesized, and then amplified with PCR using OneStep RT-PCR kit (Qiagen One step RT-PCR kit). The cDNA obtained from human brain extract was used as a control. PCR was performed in a 20 μL reaction solution composed of 5x Qiagen OneStep RT-PCR buffer, dNTP mix, OneStep RT-PCR Enzyme Mix, RNase inhibitor, forward and reverse primers (0.4 μM), and variable volume of template RNA and RNase free water. The RT-PCR conditions were as follows: 30 min at 50°C for reverse transcription, and then for PCR, 15 min at 95°C followed by 30 cycles of 94°C for 30 s, Tm for 30 s, and 72°C for 1 min, and final extension for 10 min at 72°C. Primer sequences (forward, reverse) and lengths of the amplified products are given in Table 2.2. The expression of neural specific genes is expressed relative to the housekeeping gene β-Actin. The PCR products were size fractionated by 2% agarose gel eletrophoresis, stained with ethidium bromide, and visualized by UV illuminator.

47

Table 2.2. The primer sequences and the PCR product (amplicon) sizes in base pairs (bp)

Gene	Primer Sequence (Forward–Reverse)	Product Size (bp)
Housekeeping gene β-Actin	5'-AACGGTGAAGGTGACAGCA-3' 5'-TGTGTGGGACTTGGGAGAGG-3'	202
Nestin	5'-TTGCCTGCTACCCTTGAGA-3' 5'-CTGTTTCCTCCCACCCTGT-3'	192
Neurogenic differentiation 1 (NeuroD1)	5'-TTCTCAGGACGAGGAGCAC-3' 5'-CGGGCGTTAGCCTTCAT-3'	243
Hairy and enhancer of split 1 (HES1)	5'-TGCTTTCCTCATTCCCAAC-3' 5'-TCTCCCAGTATTCAAGTTCCTG-3'	243
Microtubule-associated protein2 (MAP2)	5'-CCTCCAGCACAAGAAGCAG-3' 5'-GGCAAGACACATCGGCAAAT-3'	238
Glial fibrillary acidic protein (GFAP)	5'-TCAACTCACCGCCAACAG-3' 5'-CCAGCGACTCAATCTTCCTC-3'	197
Neuron-specific enolase 2 (Enolase2)	5'-GCTGCTCCTTGGCTTACCT-3' 5'-TGACGCTCCCATCACAGA-3'	192
Retinoic acid receptor type-α (RARA)	5'-TTCACCACCCTCACCATC-3' 5'-TCTCCGCATCATCCATCT-3'	232
Nuclear receptor related-1 (Nurr-1)	5'-AGTATGGGTCCTGCCTCA-3' 5'-CGTCGTAGCCTGTGCTGTAG-3'	198
Neurogenin1 (ngn1)	5'-AGTCAGCAGGCAATAGATGG-3' 5'-AGCCAGTCACAAGGAGGTT-3'	245
Paired box gene 6 (Pax6)	5'-ATTCCACAACCCACCACA-3' 5'-CATAACTCCGCCCATTCA-3'	214

2.2.2.1.3. Characterization of Isolated Wharton's Jelly MSCs

2.2.2.1.3.1. Evaluation of Cell Morphology

Isolated human MSCs cultured on TCPS were examined under inverted phase contrast microscope (Olympus IX 70, Japan) and recorded with camera after the isolation and several passages.

To investigate the morphology and cytoskeletal organization of cells the isolated MSCs derived from both sources were stained with Phalloidin-DAPI. The cells were fixed with 4% PFA for 15 min, and then after permeabilization with 0.1% Triton X-100 (in PBS), non-specific binding was blocked by 1% BSA for 30 min at 37^0C as in section 2.2.2.1.2.2. WJ MSCs were stained with FITC-conjugated Phalloidin (1:100 in 0.1% BSA) for actin filaments, and following staining their nucleus with DAPI (1:5000 in PBS) for 10 min the cells were examined via fluorescence microscopy (Olympus IX 70, Japan, with inverted reflected light fluorescence observation attachment).

2.2.2.1.3.2. Growth Kinetics of Isolated WJ MSCs

Isolated WJ MSCs cultured in growth medium #2 and #4 (at passage 2 and 1, respectively) were seeded into 24 well plate at a density of 10^4 cells/well. The cells were cultured at 37^0C in a CO_2 incubator. The cell number of samples in triplicate was determined by Cell Titer 96* AQueous One Solution Cell Proliferation Assay (MTS Assay) at the end of 24, 48, 72, 96, 144, 192 and 240 h incubation periods.

The principle of MTS assay is based on the conversion of MTS/PES solution (convenient solution combines PES, a chemically stable electron coupling reagent, and MTS, a novel tetrazolium compound) into a water-soluble formazan that absorbs light at 490 nm. For this, the growth medium of cells in the 24 well plate was discarded, and MTS/PES working solution (0.5 or 1 mL, 10% MTS/PES solution in the expansion medium prepared with low glucose DMEM) was placed on cells. The cells were incubated for 2 h at 37^oC in the CO_2 incubator. A solution

of 200 µL was transferred into a 96 well plate and absorbance of the product produced by MTS assay was determined at 490 nm with Elisa Plate Reader (Model Maxline, Molecular Devices, (USA)). The obtained absorbance was correlated with the cell number using a calibration curve constructed with known cell numbers (Appendix C).

2.2.2.1.3.3.   Osteogenic Differentiation of Isolated WJ MSCs

Isolated WJ MSCs at P3 were seeded at 10^4 cells/well into 24 well plates and cultured in the expansion medium #2 and #4. When the cells reached confluency, osteogenic induction was applied like in section 2.2.2.1.2.3. for 14 days in CO_2 incubator at 37^oC.

At the end of incubation differentiation to osteoblasts was assessed via ALP activity. The cells on each well of 24 well plate were lysed with 0.2% (v/v) Triton X-100 (in 10 mM pH7.5 Tris HCl buffer), and sonicated for 5 min at 25 Watts on ice. The samples were centrifuged at 2000 rpm for 10 min at 4^0C, and the rest of the protocol was applied like in section 2.2.2.1.2.3 using ALP activity kit (Randox). The activity was expressed as nmol of substrate converted to product/min/300 µL of cell lysate (taken from a single well of 24 well plate), considering the calibration curve for the enzymatic product (Appendix B.1b). In order to prove the osteogenic differentiation von Kossa staining was carried out to show calcium deposition upon differentiation. After fixation with 4% PFA, the cells were rinsed with distilled water to carry out von Kossa staining. The cells were exposed to ultraviolet radiation (UV C) in 1% aqueous silver nitrate for 20 min and then washed with distilled water. After UV exposure, the stained cells were incubated in 5% sodium thiosulfate for 5 min to remove unreacted silver, and following washing cells were examined under a light microscope (Olympus IX 70, Japan).

2.2.2.1.3.4. Chondrogenic Differentiation of Isolated WJ MSCs

Isolated WJ MSCs at P3 were seeded at 10^4 cells/well into 24 well plates in expansion medium #4 until confluency. In order to induce chondrogenic differentiation MSCs were grown for 14 days in medium DMEM supplemented with Pen/Strep (100 units/mL-100 mg/mL), 1% nonessential aminoacids, 50 µg/mL ascorbic acid, 10 nM dexamethasone, 5 µg/mL bovine insulin and 5 ng/mL TGFβ1. Similarly MSC control cultures were maintained in parallel without chondrogenic supplements. All MSC cultures were maintained in CO_2 incubator at 37^oC and medium was changed twice a week.

Chondrogenic differentiation was determined by Alcian blue staining of the proteoglycans and by detection of type II collagen and aggrecan, typically found in articular cartilage. Differentiated cells were fixed in 4% PFA after 14 days of culture and stained with 1% (w/v) Alcian Blue (pH 2.5, in 3% acetic acid) solution for 30 minutes. Following washing with distilled water, the photomicrographs of cells were obtained under a light microscope. For immunostaining, the cells, fixed after 14 days of culture, were permeabilized with 0.1% Triton X-100 (in PBS) for 5 min, and following PBS wash the cells were incubated in 1% BSA blocking solution for 30 min at 37^0C. The cells were incubated in primary antibodies, anti-Collagen Type II or anti-aggrecan (1:100 in 0.1% BSA) for 1 h at 37^0C, and then after washing they were kept in Alexa Fluor 488 labeled secondary antibody solution (1:100 in PBS) for 1 h at 37^0C. Following nuclei staining with DAPI (1:5000 in PBS) for 10 min, the cells were examined via fluorescence microscopy (Olympus IX 70, Japan, with inverted reflected light fluorescence observation attachment).

2.2.2.1.3.5. Neural Gene Expression of Undifferentiated Isolated WJ MSCs

Neural gene expression analysis of WJ MSCs (at P2, P3, and P4) isolated from UCM were done by total RNA isolation protocol as mentioned in section 2.2.2.1.2.5. Neuroblastoma cells were used as the control to optimize primers. RT-PCR was performed using Robust OneStep RT-PCR kit in a 20 µL

reaction solution composed of 10x Robust reaction buffer, $MgCl_2$, dNTP mix, M-MulVRT RNaseH, DyNAzyme Ext Polymerase, RNase inhibitor, forward and reverse primers (0.4 μM), and variable volume of template RNA and RNase free water. The RT-PCR conditions were as follows: 45 min at 48°C for reverse transcription, and then for PCR 2 min at 94°C followed by 30 cycles of 94°C for 30 s, Tm (55^0C) for 30 s, and 72°C for 1 min, and final extension for 10 min at 72°C. Primer sequences (forward, reverse) and lengths of the amplified products are given in Table 2.2. The expressions of neural specific genes were analyzed relative to the housekeeping gene β-Actin after gel electrophoresis (2% agarose containing ethidium bromide).

2.2.2.1.4. Differentiation of Human MSCs into Neural Cell Lineages

Human WJ MSCs, at approximately 90% confluence, were trypsinized and then seeded on laminin1 coated or untreated TCPS 24 well plates in preinduction medium (growth medium with or without FCS supplemented with 10 ng/mL EGF, 10 ng/mL bFGF and 50 μM forskolin). The valproic acid (VA, 2 mM) was added to some set of samples to check their effect on the differentiation of human MSCs. After 24 hours of incubation in the preinduction medium, the medium was refreshed with differentiation medium containing different combinations of the following growth factors and chemicals: B27 supplement, valproic acid, retinoic acid (RA), Insulin-like Growth Factor 1 (IGF1), ciliary neurotrophic factor (CTNF), Interleukinβ1 (ILβ1), Interleukin6 (IL6), Nerve Growth Factor (NGF), 5-azacytidine, β-mercaptoethanol (βME), dimethyl sulfoxide (DMSO). After 3 to 4 days, media was refreshed. After 7 or 14 days of differentiation treatment, cells were studied by light microscopy and some samples of cells were stained with FITC labeled Phalloidin and DAPI for cell morphology analysis. Moreover, the samples were analyzed in detail for differentiation by RT-PCR and immunocytochemistry.

2.2.2.1.4.1. Protein Expression Analysis of MSCs by Immunocytochemistry Upon Neural Induction

Immunocytochemistry was carried out using standard protocols. Human MSCs were fixed with 4% PFA for 15 min at room temperature and then washed with PBS. The cells were incubated in 100 mM glycine for 15 min to saturate reactive PFA groups. After washing with PBS, the cells were permeabilized by Triton X-100 (0.1% in PBS, PBST) treatment for 5-10 min. Following excessive washing, the cells were incubated in blocking solution (1% BSA in PBS) at 37^0C for 30 min to prevent nonspecific binding of antibodies. MSCs were incubated with primary antibodies at 4^0C overnight or 37^0C for 1 h. Primary antibodies and dilutions for human WJ MSCS were as follows: anti-β-Tubulin III (1:200 in 0.1% BSA), and anti-GFAP (1:200 in 0.1% BSA). Both were monoclonal. Following incubation of primary antibodies, the cells were washed with PBS and then the fluorescence labeled secondary antibodies Alexa Fluor 488 or Alexa Fluor 532 (1:100 in PBS) was applied for 1 h at 37^0C, and then washed with PBST, and subsequently with PBS. The cells were counterstained with DAPI (1:1000 in PBS) for 10 min, and following washing with PBS the cells were examined with fluorescence microscope (Olympus IX 70, Japan, with inverted reflected light fluorescence observation attachment).

2.2.2.1.4.2. Gene Expression of MSCs Analyzed by RT–PCR upon Neural Induction

MSCs induced by neural treatment were lysed and their RNA was isolated according to the protocol explained in section 2.2.2.1.2.5. Specific neural markers were chosen to check differentiation of MSCs into neural cells. RT-PCR analysis was carried out according to section 2.2.2.1.3.5. which was applied for isolated WJ MSCs.

2.2.2.2.   *In Vitro* Studies of Mouse NSCs

2.2.2.2.1.   Culture and Differentiation of NSCs

Balb C mouse neural stem cells (NSCs) (CRL-9392; obtained from ATCC) were cultured in a growth medium that contains Dulbecco's Modified Eagle Medium:Ham's Nutrient Mixture F12 (DMEM/F12; 1:1), human transferrin (0.01 mg/mL), bovine insulin (0.01 mg/mL), chemically defined lipids (1% v/v), sodium selenite (10 nM), Pen/Strep (100 units/mL/100 mg/mL) and supplemented with mouse EGF (50 ng/mL). The cells were cultured on fibronectin (5 µg/cm^2) coated TCPS flasks at 37°C in a humidified 5% CO_2 incubator, and the growth medium was replaced every two days. When NSCs reached 80% confluency, the cells were detached by incubation in 0.05% Trypsin-EDTA solution for 30 s. To inactivate trypsin, same volume of trypsin inhibitor (0.1% in PBS) and the growth medium, of which volume was at least five times more than Trypsin-EDTA volume, were added. The cells were pelleted by centrifugation for 5 min at 3000 rpm, and then the pellet was resuspended to be transferred to a new flask or to be seeded on the scaffolds.

NSCs were differentiated into neuron upon removal of mouse EGF from the growth medium and the addition of 10% FCS to this EGF-free medium leads to differentiation of NSCs into astrocytes.

2.2.2.2.2.   Evaluation of NSCs Differentiation by Microscopy

The change in morphology of NSCs upon neural induction was examined by light microscope. Specific neural protein expression was analyzed by standard immunocytochemistry protocol (Section 2.2.2.1.4.1.). NSCs in an undifferentiated form and after differentiation into neuron and astrocytes were stained with primary antibodies monoclonal anti-β-Tubulin III and monoclonal anti-GFAP, and followed by staining with secondary antibodies Alexa Fluor 488 or Alexa Fluor 532 (1:100 in PBS), respectively. After DAPI counterstaining, the cells were examined with fluorescence microscope.

2.2.2.3. Behavior of Stem Cells on Electrospun Fibrous Mats and Micropatterned Films

2.2.2.3.1. Seeding of Stem Cells on Scaffolds

The scaffold components, the electrospun fibrous mats and the porous micropatterned films, were sterilized with 70% ethanol for 2 h at 4^0C, and then after washing with PBS scaffolds were dried. For protein coating the scaffolds were covered with fibronectin (5 µg/cm^2) or laminin1 (1 µg/cm^2) for NSCs and MSCs, respectively. After drying the scaffolds were ready to be seeded with cells.

Mouse NSCs were detached from the flask and counted by Trypan Blue staining or Nucleocounter (Chemometec Biolab, Denmark). NSCs were seeded onto fibronectin adsorbed micropatterned films and electrospun mats at a density $5x10^3$ or $2x 10^4$ cells / sample (1x1 cm^2). The cells on electrospun mats were cultured with the growth medium contains EGF without differentiation, while the cells on micropatterned films were cultured with growth medium for 2-4 days and then cultured with astrocyte induction EGF-free medium in the presence of 10% FCS.

Isolated WJ MSCs were counted like NSCs and seeded onto laminin1 coated micropatterned films and electrospun mats at a density $5x10^3$ or $2 x10^4$ cells/ sample (1x1 cm^2), and then the cells were cultured in the appropriate growth medium in a humidified CO_2 incubator.

2.2.2.3.2. Proliferation and Cell Activity of Stem Cells on Scaffolds

Cell activity and proliferation of NSCs and isolated WJ MSCs on the electrospun mats and the micropatterned films were determined by Cell Titer 96* AQueous One Solution Cell Proliferation Assay (MTS Assay).

MTS assay was carried out after a day of cell seeding to determine the initial number of attached alive cells and after 7 and 14 days of culture to investigate cell proliferation on the polymeric scaffolds and TCPS, a positive control. At the end of 1, 7 and 14 days, the scaffolds were transferred into clean wells and the cell number on each sample was determined in triplicate with MTS

assay. MTS/PES working solution (0.5 or 1 mL, 10% MTS/PES solution in the expansion medium prepared with low glucose DMEM) was added on films and the control TCPS wells, and then incubated for 2 h at $37^{o}C$ in the CO_2 incubator (mentioned in section 2.2.2.1.3.2.). The absorbance of the product of the MTS assay was quantified at 490nm with Elisa Plate Reader (Model Maxline, Molecular Devices, (USA)), and then the cell number was determined using a calibration curve constructed for each type of cells with known cell numbers (Appendix C).

2.2.2.3.3. Cellular Organization and Alignment on Scaffolds

NSCs and isolated WJ MSCs organization and their alignment on the electrospun mats and the micropatterned films were investigated by fluoresence and confocal microscopy at the end of 2-4 days of culture.

For fluorescence and confocal microscopy examination stem cells were fixed with 4% PFA for 15 min. The cells were stained with FITC conjugated Phalloidin -DAPI (Section 2.2.2.1.3.1.) to investigate cytoskeleton organization of cells on scaffolds and then examined under fluorescence microscope using a 488 nm filter and a UV filter (330-385 nm). For cell organization on the micropatterned surfaces and on/in the fibrous mats the cells were stained with Acridine Orange to be examined with confocal microscope with 488 nm laser excitation. Stem cells were permeabilized with 0.1 M HCl for 45 s, and then stained with Acridine Orange for 15 min at room temperature followed by excessive washing with distilled water.

2.2.2.4. Formation of Tubular Construct and Stem Cells Behaviour in 3D Scaffold

Stem cells were seeded onto the components of the final construct separately. After culturing cells on these scaffolds for a week, the micropatterned film was rolled over electrospun mat. The final 3D construct was restrained in tubular form with elastic bands or fixed by suturing (3-4 mm in diameter, ca. 30 mm in length) (Figure 2.5).

Mouse NSCs were seeded onto fibronectin adsorbed sterilized scaffold components at a density $6x10^4$ - 10^5 cells/ sample (1x3 cm^2), while human MSCs were seeded on laminin1 coated surfaces at $7x10^4 – 10^5$ cells/ sample (1x3 cm^2). NSCs were grown on electrospun mats with the expansion medium; however, NSCs were differentiated into astrocytes on the porous micropatterned films with EGF free medium in the presence of 10% FCS following expansion of NSCs in undifferentiated form for 2-4 days. On the other hand, isolated WJ MSCs seeded at P4 on the electrospun mats were differentiated into neuron cells (determined according to differentiation studies results given in section 3.2.1.3), while MSCs seeded at P3 on the porous micropatterned films were cultured with the expansion medium to maintain them in undifferentiated state. Stem cells on 3D construct were cultured in an appropriate medium in the presence of supporting cells (mouse astrocytes or human MSCs) on micropatterened films to facilitate, maintain and/or enhance differentiation of stem cells on the fibers.

The components of the final construct were separated, and then the cell viability on the electrospun fiber and micropatterned film parts was determined separately by MTS assay (Section 2.2.2.3.2). The cell organization and alignment tendency of cells were investigated by Acridine Orange staining as described in section 2.2.2.3.3. Moreover, the differentiation of stem cells on the scaffolds was determined by immunocytochemistry (Section 2.2.2.1.4.1) using appropriate antibodies and by RT-PCR analysis for WJ MSCs (Section 2.2.2.1.4.2).
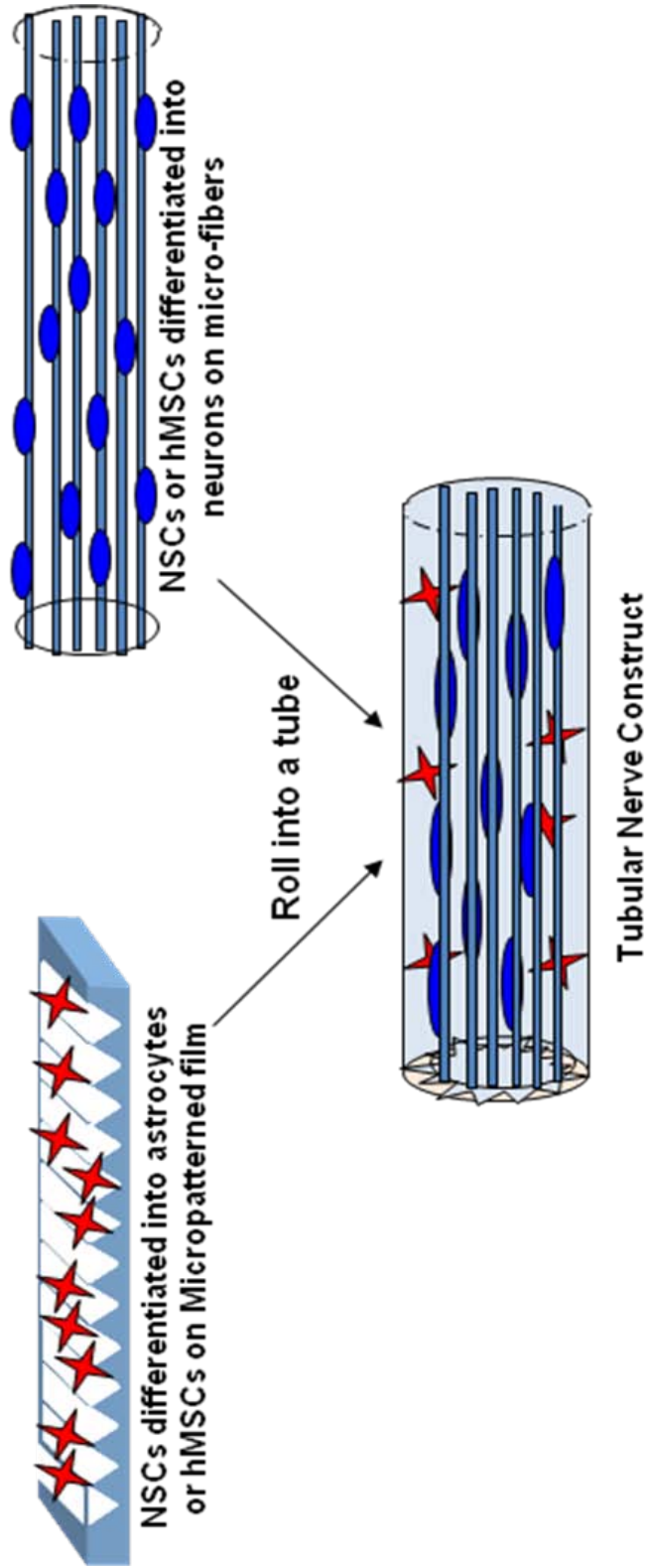
Figure 2. 5. The design of the guided nerve tube

Labels within the figure:

NSCs or hMSCs differentiated into neurons on micro-fibers

NSCs differentiated into astrocytes or hMSCs on Micropatterned film

Roll into a tube

Tubular Nerve Construct

CHAPTER 3

RESULTS AND DISCUSSION

3.1. Characterization of Scaffolds

3.1.1. Surface Topography and Dimension Analysis of Micropatterned Films

The micropatterned Si inclined wall (IW:A4) templates were produced via photolithography followed by wet etching, whereas the perpendicular wall (PW:B1) templates were obtained by reactive ion etching after photolithography (Figure 3.1.a-b). Negative PDMS replica of B1 Si wafer was also used as a mold to prepare polymeric film (Figure 3.2.a). The pattern on both templates and on PDMS replica was successfully transferred onto the polymeric films (Figure 3.1.c-d and Figure 3.2.b, respectively). The dimensions of the polymeric films were determined from the cross-section of the films observed by light microscopy and from SEM images. The dimensions of the polymeric films obtained by solvent casting were slightly different from the dimensions of the templates, even in PDMS mold (Table 3.1).

The polymeric film with the micropattern was designed to serve as the exterior of the final tubular nerve construct (shown in Figure 2.5 in section 2.2.2.4). Thus, the polymeric film had to be permeable to the nutrients to allow cell growth within the construct. It also had to be flexible to some extent in order to be able to fix the tissue engineered construct to the native nerve tissue. In the preliminary studies micropatterned films were prepared with PHBV and P(L-D,L)LA blend, and for the final construct PLGA was added to increase film flexibility. It was observed

that addition of PLGA made the film not just flexible but also slightly porous (Figure 3.3). In order to enhance the porosity PEG was added to the film composition and was then removed after solvent casting by leaching in distilled water. It can be seen from the SEM images that the films obtained after PEG removal are fairly porous and had undisrupted micropatterns (Figure 3.4). The porous structure on the surface was also seen in the bulk of the film from Figure 3.4c-d. The porous micropatterned polymeric film was successfully transferred from PDMS with desired dimensions.
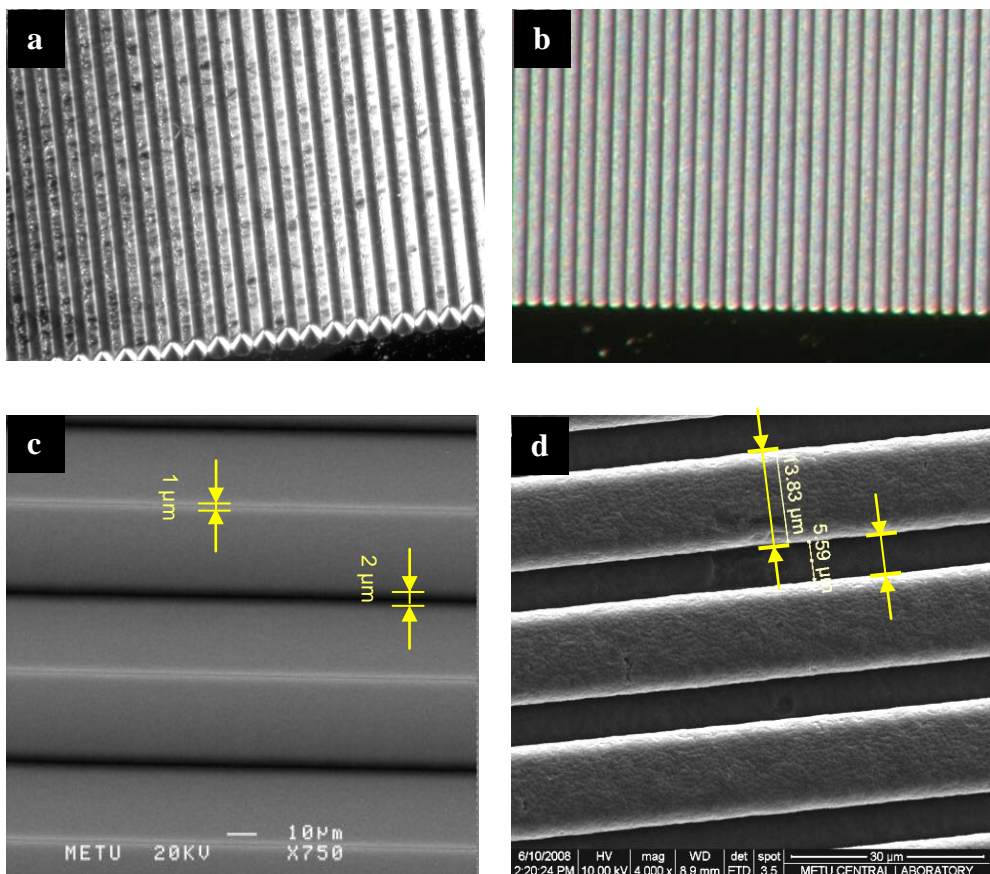
Figure 3.1. Micrographs of micropatterned templates and films. Templates as observed by stereomicroscopy: a) inclined wall A4, and b) 90^0 wall B1 (x33.75). Scanning electron micrographs of micropatterned PHBV-P(L-D,L)LA films: c) MP A4, and d) MP B1.
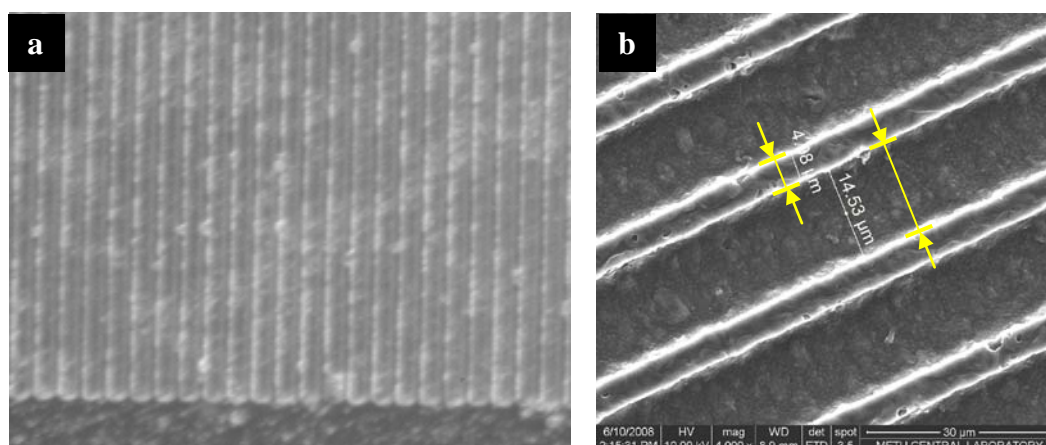
Figure 3.2. a) Micrograph of PDMS replica of B1 template obtained by stereomicroscopy (x 33.75), b) Scanning electron micrograph of a PHBV-P(L-D,L)LA film obtained from the PDMS replica of B1.

Table 3.1. The dimensions (wall angle (θ), ridge width (RW), groove width (GW) and groove depth (GD)) of the templates and micropatterned films produced from them

	Wall	Code	θ (^{0})	RW (μm)	GW (μm)	GD (μm)
Template	IW	A4	54.7^0	2	1	30
	PW	B1	90.0^0	5	14	5
	PW	B1 PDMS	90.0^0	15	5	5
MP Film	IW	A4	54.7^0	1	2	30
	PW	B1	90.0^0	14	5.5	5
	PW	B1 PDMS	90.0^0	5	14.5	5
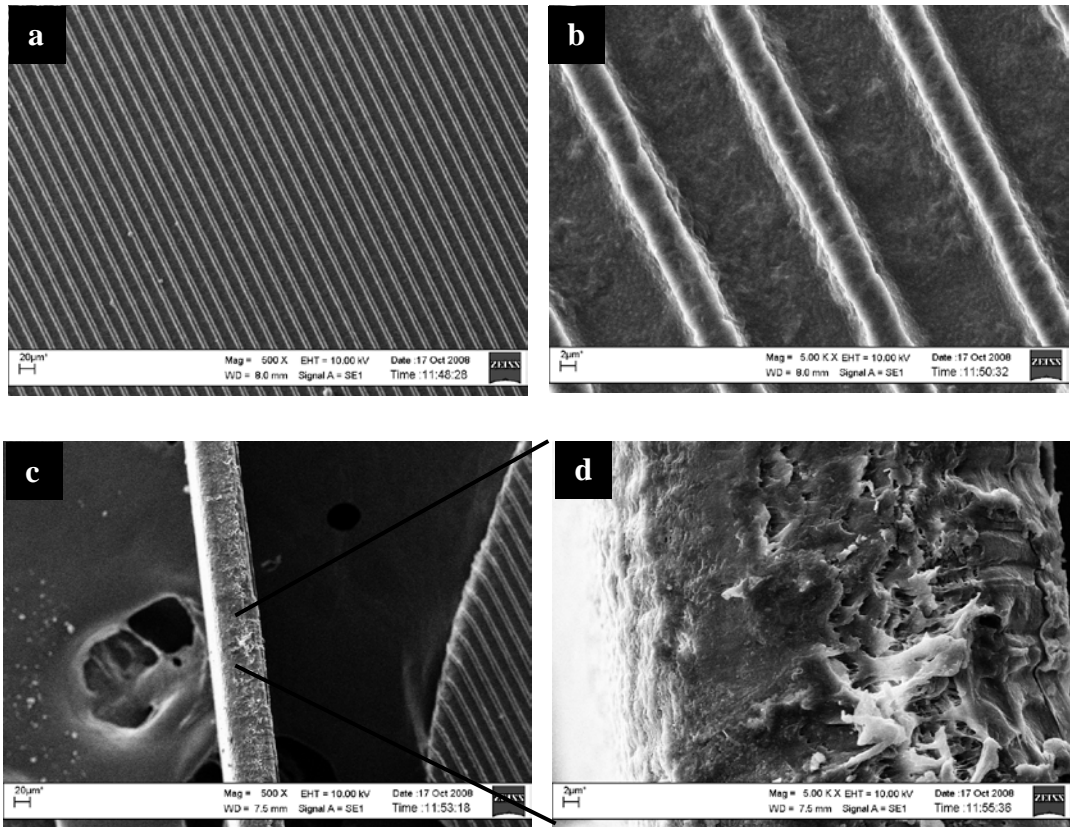
Figure 3.3. SEM images of PHBV-P(L-D,L)LA-PLGA films obtained from the PDMS replica of B1. a-b) top views, and c-d) cross-sections at different magnifications.
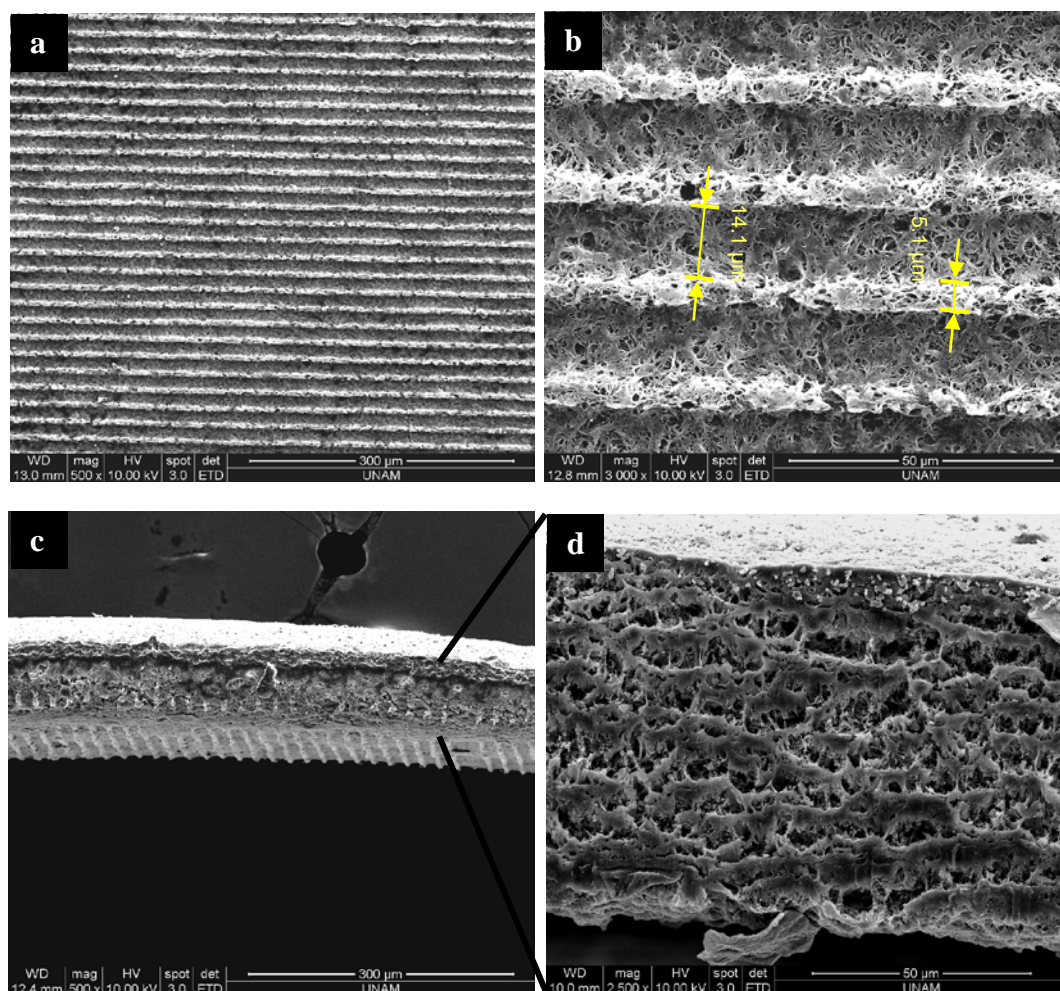
Figure 3.4. SEM images of porous PHBV-P(L-D,L)LA-PLGA films. The patterned film was obtained from the PDMS replica of B1 and then PEG was leached out in distilled water. a-b) top views, and c-d) cross-sections at different magnifications.

3.1.2.   Porosity of the Polymeric Films

The porosity of the PHBV-P(L-D,L)LA-PLGA films obtained after leaching out the PEG was assessed using the confocal microscopy images of the micropatterned films by the use of the NIH Scion Image program. Total porosity (surface and bulk) was calculated by taking images from layers (1 µm in z-direction) of three different regions of two separate micropatterned films (Figure

3.5). The average porosity was determined as 58.95 ± 2.42 (%). SEM image (Figure 3.4.b) shows that the maximum pore size is around 4-5 µm, which is smaller than the size of both the cell sources used in this study. Thus, the porous micropatterned film is permeable to nutrients, however, would not allow the ingrowth of the cells in the film. The cells would not and should not penetrate into the film, while they were stay on the surface, recognize the micropattern and align along its axis as will be seen in the alignment studies in the following sections.
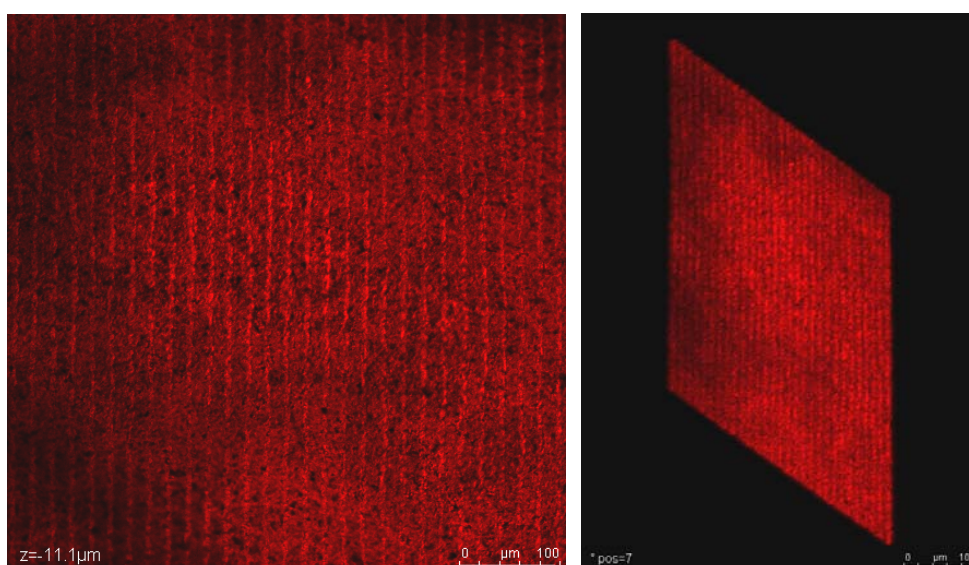
Figure 3.5. Confocal micrographs of porous micropatterned films after Nile Red staining (x200, scale bar: 100 µm)

3.1.3.   Mechanical Properties of the Polymeric Films

The tissue engineered tubular construct is designed to be attached to the ends of the native nerve tissue in the body either through suturing the outer film part or with biological glue. The outer region should be able to withstand the tensile

stress during suturing. For this reason, the effect of PLGA and porosity incorporation on the mechanical properties of polymeric films was investigated.

In tensile testing, a gradually increasing tensile force is applied to a sample until it fails (breaks). Strain (ε) is the ratio of change in the length to original length, and is directly proportional to the stress applied (σ). The stress-strain graph describes the relationship between the stress and the strain (Figure 3.6). In elastic region of the graph (initial, linear) the load is not enough to cause permanent translation of the molecules and deformation is reversible. Beyond this region the applied stress produces permanent changes to a sample and called as plastic deformation if the material is viscoelastic. The ultimate tensile strength is defined as the highest tensile stress a material can withstand. The modulus of elasticity (E) describes the relationship of stress to strain within the elastic region and gives information about the material's stiffness. Elongation at break is the strain on a sample before it breaks and is expressed as a percent or a fraction.

In the tensile tests of this study, the modulus of elasticity, ultimate tensile strength and elongation at break values of three different polymers were determined (Table 3.2). The results showed that incorporation of PLGA into PHBV-P(L-D,L)LA film led to a 23% and 32% decrease in UTS and elastic modulus, respectively, and a 12% increase in elongation at break. These indicate that PLGA incorporation made the film less strong, less hard but more extensible. Upon porosity incorporation UTS and elastic modulus were decreased more significantly (85% and 92%, respectively) and the elongation at break percent was increased also significantly (by 24%). These imply that incorporation of PLGA affected the tensile properties of PHBV-P(L-D,L)LA, but the effect was more pronounced upon porosity incorporation.
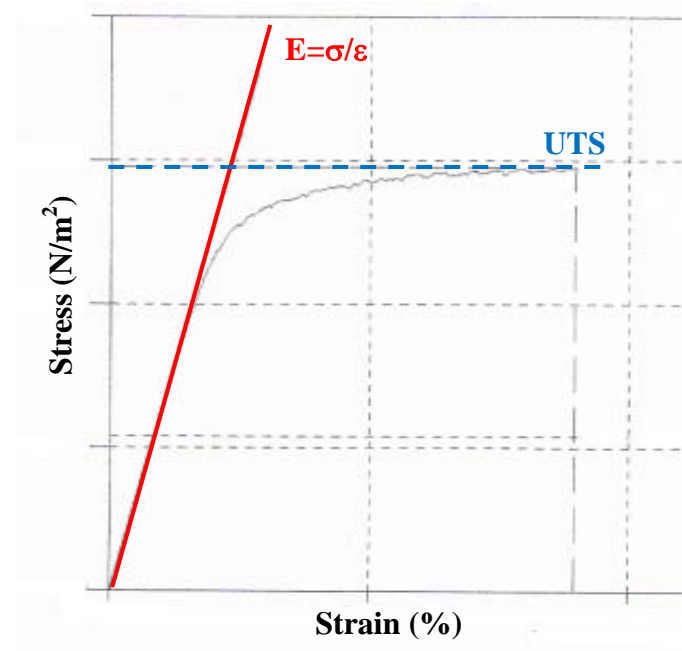
Figure 3.6. A representative stress-strain curve

Table 3.2. Tensile test results of polymeric films.

Sample	UTS (MPa)	E (MPa)	EAB (%)
PHBV5-P(L-D,L)LA	26.94 ± 6.28	1.54 ± 0.01	7.60 ± 0.07
PHBV5-P(L-D,L)LA-PLGA	20.81 ± 1.47	1.05 ± 0.23	8.54 ± 0.15
Porous PHBV5-P(L-D,L)LA-PLGA	3.13 ± 0.44	0.08 ± 0.02	10.57 ± 0.89

UTS: ultimate tensile strength, E: modulus of elasticity, EAB: elongation at break

3.1.4. Physical Characterization of Electrospun Fibrous Mat

In the preparation of electrospun fibers the parameters (polymer concentration, flow rate, applied potential and the distance between the two poles (needle and collector)) were optimized to obtain uniform, defect-free, aligned fibers. To improve the fiber quality a solvent DMF with a high dielectric constant (36.7 $C^2m^{-2}N^{-1}$ at 25ºC) was added to the polymer solution. By increasing the conductivity of the polymer solution, the higher attractive forces created between the metal collector and the syringe tip was expected to lead to more straight and uniform fibers without any fusion or beads (Ndreu et al., 2008).

One of the parameters, polymer concentration, was found to be very influential on fiber diameter. It was not possible to obtain a PHBV5-PLGA fibrous mat using a 5% (w/v) polymer solution even when the DMF content was high. Aligned PHBV5-PLGA fibrous mat with fibers 950 nm in diameter was obtained (with some beads) using a 10% (w/v) polymer solution (Figure 3.7.a-b). The best electrospun fibrous mats were obtained using 15% (w/v) PHBV5-PLGA solution (Figure 3.7.c-e). Electrospun fibers were well aligned and the diameter of the fibers was around 1.5 µm (Figure 3.7.e). Unlike PHBV, PLGA is soluble in acetone; therefore, the fibrous mat was treated with acetone to study the PLGA and PHBV5 mixing and their respective locations in the mat (Figure 3.8). It was observed that upon acetone treatment of PHBV5-PLGA PLGA dissolved out of fibers and left nicks (Figure 3.8.f). The acetone treatment was, however, not effective on PHBV fibers (Figure.3.8.b). SEM results showed that PHBV-PLGA fibers do not have core shell structure. The scratches indicate that PLGA is generally found mixed with PHBV along the fiber; however, the breaks imply an improper mixing of the two polymers in some regions of the fibrous mat (PLGA rich regions broke).
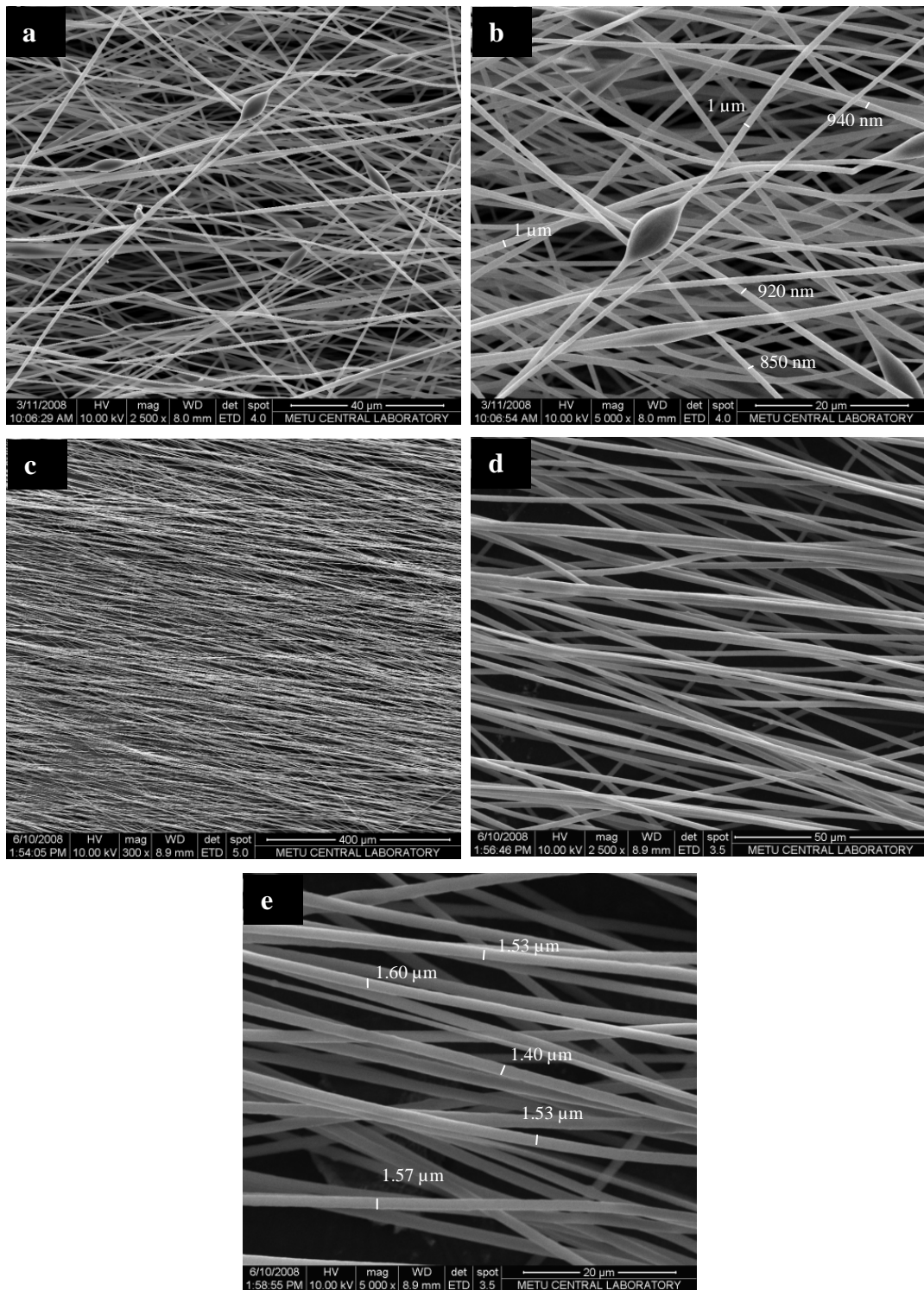
Figure 3.7. SEM of PHBV-PLGA fibers prepared under constant voltage (18 kV) and flow rate (20 µL/min) a-b) with a 10% (w/v) polymer solution with a distance of 15 cm and c-e) with a 15% (w/v) polymer solution with a distance of 25 cm.
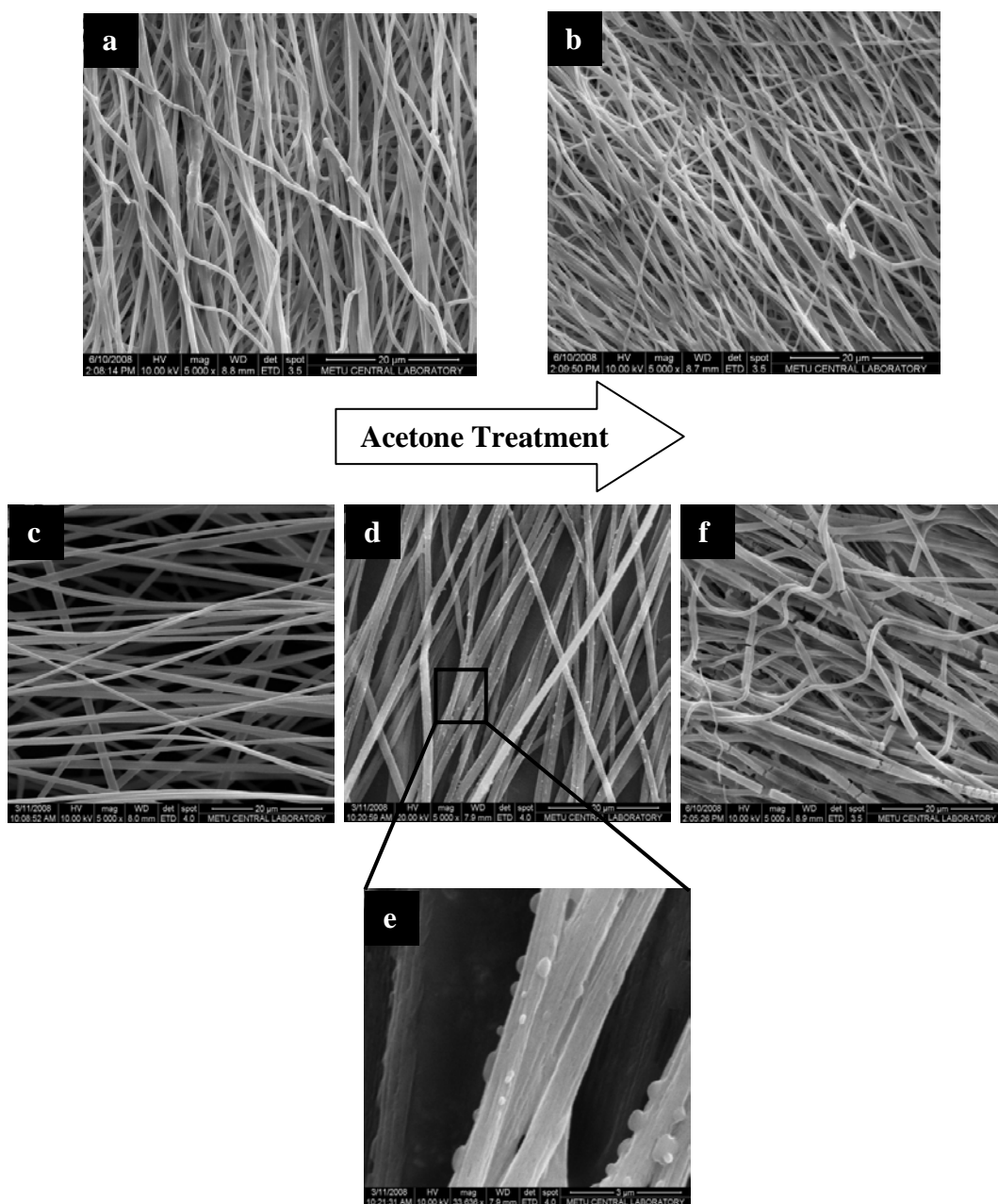
Figure 3.8. SEM of PHBV (5%, w/v) fibers prepared under 24 kV and 20 µL/min flow rate with a distance of 20 cm. a) before and b) after 2 h acetone treatment. SEM of PHBV-PLGA (15%, w/v) fibers prepared under optimized conditions: c) before acetone treatment, d) after acetone wash for a while, e) a closer view of (d) and f) after 2 h of acetone treatment.

3.1.5. Erosion of Polymeric Films and Electrospun Mats

In tissue engineering the disappearance of the scaffold in the body with time is an important point to be considered in the design of a scaffold. Since during healing process the removal rate of an implanted scaffold should match the formation rate of native ECM. Thus, the erosion rates of electrospun fibrous mats of PHBV5-PLGA and films of PHBV5-P(L-D,L)LA, PHBV5-P(L-D,L)LA–PLGA and porous PHBV5-P(L-D,L)LA–PLGA were investigated. Three sets of samples of fibrous mats and films were incubated in 30 mL PBS at 37^0C for 90 days. The weights of the dried samples were determined at 10 days intervals. Weight remained (Wr) was determined as: Wr (%) = 100-((Wi-Wf)/Wi x 100) where Wi is initial weight, and Wf is final weight. All measurements were expressed as means ± standard deviation (sd). The change in weight by time for the electrospun mats and the polymeric films was shown in Figures 3.9 and 3.10, respectively.

The weight of PHBV-PLGA electrospun fiber samples changed steadily with time (Figure 3.9). At the end of 90 days there was a 80% decrease in the sample weight which was probably due to the loss of mostly PLGA and on a small amount PHBV as expected from the degradation rate of PLGA being higher than that of PHBV (Lu et al., 2000, Ferreira et al., 2001). The weight of PHBV-P(L-D,L)LA films remained almost stable for the whole duration (5% decrease in weight) (Figure 3.10). However, incorporation of PLGA increased the erosion rate of the films. Indeed a sharp 15% decrease in weight was seen between days 20 and 30, and the total weight loss was around 35%. Surprisingly the porous PHBV-P(L-D,L)LA-PLGA films had slower erosion rates (with a total weight loss of ca. 25%) compared to nonporous ones. A faster erosion in porous structures was expected due to higher penetration of the solvent (water). However, if bulk erosion with PLGA takes place due to inability of the degradation product, lactic acid and larger molecules, leaving the bulk then it is possible that the porous one may not have faster rate of erosion. Thus, the acidic degradation products of the porous films could be removed via pores.
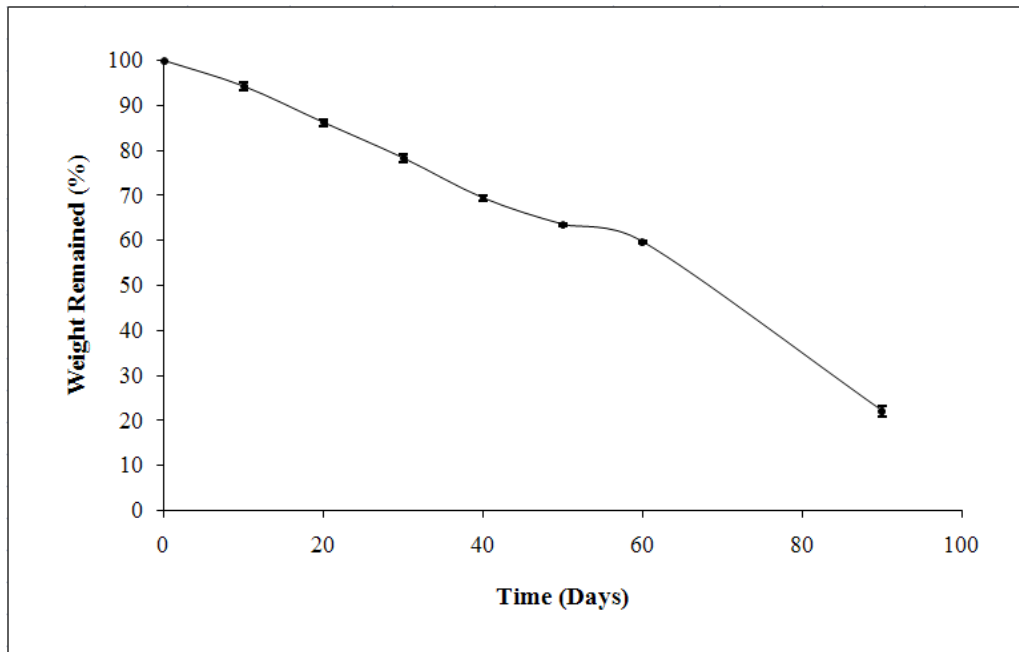
Figure 3.9. Erosion profile of PHBV5-PLGA electrospun fibrous mat.
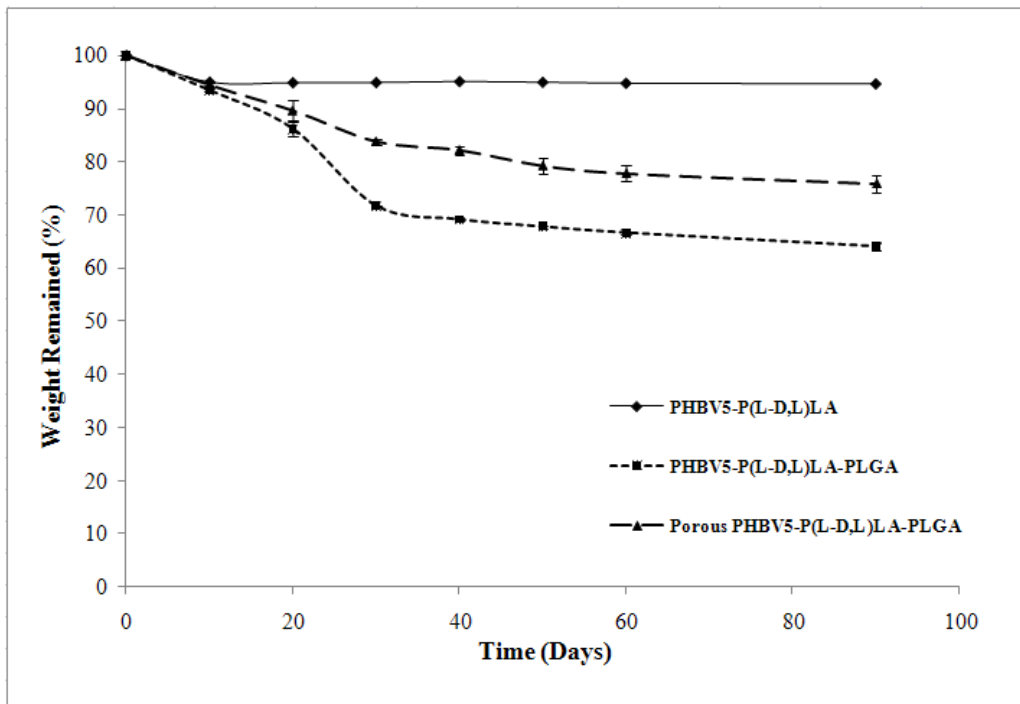
Figure 3.10. Erosion profile of polymeric films.

71

3.2.   *In Vitro* Studies

3.2.1.   *In Vitro* Studies of Human MSCs

3.2.1.1.   Comparison of Bone Marrow and Wharton's Jelly-derived MSCs

3.2.1.1.1.   Flow Cytometric Analysis

The specific cell surface antigens of human BM and WJ (P2, P3 and P4) MSCs were analysed by flow cytometry. Positive cells were counted and compared with the corresponding immunoglobulin isotypes (Figure 3.11). The absolute positive cells were calculated considering the intersection of isotype control and positive sample (Figure 3.11.b-c). The expression of surface antigens of MSCs derived from BM and WJ are given in Table 3.3 based on isotype controls. MSCs derived from both cell sources were negative for hematopoietic markers CD34, CD45, and also for CD133 regardless of passage number. However; MSCs derived from both sources were strongly positive for MSC markers CD73, CD44, CD90, and also for HLA-ABC. BM MSCs were positive for CD106 and HLA-DR but its expression decreased by increase in passage number. However, WJ MSCs were negative for HLA-DR and expressed CD106 at low level at passages 2 and 4; in fact they had no CD106 expression at passage 4. MSC antigen CD105 was expressed in both cell sources but the increase in passage number leads to decrease in its expression especially in WJ MSCs. The expression of CD49d was completely negative in BM MSCs, while this antigen was slightly expressed by WJ MSCs and this low expression decreased by increase in passage number. The expression of CD29 was significantly low in BM MSCs compared to high expression in WJ MSCs, but this antigen was found to be present on BM MSCs obtained from another donor in amount comparable to that of WJ MSCs.

The flow cytometry results are consistent with previous studies and confirmed that MSCs express specific surface markers like CD105, CD73, CD44, CD90, and also HLA-ABC, and are negative for hematopoietic markers CD34, CD45 and also for CD133 (Bieback et al., 2004, Pittenger and Martin, 2004, Wang

et al., 2004). Unlike in BM MSCs, WJ MSCs were negative for immunogenic antigen HLA-DR, and this is in agreement with the results of Weiss et al.2006. The absence of HLA-DR in WJ MSCs in this study implies that these cells will be less prone to immune rejection in case of allogenic transplantation, because it is known that HLA-DR antigens are responsible for triggering humoral immune response (Burlingham et al., 2000). BM MSCs were also found to be moderately positive for the vascular cell adhesion molecule CD106, as expected according to several recent studies (Bieback et al., 2004, Pittenger and Martin, 2004), while WJ MSCs had low expression of this antigen. A significant decrease in CD105 expression in WJ MSCs by increase in passage number was shown also by Weiss et al. 2006. Simultaneusly, more dispersed cell clusters were seen in the dot-plot of flow cytometry data because of being non uniform in size as passage number increased from 2 to 4 in WJ MSCs. Therefore, this outcome points out that it would be better to use low passage number WJ MSCs, when all the cells in the population are in their undifferentiated state, in cell differentiation studies. A drop in proliferation rate and increase in granularity was obtained in WJ MSCs as the passage number increased from 2 to 4, implying that either the source used was not optimal or that the expansion medium used in this study (DMEM with 10% FCS, commonly used medium for BM MSCs growth) was not suitable for these cells. FCS contains some growth factors and its use in large amounts in expansion medium may promote unintentional differentiation or stem cell differentiation to unpredictable cell lineages.
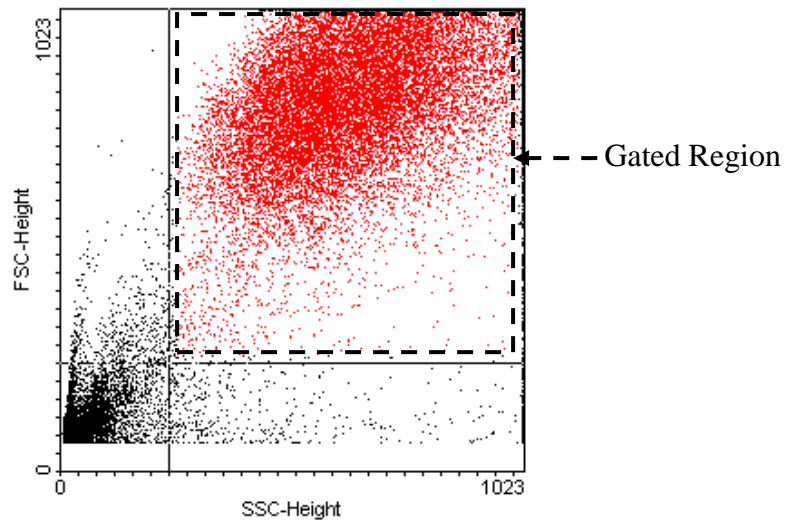
(a)
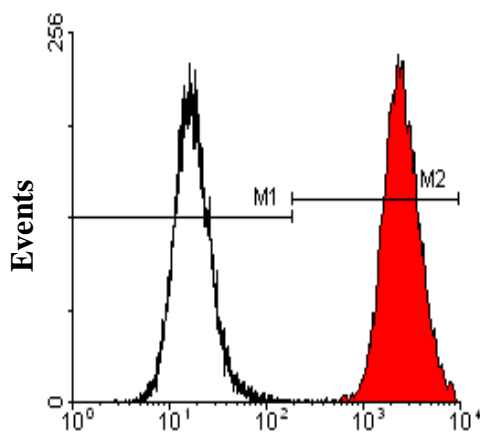
(b)
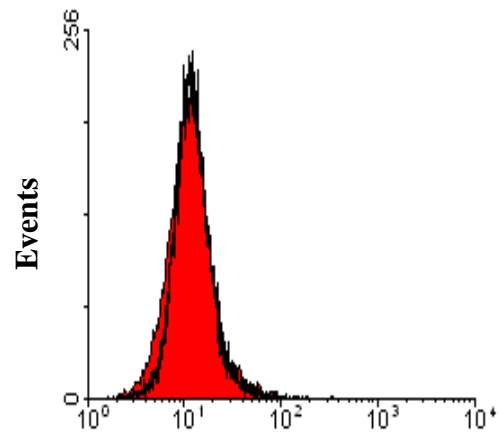
(c)

Figure 3.11. a) The forward scatter versus side scatter dot-plot illustrates the gating strategy . The representative histograms for different antigen expression: b) positive expression of CD73, and c) negative expression of CD45 for bone marrow MSCs. The shaded area shows the profile of the gated positive cells, while the unfilled area shows the gated isotype control.

Table 3.3. The expression of surface antigens of MSCs derived from bone marrow and Wharton's Jelly based on isotypes

Surface Antigen	BM MSCs %*			WJ MSCs %*		
	P2	P3	P4	P2	P3	P4
CD105	98.2 ± 0.2	96.3 ± 2.1	91.2 ± 4.0	97.2 ± 0.1	85.6 ± 14.4	55.8 ± 1.1
CD106	83.4 ± 13.6	79.5 ± 12.8	63.5 ± 9.2	22.4 ± 13.6	11.1 ± 15.7	0.0 ± 0.0
CD49d	0.7 ± 0.5	0.0 ± 0.0	0.0 ± 0.0	17.4 ± 9.9	10.2 ± 3.3	6.1 ± 2.3
CD90	99.9 ± 0.0	99.8 ± 0.2	99.8 ± 0.0	99.8 ± 0.1	100.0 ± 0.0	93.5 ± 8.6
CD44	98.2 ± 0.8	96.7 ± 1.8	95.3 ± 0.3	87.2 ± 7.8	91.1 ± 7.0	80.6 ± 3.0
CD73	99.9 ± 0.2	100.0 ± 0.0	99.0 ± 0.1	92.7 ± 9.7	99.1 ± 1.3	96.3 ± 2.5
CD29	36.0 ± 7.5	40.3 ± 13.8	31.0 ± 1.8	91.6 ± 8.8	92.8 ± 3.5	70.0 ± 29.6
HLA-ABC	99.8 ± 0.1	99.7 ± 0.2	98.5 ± 0.0	93.0 ± 9.8	99.6 ± 0.1	98.1 ± 2.0
CD45	0.3 ± 0.4	1.0 ± 1.4	0.0 ± 0.0	0.0 ± 0.0	0.0 ± 0.0	0.0 ± 0.0
CD34	0.0 ± 0.0	0.0 ± 0.0	0.0 ± 0.0	0.0 ± 0.0	0.0 ± 0.0	0.0 ± 0.0
HLA-DR	89.3 ± 1.8	78.9 ± 8.1	67.1 ± 1.6	0.0 ± 0.0	0.0 ± 0.0	0.0 ± 0.0
CD133	0.0 ± 0.0	0.0 ± 0.0	0.0 ± 0.0	0.0 ± 0.0	0.0 ± 0.0	0.0 ± 0.0

*Percentage of positive cells (Intersection of isotype control and positive sample considered for calculation of absolute positives).

3.2.1.1.2. Evaluation of Cell Morphology by Staining Actin Filaments and Nucleus of MSCs

Human MSCs derived from BM and Wharton's Jelly show the flat-polygonal or spindle-shape fibroblastic morphology (Figure 3.12). It was observed that BM MSCs were to form a strict monolayer, whereas WJ MSCs were able to exceed a monolayer by crossing over each other. The other significant difference between the two cell types, WJ MSCs were more heterogeneous and usually larger in size compared to bone marrow derived MSCs.
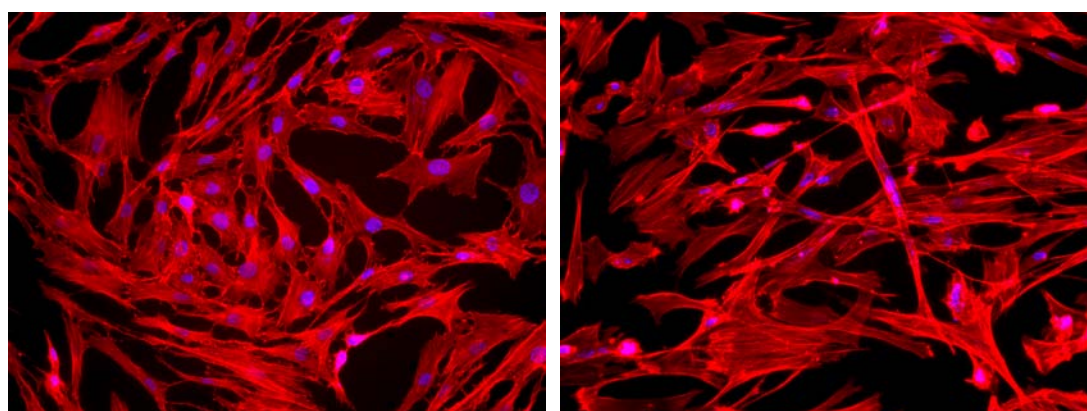
(a)   (b)

Figure 3.12. Fluorescence micrographs showing MSCs (P3) from human a) bone marrow, and b) Wharton's Jelly (original magnification: x200). Red: F-actin stained with Alexa Fluor 546 labeled Phalloidin, blue: cell nuclei stained with Hoechst 33342.

3.2.1.1.3. Osteogenic Differentiation of Human MSCs

Osteoblasts secrete alkaline phosphatase (ALP) an extracellular enzyme during the early stages of mineralization, and the level of this enzyme is an indicator of osteogenic differentiation in *in vitro* studies. Using cell lysates ALP

activity of cells was determined spectroscopically by the determination of the product amount at the end of 1h incubation at 37°C for the enzymatic reaction. The activity results were expressed as µmol of substrate converted to product/min/250 µL of lysate using the calibration curve for the enzymatic product (Appendix B1.a). Upon osteogenic induction for 21 days BM MSCs showed significantly high ALP activity (349.86 ± 16.11 µmoles substrate consumed/min) compared to WJ MSCs (7.13 ± 7.82 µmoles substrate consumed/min). This can be attributed to BM MSCs' being already committed to enter the osteoblastic lineage; even undifferentiated BM MSCs show ALP activity. On the other hand, the determined WJ MSCs ALP activity was not very reliable the value being equal to its standard deviation. The ALP level could have been much lower like in nmol range so it could not be detected accurately.

3.2.1.1.4. Adipogenic Differentiation of Human MSCs

Compared to undifferentiated MSCs (control), human MSCs from both sources induced with adipogenic stimulants for 21 days demonstrated a shift in cell morphological features from a primarily slender elongated morphology to a relatively spherical cell phenotype (Figure 3.13). The adipogenic differentiation was observed with cells which stained positive for lipid vacuoles by Oil Red-O. The morphology change and increase in oil vesicles' amount were more significant in BM MSCs compared to WJ MSCs. Thus, the more oil vesicle formation and the higher ALP activity seen in BM derived MSCs indicate that BM MSCs can be in a later stage in mesodermal lineage compared to WJ MSCs. An immature adipogenic differentiation of WJ MSCs compared to BM MSCs was shown by Karahuseyinoglu et al. (2007), too. Considering WJ MSCs in an early stage in mesodermal lineage, these cells might need additional growth factors and/or longer time for complete differentiation into osteoblasts and adipocytes.

	Control	**Differentiation into Adipocyte**
Bone Marrow MSCs		
Wharton's Jelly MSCs		
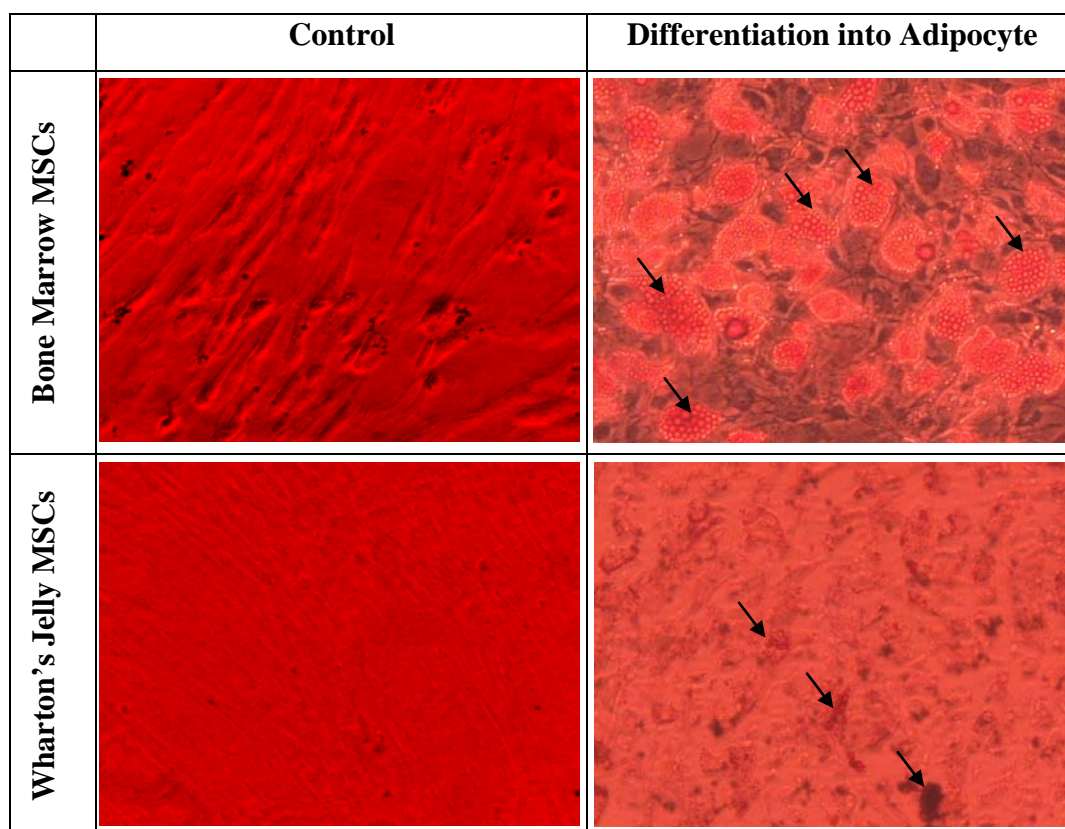
Figure 3.13. Light microscope images of human BM and WJ derived MSCs: cultured in regular medium for 21 days in the absence of adipogenic stimulants as a control and subjected to adipogenic induction medium for 21 days (original magnification: x200). The arrows show the oil vesicles formed upon adipogenic differentiation.

3.2.1.1.5. Neural Gene Expression of Undifferentiated MSCs

The molecular mechanism of neural differentiation, which needs to be known to design experimental protocols to achieve complete differentiation of MSCs into functional mature neurons and glial cells, is not clear. It is known that an increase in cAMP by differentiation inducing agents activates the classical PKA pathway and starts the early steps of neural differentiation, while they are not able to maintain this process, and therefore, it is not useful for long-term *in vitro* survival of neurons (Jori et al., 2005). To understand the molecular mechanism of neural

differentiation it has to be known whether MSCs express genes of early neural proteins and/or transcription factors involved in neural development.

Undifferentiated BM and WJ MSCs were tested for their expression of neural specific markers. PCR primers for these markers were designed de novo, so they were proven to be specific for the mRNA of interest by using cDNA from human adult brain (Figure 3.14). The single bands obtained at the expected size by RT-PCR analysis showed that our primer design and PCR conditions were optimized successfully. Most of the specific neural gene products were found to be expressed in brain tissue. However, early neural markers NeuroD1 and Neurogenin1 were expressed in very low amounts (almost none) in the human adult brain.

RT-PCR results of untreated human MSCs derived from both BM and WJ (Figure 3.14) indicated that these cells do not express the astrocyte marker GFAP and early neural markers Pax6, and express NeuroD1 at a very low, almost undetectable, level. The other early neural marker Neurogenin1 was expressed at a low level in MSCs derived from both sources at all passages. The genes NeuroD1 and Neurogenin1 could not be seen clearly in human brain and MSCs, therefore, their PCR products were sequenced. However, hMSCs derived from both sources at all passage numbers used had high expression of HES1, Enolase2, Nurr1, nestin and RARA. The presence of retinoic acid receptor, alpha (RARA) is a significant clue for the ability to differentiate since MSC differentiation to neural cells with retinoic acid is impossible in the absence of its receptor. The adult neural marker MAP2 was expressed in hMSC from both sources, but significantly expressed in BM MSCs at P3.

The expression of early and mature neural and glial genes by human BM and WJ MSCs was studied with RT-PCR to investigate the capacity of MSCs to differentiate into mature neurons and glial cells. It was revealed that most of the early neural lineage markers were expressed in human MSCs from both sources, suggesting neural differentiation potential. Several studies with MSCs of animals and humans showed that these stem cells are able to cross the barriers of different lineages, like mesodermal origined MSCs that can express the specific genes of neuroectodermal lineage (Woodbury et al., 2000, Tondreau et al., 2004, Bossoasco

et al., 2005, Kondo et al. 2005, Wislet-Gendebien et al., 2005, Hermann et al., 2006). Thus, stem cells could express a wide variety of genes at low basal levels (Blondheim et al., 2006). Modulation of transcription factor expression and activation of these genes might result in transdifferentiation of the adult stem cells. Even though the low expression of early neural genes could not directly show that these adult stem cells would become neural cells, it implies their potential for neural differentiation.

Neural Markers	Mw	DNA marker	β-Actin	Pax 6	Neurogenin1	Neuro D1	Nurr1	RARA	HES1	Nestin	Enolase 2	MAP2	GFAP
Human adult brain extract	300bp / 150bp												
Bone Marrow MSC Passage 2	300bp / 150bp												
Bone Marrow MSC Passage 3	300bp / 150bp												
Bone Marrow MSC Passage 4	300bp / 150bp												
Wharton's Jelly MSC Passage 2	300bp / 150bp												
Wharton's Jelly MSC Passage 3	300bp / 150bp												
Wharton's Jelly MSC Passage 4	300bp / 150bp												

Figure 3.14. RT-PCR results for the gene expression of the early neural proteins and transcription factors in untreated human WJ and BM MSCs, compared to the expression at the corresponding human adult tissue (30 cycles). β-actin was used an internal standard.

In order to find a clue for the neural differentiation predisposition of MSCs, the expression of specific transcription factors NeuroD1, Nurr1, Pax6, and HES1 was investigated, because these are directly or indirectly involved in neurogenesis and transiently expressed in neural precursor cells. In addition, the expression of NSC marker protein nestin, Enolase2, and mature astrocyte and neuron proteins GFAP and MAP2, respectively, were investigated. The potential role of some transcription factors and proteins in modulating neural phenotype will be discussed below.

An orphan receptor belonging to the nuclear receptor superfamily, Nurr1, which activates endogenous tyrosine hydroxylase in neural progenitor cells in the brain (Sakurada et al., 1999), is expressed in the early stages of embryogenesis, and also continues to be expressed into adulthood (Zetterstrom et al. 1996). Even though it was present at low levels, Nurr1 was expressed in the adult human brain as expected; and MSCs from both sources highly expressed this transcription factor. The expression of the other early neural markers, ngn1 and NeuroD1, could not be clearly seen in adult human brain, probably due to their being early neural markers. NeuroD1 expression was absent in both BM and WJ MSCs, but in contrast to adult brain cells these cells slightly expressed ngn1. The expression of NeuroD1 was not clearly detected in some studies carried out with MSCs from human bone marrow (Hermann et al., 2004) and also in the cells from umbilical cord blood (Habich et al., 2006). Helix-loop-helix protein HES1 negatively regulates the development of CNS. Scintu et al.(2006) showed that HES1, involved in differentiation of BM MSCs into neural cells, was expressed in undifferentiated human BM MSCs. Its expression was significantly increased upon induction, and then decreased as neural differentiation proceeded.

The expression of nestin observed in the human MSCs derived from both sources is an important clue to show that these stem cells have already expressed neural lineage markers without induction. It was reported that the expression of nestin was seen in MSCs, and upon induction the expression was decreased in a significant and progressive manner (Scintu et al., 2006). Thus, the expression level of nestin should be followed during trandifferentiation of MSCs into neural cells.

The constitutive expression of transcription factors and proteins, which has significant roles in neural development, by BM and WJ MSCs suggests that these cells can retain the ability for neural differentiation. Besides these early neural markers, the adult glial and neural markers were investigated. The astrocyte intermediate filament protein, GFAP was found in differentiated astrocytes in brain, but this mature astrocyte marker was not expressed in undifferentiated human MSCs. Even though some researchers showed GFAP expression in undifferentiated MSCs from bone marrow (Hermann et al., 2004, Bossolasco et al., 2005) and umbilical cord matrix (Mitchell et al., 2003), the expression of GFAP was not expected in these cells as was the case in several studies with rats and humans (Dezawa et al., 2004, Jeong et al., 2004, Tao et al., 2005, Habich et al., 2006). There was a controversy in the literature about the mature neuron marker, MAP2 expression as in the case of GFAP. The low level expression of MAP2 by MSCs was reported in some studies (Jeong et al., 2004, Tao et al., 2005); but in several other studies MAP2 expression was not detected in MSCs (Dezawa et al., 2004, Habich et al., 2006). In the present study of this section, MAP2, which was highly expressed in mature neurons of the brain, had low expression in the Wharton's Jelly MSCs and had a moderate expression in bone marrow MSCs, with especially significant expression seen at P3.

The expression of retinoic acid receptor is not directly involved in neural development. However, MSCs can be differentiated into neuron-like cells under *in vitro* conditions in the presence of agents such as retinoic acid and other growth factors (Sanchez-Ramos et al., 2001). Thus, for the differentiation of MSCs to neural cells with retinoic acid the expression of its receptor, RARA, is required. In the present study, its high level expression in undifferentiated MSCs implies that bone marrow and Wharton's Jelly MSCs might differentiate into neurons upon induction by retinoic acid combined with appropriate supplements.

3.2.1.2. Characterization of Isolated Wharton's Jelly MSCs

3.2.1.2.1. Evaluation of Cell Morphology by Microscopy

Wharton's Jelly MSCs were isolated from umbilical cord of two different women (A and B) and cultured in four different media (Section 2.2.2.1.1). According to the light microscope examination of the cell migration from tissue and their morphology, no significant difference was observed in terms of source, and the best media were #2 (DMEM low glucose:HAMF12 (1:1) with 10% FCS, 100 U/ml penicillin, 100 μg/ml streptomycin, 1 ng/ml of basic fibroblast growth factor (bFGF) and #4 (α-MEM: HAMF12 (1:1) with 2% FCS, 100 U/ml penicillin, 100 μg/ml streptomycin) (Figure 3.15). The cell morphology was more homogenous and most of the cells had fibroblastic morphology which is a characteristic of MSCs in both media #2 and #4. However, the cells cultured with media # 1 and # 3 were mixed, and it seems that some were differentiated. Thus, the rest of the study was continued with cells cultured in media # 2 and # 4. The light microscope image presented in Figure 3.15.a. shows that the cells start to migrate from the edge of the tissue, and then spread all over the well, and after a while they start to form embroid body-like structures (Figure 3.15.b). When the cells reached confluency, they were detached from the 6 well plate and transferred to TCPS flask as Passage 1 (Figure 3.15.d). MSCs isolated from the umbilical cord matrix have similar morphology with the cells derived from bone marrow. When the cells were grown at a low density, they mostly displayed a spindle-like shape, but when they reached confluency and started to grow in several layers, the cells became flat (Tropel et al., 2004). Earlier studies claimed that MSCs isolated from bone marrow comprise a single phenotypic population forming symmetric, spindle-shaped colonies (homology up to 98%) (Pittenger et al., 1999). More recent studies, however, indicate that single-cell derived colonies of BM MSCs are morphologically heterogeneous, containing at least two different cell types: small spindle shaped cells and large cuboidal or flattened cells (Bruder et al., 1997, Im et al., 2005). In terms of proliferative potential, the cells have been also described as small rapidly-renewing and large slowly-renewing (Reyes et al., 2001). Nevertheless, the latest

findings show that MSC colonies contain as much as three types of cells. The third fraction was described to be composed of very small rapidly self-renewing cells (Colter et al., 2001), which are reported as the earliest progenitors and possess the greatest potential for multilineage differentiation. The examination of these cells revealed that they were about 7 μm in width and had a high nucleus-to cytoplasm ratio. The indicated heterogeneous morphology was also seen in the isolated WJ MSCs in this study. There were small spindle-shaped and flattened cells in the culture. Moreover, it was revealed from light microscope examination that the cell size change when cultured in different media. MSCs cultured in medium #2 were smaller than the ones cultured in medium #4, and this change in cell size was seen in control samples in Figure 3.20 (Section 3.2.1.3.1).
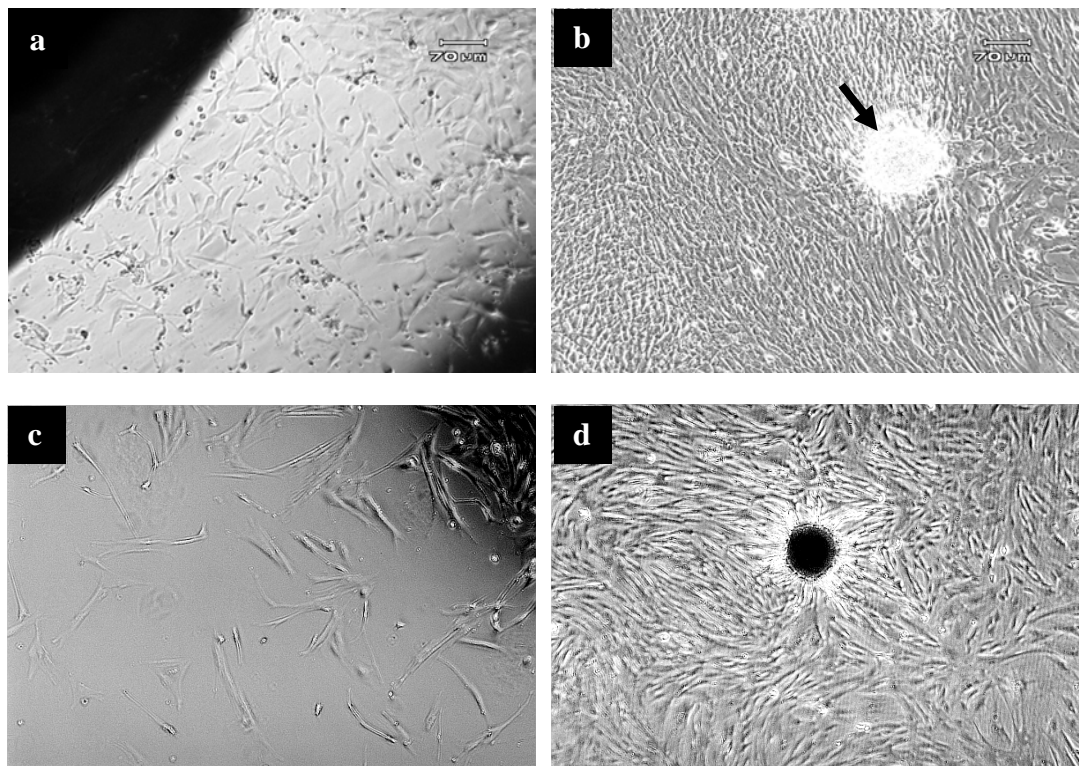
Figure 3.15. Light microscope images of isolated human Wharton's Jelly MSCs on TCPS: after 17 days of isolation a) A4 cells, and b) A2 cells; c) after 25 days of isolation B2 cells; d) B4 cells at passage 1 (A and B: two different donors, #2 and #4: two different media) (x100).

3.2.1.2.2. Growth Kinetics of Isolated WJ MSCs

The cell growth kinetics plots give information about doubling time of the cell line. The doubling time of the population is calculated from log phase (exponential part) of the graph and used to evaluate the response of the cells towards different inhibitory or stimulatory conditions, especially in stem cell studies since the multiple stem cell fates are regulated by both intrinsic and extrinsic controls. Determination of population doubling time is a useful point to be considered during the calculation of cell yields and the dilution factor required at subculture.

In WJ MSCs studies the population doubling time, approximately 60-85 hours in early passages, dramatically declined as the passage number increases (Sarugaser et al., 2005, Karahuseyinoglu et al., 2007), and the number of population doublings vary from group to group (Weiss et al., 2006, Conconi et al., 2006, Lund et al., 2007), ranging from 20-60 until cells reach a replicative senescence without any sign of abnormal karyotype.

The growth curves of WJ MSCs were obtained by plotting increase in number of cells (Log number of cells) against time (h). The number of cells was determined by MTS assay using calibration curves for WJ MSCs grown in each culture conditions (Appendix C). The population doubling time of the isolated WJ MSCs in this study was determined as 25.5 h and 26.5 h for cells cultured in medium #2 and #4, respectively (Figure 3.16). MSCs reached growth saturation after about 200 h of incubation. It was revealed from growth curves that the difference in culture media was not effective on MSCs growth kinetic.
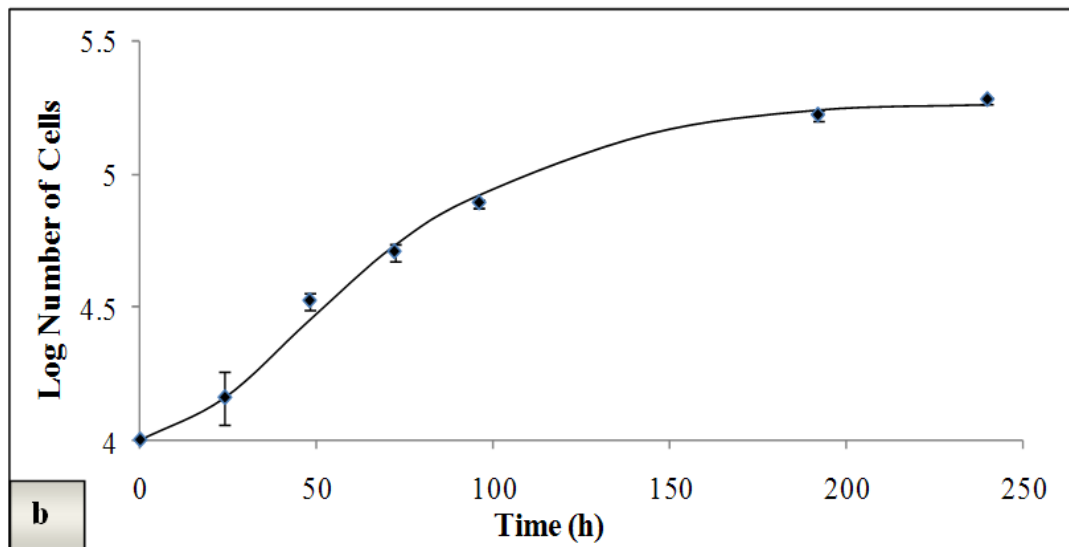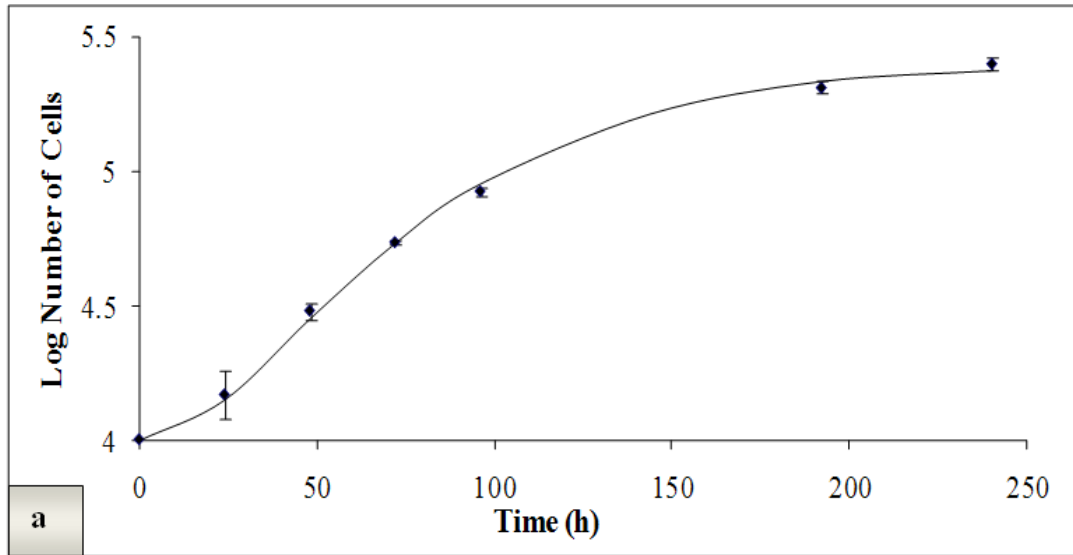
Figure 3.16. Growth kinetics of WJ MSCs cultured with growth medium: a) #2 (doubling time 25.5 h), and b) #4 (doubling time 26.5 h).

3.2.1.2.3. Osteogenic Differentiation of Isolated WJ MSCs

The enzymatic activity results were expressed as nmol of substrate converted to product/min/300 µL of lysate using a calibration curve for the enzymatic product (Appendix B1.b). ALP activity of isolated WJ MSCs induced by osteogenic stimulants for 14 days was about two times higher than the ALP activity of the control cell which was WJ MSCs cultured with same medium in the absence of osteogenic stimulants (Table 3.4). The results showed that ALP activities of WJ MSCs cultured in medium #2 and #4 were not distinctively different. Thus, it implies that ALP activity does not depend on the culture medium used for the growth of cells before differentiation. As indicated in section 3.2.1.1.3. the increase in ALP activity shows the differentiation of isolated WJ MSCs into osteoblasts. ALP activity of WJ MSCs could not be detected properly at µmole level, therefore, ALP activity of isolated WJ MSCs were determined in nmole level. In addition the osteogenic induction periods for WJ MSCs used at MGH and Tufts University, Boston (USA) (21 days) and the ones isolated at METU (14 days) were not same, thus it is not feasible to compare their ALP activities.

The other indicator of osteoblastic differentiation is von Kossa staining for calcium deposition which starts to be formed upon osteogenic induction. Compared to control cells, WJ MSCs induced with osteogenic stimulants for 14 days have calcium depositions which were stained red-brown (Figure 3.17). The calcium deposition was seen much more in MSCs grown in medium #2 compared to medium #4.

ALP activity and von Kossa staining results showed that MSCs, grown in medium #2 before differention, had slighthly higher tendency to differentiate into osteoblasts. The indications of osteoblastic differentiation like the increase in ALP activity and the von Kossa staining were not distinct at the end of 14 days. This could be made more distinct upon extension of the differentiation duration.

Table 3.4. ALP activity of WJ MSC (P3) cultured in growth media #2 and #4 as control and with osteogenic induction medium for 14 days

WJ MSCs	ALP Activity (nmoles substrate consumed/min)	
	Control	**Osteogenic Differentiation**
Medium #2	0.702 ± 0.061	1.623 ± 0.197
Medium #4	0.666 ± 0.127	1.280 ± 0.203
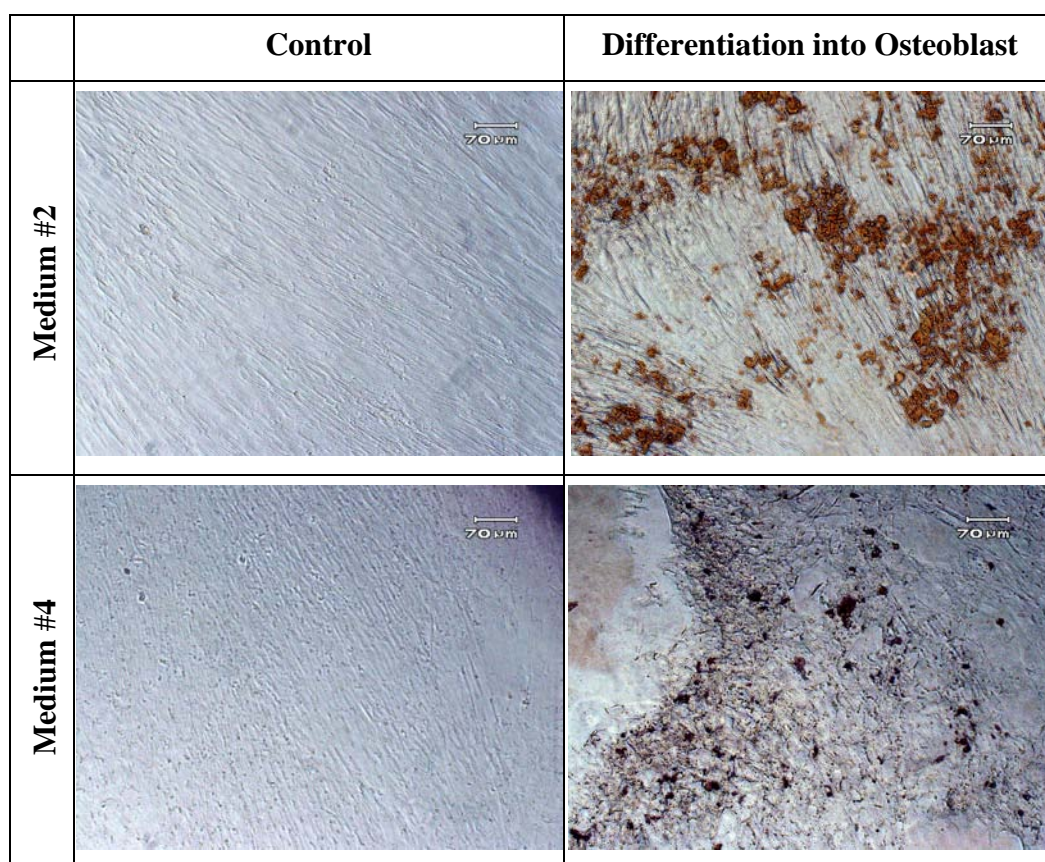
Figure 3.17. Light microscope images of WJ MSCs (P3) cultured with growth medium #2 and #4 as control and with osteogenic induction medium for 14 days after von Kossa staining (x100).

3.2.1.2.4. Chondrogenic Differentiation of Isolated WJ MSCs

Isolated WJ MSCs, grown in medium #4 and seeded at passage 3, demonstrated a shift in cell morphological features from a primarily slender, elongated morphology to a relatively spherical cell phenotype upon chondrogenic induction. WJ MSCs were cultured for 14 days in the presence of chondrogenic stimulants and, as a control, in the absence of stimulants. To confirm chondrogenic differentiation the cells were stained with Alcian Blue for mucopolysaccharides and immunostained with anti-collagen type II and anti-aggrecan which are normally secreted by chondrocytes. Compared to the control, Alcian Blue staining showed, with intense blue color, that chondrogenic differentiation increased the amount of polysaccharides (Figure 3.18). In addition, the secretion of collagen type II and aggrecan was increased upon chondrogenic induction (Figure 3.19).
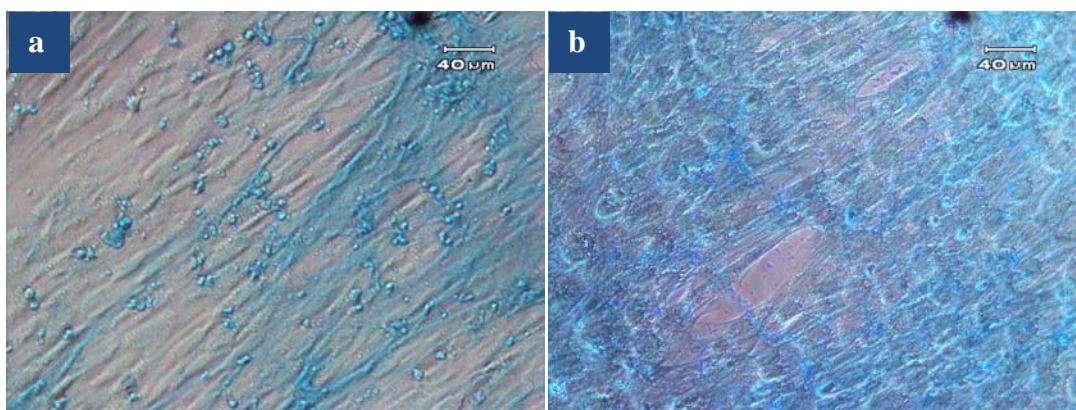
Figure 3.18. Light microscope images of WJ MSCs a) control, and b) subjected to chondrogenic induction for 14 days. Alcian Blue staining (x200).

The major function of BM MSCs is to form a tissue framework to provide mechanical support for the hematopoietic cell system. BM MSCs secrete a number of extracellular matrix proteins including fibronectin, laminin, collagen and proteoglycans (Devine and Hoffman, 2000). In this study, all indicators of chondrogenic differention were seen slightly in the controls (Figure 3.18 and 3.19). This indicates that WJ MSCs secretes some extracellular matrix components and form their own biological environment like BM MSCs which play a significant role in bone marrow microenvironment.

	Control	Differentiation into Chondrocyte
Collagen Type II		
Aggrecan		
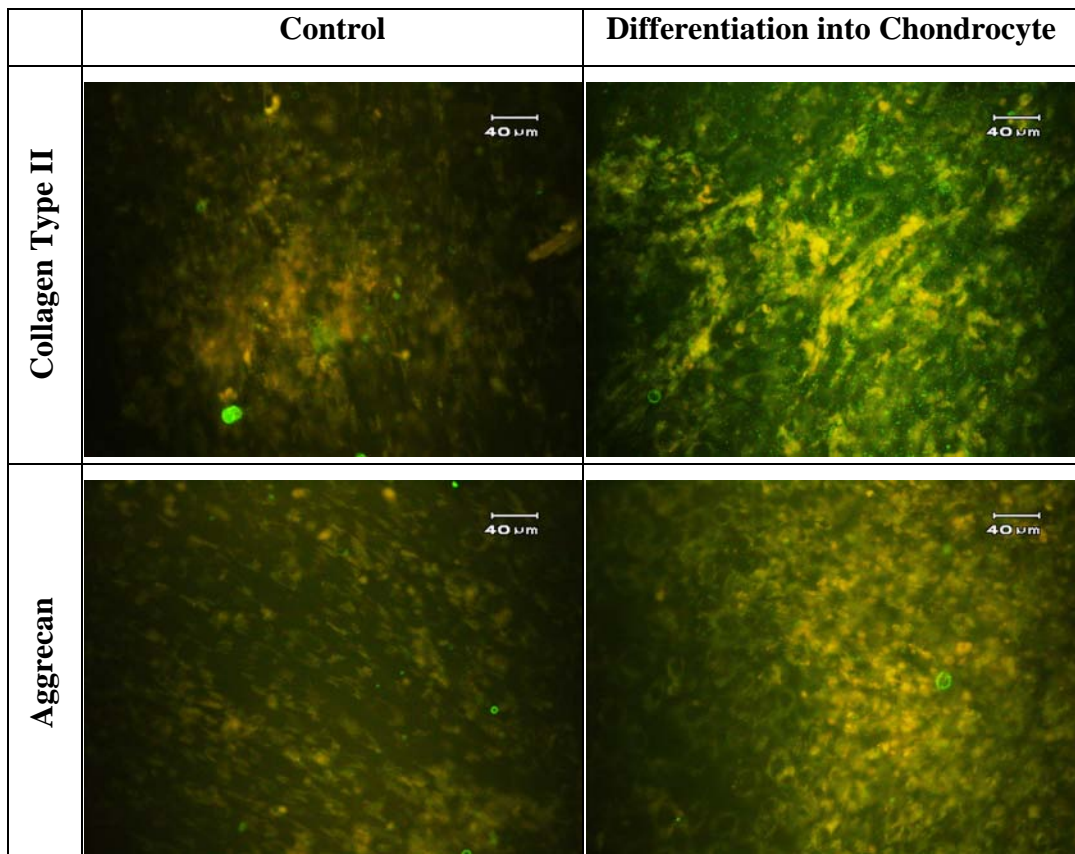
Figure 3.19. Immunofluorescence analysis of collagen type II and aggrecan expression of WJ MSCs with medium lack of induction (control) and with chondrogenic induction medium for 14 days (x200).

3.2.1.3. Differentiation of Human MSCs into Neural Cell Lineages

3.2.1.3.1. Morphology of Cells upon Neural Induction

It has been commonly known that MSCs have an intrinsic potential to differentiate into mesodermal lineages like osteoblasts, chondrocytes and adipocytes under appropriate conditions, but they do not have a tendency to differentiate into other lineages. In recent years, a large number of studies have shown that the cells can transdifferentiate into lineages derived from the neuroectoderm (Phinney and Prockop, 2007). As a result research is concentrated on establishing the molecular mechanisms that regulate adult stem cell plasticity and also on developing ways to use it in therapy. These efforts have led to the publication of many protocols for inducing adult stem cells to differentiate *in vitro* across germinal boundaries, a process referred to as transdifferentiation. In most neural differentiation studies, several inducing agents have been used separately or in combination, and then their effect on neural gene expression was analyzed (Mitchell et al., 2003, Karhuseyinoglu et al., 2007).

MSCs were seeded on uncoated or laminin1 coated TCPS 24 well plate, and incubated in the preinduction medium for 24 h, followed by incubation in the neural induction medium. Detailed information on the conditions of seeded WJ MSCs used in neural differentiation, differentiation protocol and the examinations of cells upon induction are given in Table 3.5. In general MSCs incubated with preinduction medium containing valproic acid (VA) have the structures of cell bodies with long, thin processes and fibrillar extensions. The presence of this specific structure was enhanced upon retinoic acid treatment, especially at moderate concentrations, but it also led to significant cell death . The important stimulant which gave rise to larger and longer cells and enabled permanent neural like structure was VA. It is seen in Figure 3.20 that the preinduction medium without VA was not effective in changing the morphology of WJ MSCs. However, this neural morphology was not permanent when the differentiation medium contains FCS, and after the 5th day most of the cells lost their neural morphology and returned to typical MSC morphology. Thus, in order to extend the survival of

these cells in neural-like morphology, the neural induction was carried out with a medium containing a combination of the growth factor, VA, and the most important component B27 which mimics FCS.

MSCs, grown in medium #4 and then seeded at P3 and P4 on laminin1 coated 24 well plate, were cultured for 24 h in a similar manner with preinduction (PI) medium containing 50µM forskolin, 10 ng/mL human EGF, 10 ng/mL bFGF and with 2 mM VA, and then the culture continued with neural induction medium supplied with 2 mM VA, 50 ng/mL IGF1, and 2% B27. The light microscopy examinations (Figure 3.21) showed that upon neural induction cells seeded at P3 became longer, larger and thinner like the previous trials, whereas WJ MSCs seeded at P4 had dendritic or bipolar extensions resembling neural cells. These dendritic structures were common in WJ MSCs seeded at P4 after 24 h of preinduction, and then the cells with bipolar extensions became predominant and retained their neural cell morphology for a week by culturing with neural induction medium following preinduction. Thus, for the further studies on neural differentiation it was determined that WJ MSCs, grown in medium #4 and then seeded at P4 on laminin1 coated surfaces, would be cultured in the preinduction medium (the expansion medium supplied with 50 µM forskolin, 10 ng/mL human EGF, 10 ng/mL bFGF and with 2 mM VA, without FCS) for 24 h, and then continued culturing in the neural induction medium (the expansion medium supplied with 2 mM VA, 50 ng/mL IGF1, and 2% B27, without FCS) for 6 days. RT-PCR and immunocytochemistry analyses were carried out for these cells to investigate the expression of the specific neural markers.

Table 3.5. Some neural differentiation trials of WJ MSCs and the outcome

WJ MSCs (Growth/Seeding cond.)	Seeding Surface	Differentiation Medium	Neural Differentiation Protocol	Outcome
Medium #4 at P3 (10^4 cells)	Laminin1 coated / Untreated TCPS	DMEM High Glucose with 2% FCS and 0.1 mM non essential amino acids	Culture with PI medium containing VA for 24 h and then culture with medium containing 2 mM VA and 0.5-50 μM RA.	Preinduction and VA gave rise to thinner and longer cells. RA treatment formed neuron like structures especially with10 μM RA but this also led to significant cell death.
Medium #2 at P3 (10^4 cells)	Laminin1 coated / Untreated TCPS	Medium #2 without bFGF	Culture with PI medium containing VA for 24 h and then culture with medium containing 2 mM VA and 0.5-50 μM RA.	Thin and long cells were appeared upon preinduction and VA treatment especially on laminin-coated TCPS. High RA concentration brought the inevitable cell death.

Table 3.5. Some neural differentiation trials of WJ MSCs and the outcome (Cont'd)

Medium #2 and Medium #4 at P4 (5x10³ cells)	Laminin1 coated	Medium #2 without bFGF and Medium #4	Culture with PI medium containing VA for 24 h and then culture with medium containing 2 mM VA, 10 μM RA, CDL (1% v/v).	The cells became larger and thinner upon preinduction in the presence of VA but this change was transient when cultured with FCS. CDL had no effect on cell morphology (Figure 3.20).
Medium #2 and Medium #4 at P2 (10⁴ cells)	Laminin1 coated	Medium #2 without bFGF with or without FCS	Culture with PI medium containing VA or with β-mercaptoethanol or with 5-azacytidine for 24 h and then culture with medium containing different combinations of the following stimulants: 2 mM VA, 10 μM RA, 10 ng/mL NGF, 50 ng/mL IGF1, 2% B27, 20 ng/mL IL1β, 50 ng/mL IGF1, 20 ng/mL IL6, 20 ng/mL CNTF.	β-mercaptoethanol and 5-azacytidine led to cytoskeletal retraction on cells. The common cellular morphology was thin neuron-like cells in the absence of FCS. However, the neural cell morphology seen upon PI medium returned to original MSC structure in the presence of FCS.

Table 3.5. Some neural differentiation trials of WJ MSCs and the outcome (Cont'd)

Medium #2 and Medium #4 at P2 and P3 (10⁴ cells)	Untreated TCPS	α-MEM with 20% FCS	Preinduced with 1 mM β-mercaptoethanol, 100 µM RA, 5 ng/mL bFGF for 24 h and then cultured with medium containing 10 ng/mL NGF.	No significant change in cell morphology.
Medium #2 and Medium #4 at P2, P3, P4 (5x10³ and 10⁴ cells)	Laminin1 coated / Untreated TCPS	Medium #2 without bFGF and Medium #4 (Both lack of FCS)	Culture with PI medium containing VA for 24 h and then culture with two different media: 1) contains 2 mM VA, 50 ng/mL IGF1, 2% B27, with or without 20 ng/mL IL1β, and 2) contains 2 mM VA, 2% B27, 20 ng/mL IL6, 20 ng/mL CNTF.	MSCs responded to PI after 24 h at all passages by increase in size and formation of thin extensions but the significant neuron-like structure was formed in cells seeded at P4. This behavior was preserved with neural induction.

PI: Preinduction medium contains the expansion medium supplied with 50 µM forskolin, 10 ng/mL human EGF, 10 ng/mL bFGF and with or without 2 mM valproic acid (VA) in the presence or absence of FCS.

Medium #2: DMEM Low Glucose:Ham F12 (1:1) with Pen/Strep, 10% FCS, 1 ng/mL bFGF, 0.1 mM non essential amino acids.

Medium #4: α-MEM:Ham F12 (1:1) with Pen/Strep, 2% FCS and 0.1 mM non-essential amino acids.
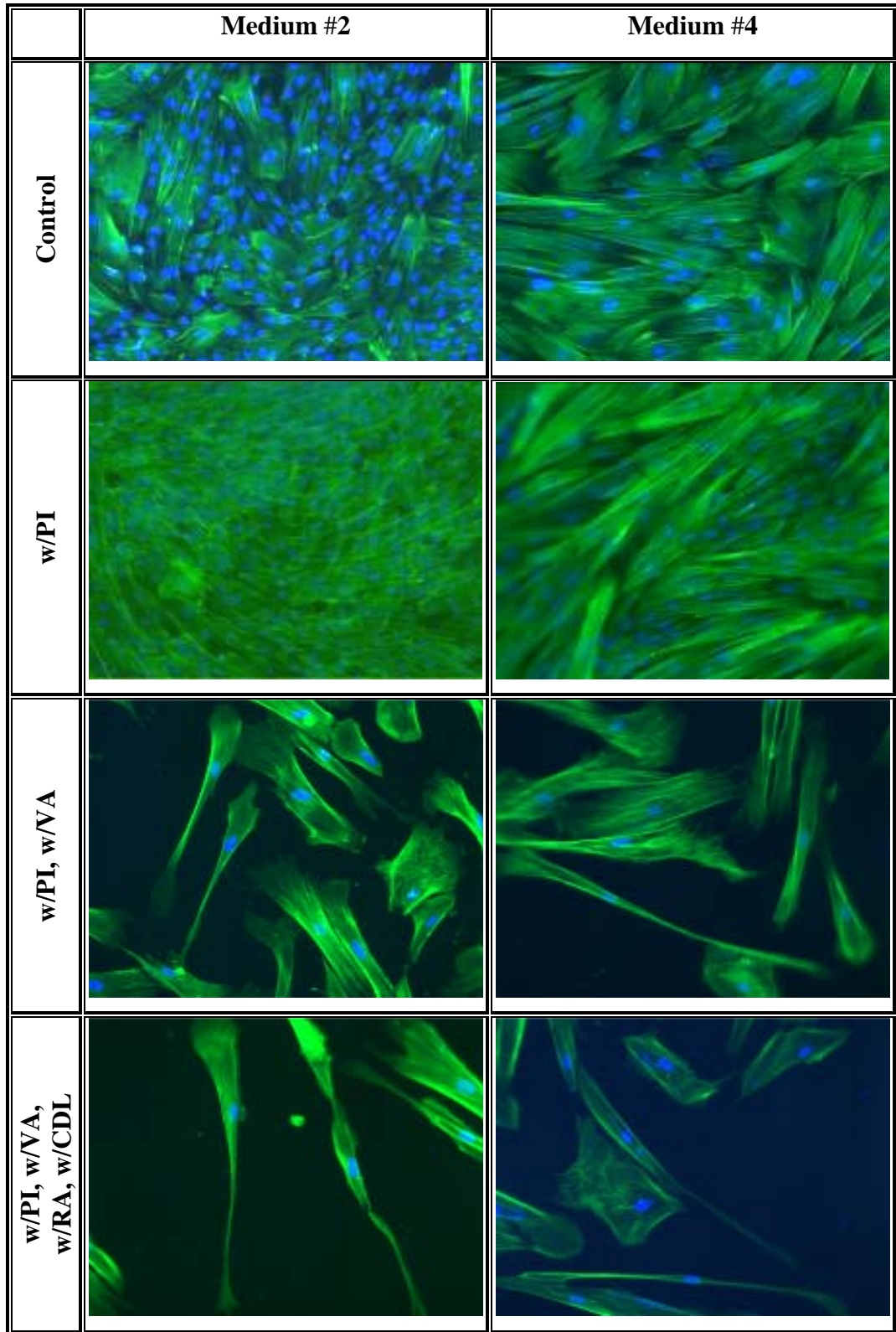
Figure 3.20. Fluorescence micrographs of Phalloidin-FITC and DAPI stained Wharton's Jelly MSCs on laminin1 coated TCPS (x100)
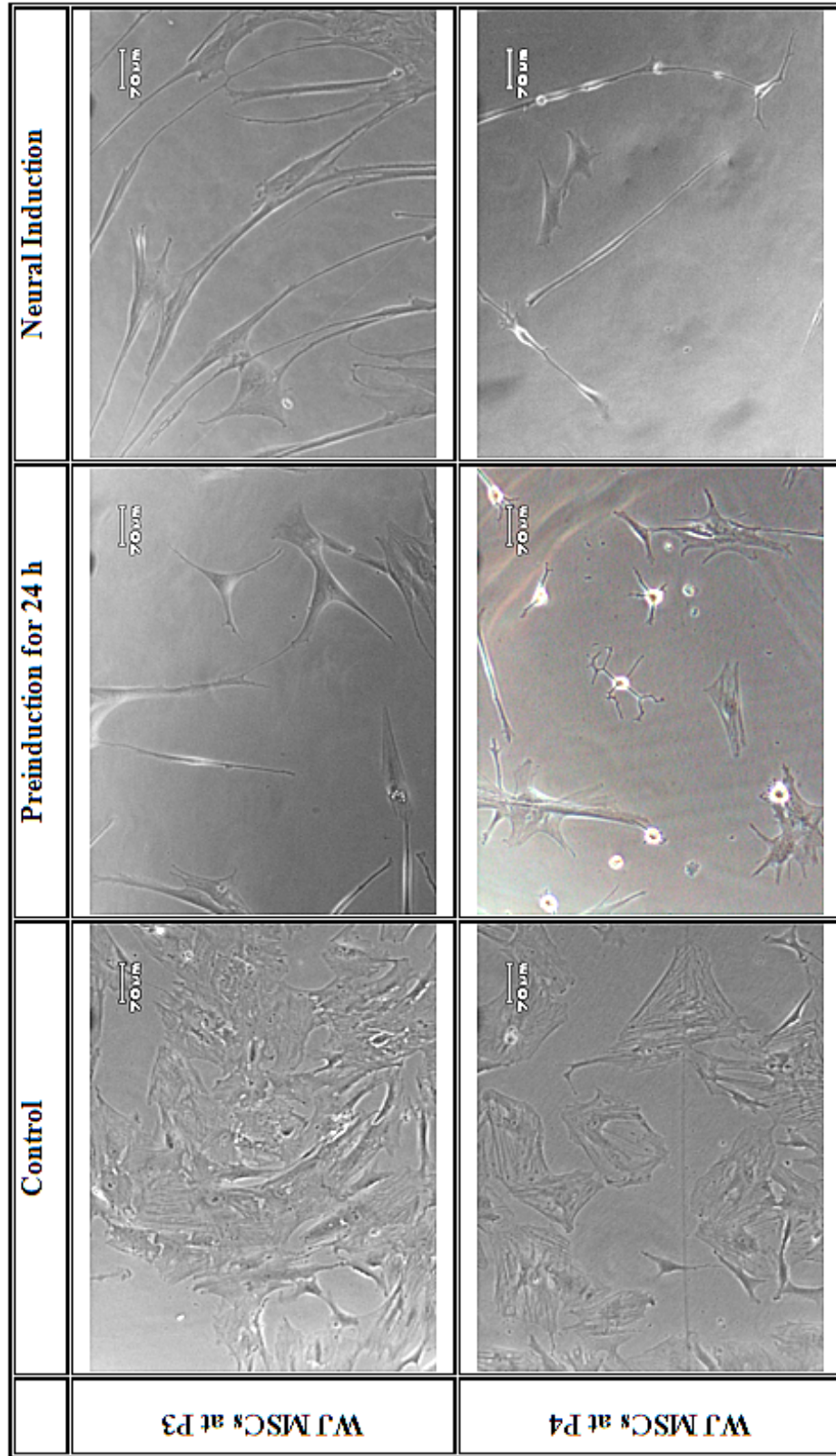
Figure 3.21. Light microscopy images of WJ MSCs (seeded at P3 and P4 on laminin1 coated 24 well plate) cultured with growth medium as a control, cultured with PI medium containing VA for 24 h, and following preinduction cultured with neural induction medium (contains 2 mM VA, 50 ng/mL IGF1, 2% B27) in the absence of FCS for 4 days (x 100).

3.2.1.3.2. Gene Expression of MSCs Analyzed by RT–PCR upon Neural Induction

As mentioned in section 3.2.1.1.5 the expression of genes of early neural proteins and/or transcription factors would give a clue about the molecular mechanism of neural differentiation and the protocol to be applied for induction.

Isolated WJ MSCs were analyzed for their expression of neural specific markers. Human neuroblastoma cell line was used as a control for optimization even the sequences of PCR primers used in this part were same with the ones used in section 3.2.1.1.5 (Figure 3.22). Some of the specific neural gene products were found to be expressed in neuroblastoma cell line such as nestin, Nurr 1, RARA, GFAP and slightly expressed MAP2.

RT-PCR results (Figure 3.22) revealed that undifferentiated human WJ MSCs (cultured in medium #4) at P2 and P3 expressed RARA and slightly GFAP, especially at P3. Thus, the expression profiles of WJ MSCs at P2 and P3 were very similar. However, this profile was slightly changed at passage 4. Besides RARA and GFAP, the faint expressions of nestin and Nurr 1 appeared at P4. Upon the determined neural differentiation cells expressed the same neural markers with MSCs at P4, but RARA expression was decreased.

There were controversial results about the expression of neural markers by human MSCs (Bossolasco et al, 2005, Dezawa et al., 2004, Hermann et al., 2004, Jeong et al., 2004, Tao et al., 2005). In a similar way, in this study, the expressions of the neural markers were different than those results in section 3.2.1.1.5. Most of the markers were not expressed by isolated WJ MSCs at METU (Figure 3.22), while they were expressed during similar studies in the USA (Figure 3.14). The sequences of the primers' and RNA isolation protocols were exactly the same. In general RT-PCR protocol was also the same but the brand of the kit was changed. The kit from Qiagen was used at MGH and Tufts University, Boston (USA), while the kit of Robust was used at METU. In addition, and more importantly the donors of WJ MSCs were different. These could lead to the changes observed in the expression of certain markers.
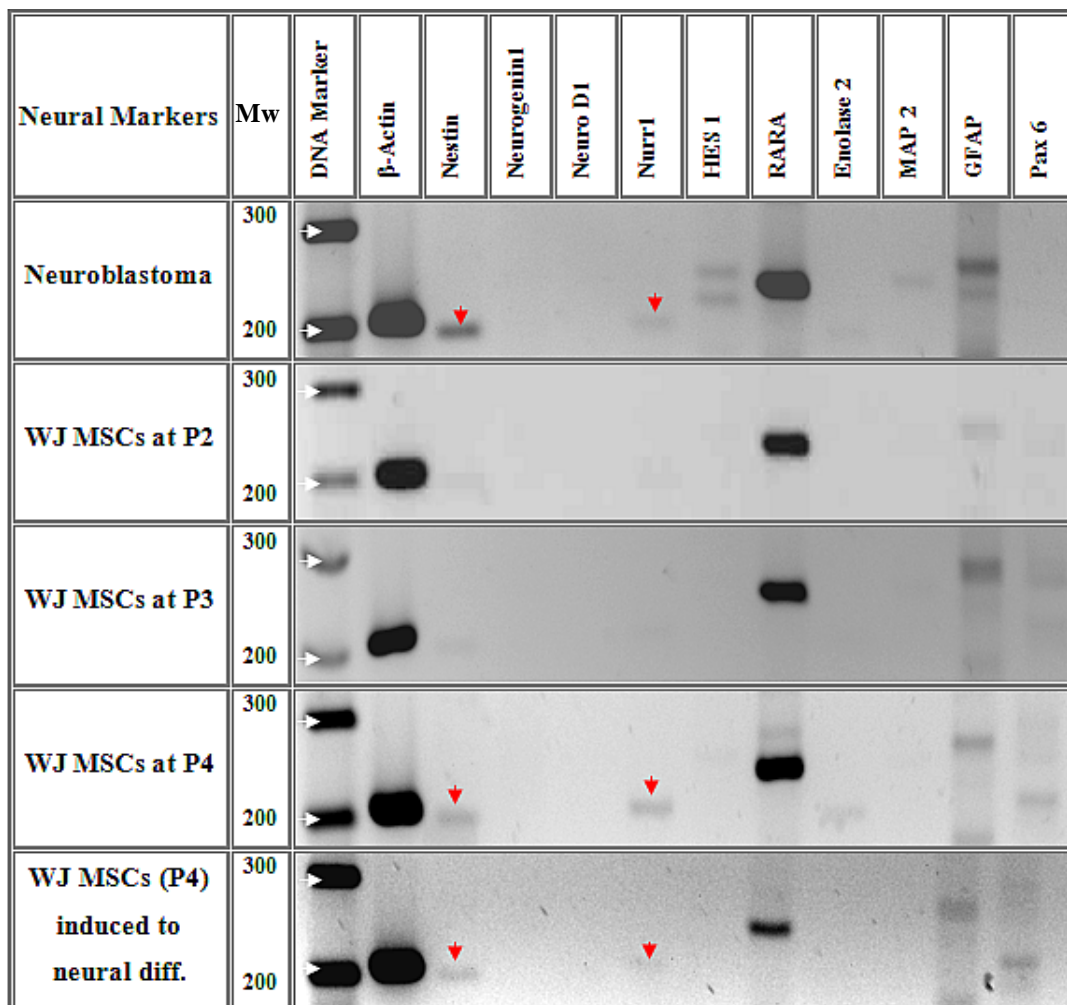
Figure 3.22. RT-PCR results for neural cell specific gene expression in undifferentiated and induced human WJ MSCs. For comparison the expression at the corresponding human neuroblastoma cell line is also presented (30 cycles).

WJ MSCs (P4) induced to neural diff.: WJ MSCs, grown in medium #4 and seeded at P4, were cultured with neural induction medium for 6 days following 24 h preinduction.

3.2.1.3.3. Protein Expression Analysis of MSCs by Immunocytochemistry Upon Neural Induction

Isolated WJ MSCs, cultured in medium #4 and seeded at P4, were induced with preinduction medium (50 µM forskolin, 10 ng/mL human EGF, 10 ng/mL bFGF and with 2 mM VA, without FCS) for 24 h and then cultured 6 more days in a medium containing 2 mM VA, 50 ng/mL IGF1, 2% B27 in the absence of FCS. At the end of the day 7 the cells were fixed with 4% PFA for immunostaining. WJ MSCs cultured with normal growth medium were used as a control since absence of FCS also has an effect on differentiation besides the stimulants. The light microscopy images demonstrated a significant change in the morphology from flat-spread cells to cells with distinctive cell body with thin extensions (Figure 3.23) as indicated in section 3.2.1.3.1.

β-Tubulin III (also designated β-4 chain) is found in the brain and dorsal root ganglia and appears to be localized to neurons of the central and peripheral nervous system, where its expression seems to increase during axonal outgrowth. The expression of the neural marker β-Tubulin III was not detected in the control, undifferentiated, WJ MSCs, whereas it was clearly seen in WJ MSCs induced with neural stimulants (Figure 3.23). After counterstaining with DAPI it was observed that the nuclei of differentiated cells were in the cell body part which was also stained with β-Tubulin III.
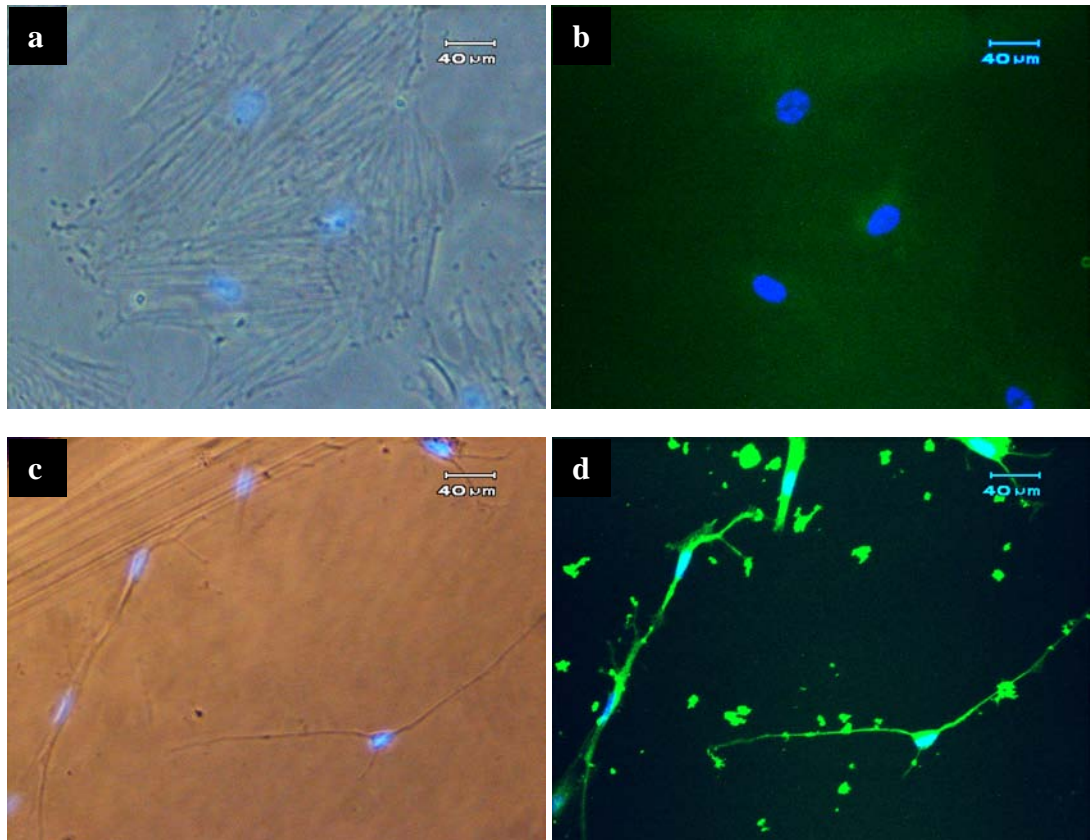
Figure 3.23. Light microscopy a and c) for cellular morphology and b and d) immunofluorescence of β-Tubulin III (Alexa Fluor 488 conjugated) expression of WJ MSCs (medium #4, P4). a-b) medium with no induction (control), and c-d) medium with neural induction for 6 days following preinduction for 24 h (x200).

3.2.2.   *In Vitro* Studies of Mouse NSCs

3.2.2.1.   Evaluation of NSC Differentiation by Microscopy

Balb C mouse NSCs were cultured in a growth medium that consisted of (DMEM)/F12, human transferrin, bovine insulin, chemically defined lipids, sodium selenite, Pen/Strep with mouse EGF. The cells were differentiated into neurons in EGF-free growth medium, whereas they were differentiated into astrocytes when 10% FCS was added to the EGF-free growth medium. The change in fibroblastic morphology of NSC upon induction was examined under light microscope (Olympus IX 70, Japan, with inverted phase contrast attachment) (Figure 3.24). It was observed that the cytoskeleton of cells became thinner upon neural induction (Figure 3.24.b), whereas the cytoskeleton had spread without any thin extension upon astrocyte induction (Figure 3.24.c).

The differentiation of NSC was demonstrated by immunocytochemistry (Figure 3.25). The expression of neural marker β-Tubulin III confirms the differentiation of NSCs into neural cells, whereas astrocyte marker GFAP expression shows the differentiation into astrocytes. β-Tubulin III was expressed by undifferentiated NSCs and widely distributed in the whole cell; however, in undifferentiated state NSCs did not express GFAP (Figure 3.25. a-b). Besides β-Tubulin III expression, NSCs, which were induced to differentiate into neurons, started to express GFAP at a low level (Figure 3.25.c-d). Upon astrocyte induction, the cells expressed GFAP significantly while they could not express β-Tubulin III (Figure 3.25.e-f).
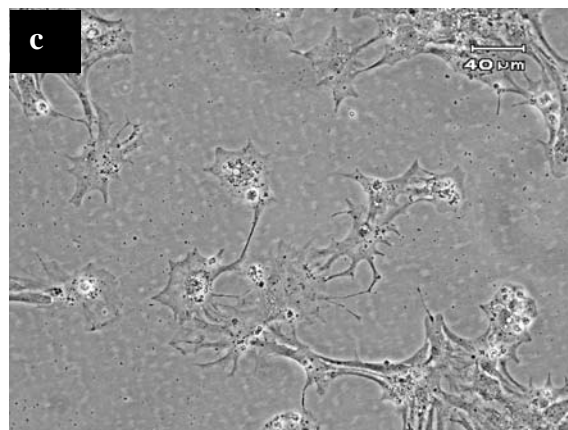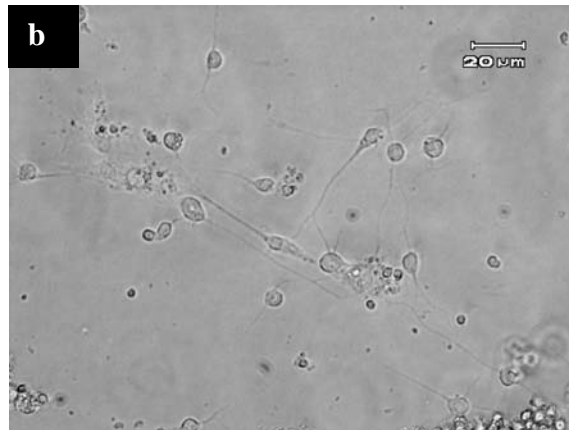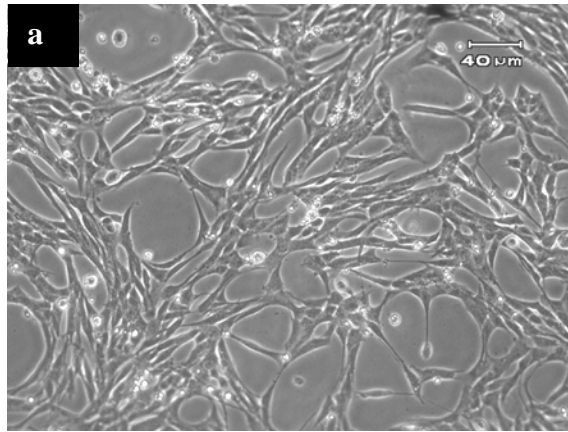
Figure 3.24. Light microscopy images of a) undifferentiated NSCs (x200), b) NSCs after neuron differentiation (x400), and c) NSCs after astrocyte differentiation (x200).
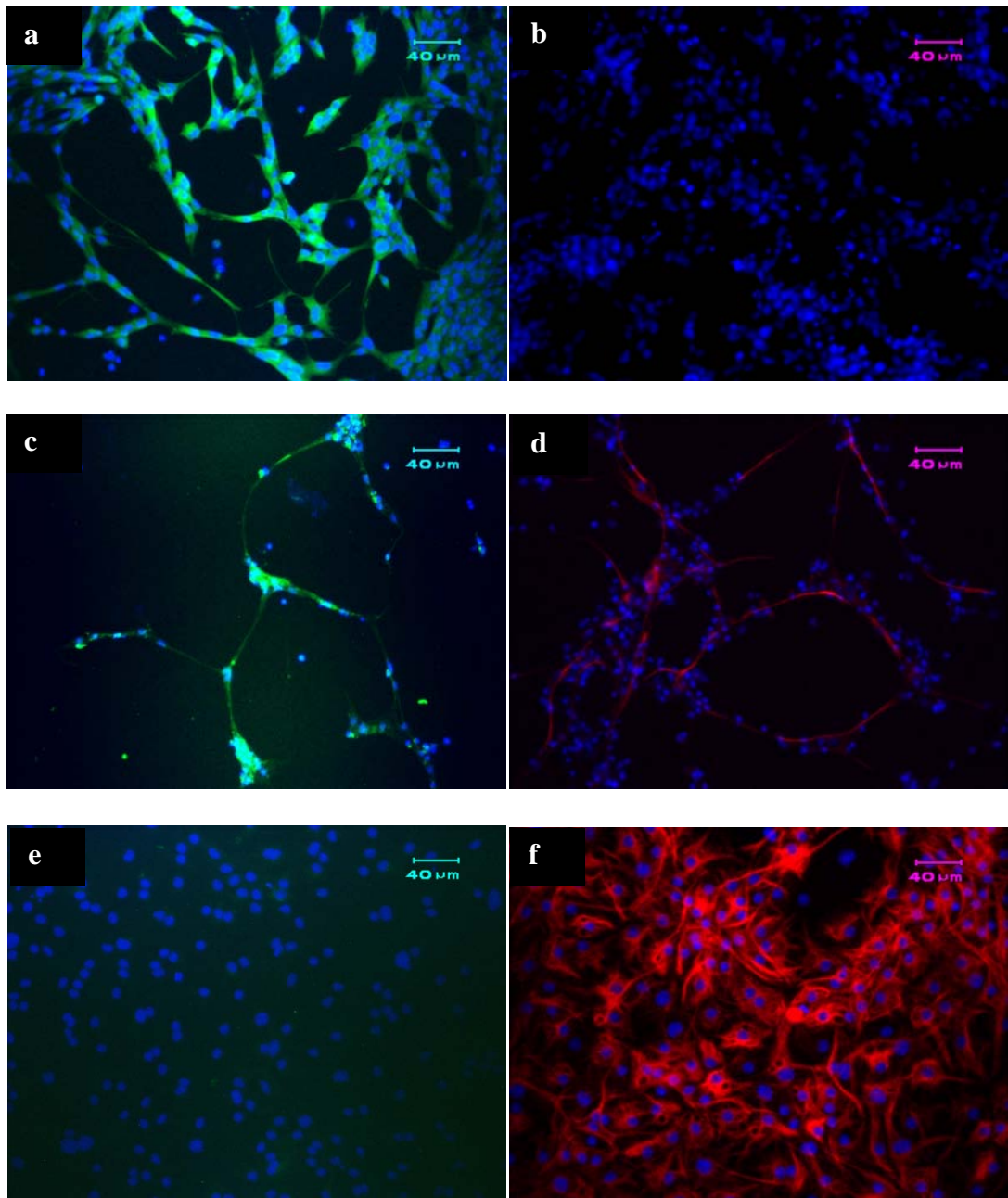
Figure 3.25. Immunofluorescence analysis of neural markers upon NSC differentiation. Undifferentiated NSCs a) β-Tubulin III-488, and b) GFAP-532; NSCs differentiated into neurons c) β-Tubulin III-488, and d) GFAP-532; NSCs differentiated into astrocytes e) β-Tubulin III-488, and f) GFAP-532 (x200).

3.2.3. Behavior of Stem Cells on Electrospun Fibrous Mats and Micropatterned Films

3.2.3.1. Cellular Organization and Alignment on Scaffolds

In order to mimic the native nerve tissue organization, the 3D tubular construct designed would have a porous, micropatterned film on the outer part and an electrospun fiber bundle within the tubular structure (as presented in Figure 2.5). Stem cells would recognize the topography on both components, and would align along the axis of each component of the construct. Human MSCs isolated from umbilical cord matrix and mouse NSCs were seeded and cultured for several days (2-4 days) on micropatterned surfaces having different groove dimensions and on aligned electrospun fibrous mats separately, and their properties such as cytoskeleton and nucleus orientation on these structures was investigated.

Before seeding the WJ MSCs, the two components of the scaffold were coated with laminin1 to enhance neural cell survival, proliferation and differentiation, especially on the fibrous mat on which WJ MSCs would be differentiated into neural cells. WJ MSC cytoskeletal organization on TCPS demonstrated that these cells have an inherent tendency to align when they start to be confluent (Figure 3.26). The reason could be that the cells interacted with other cells and had some guidance. In order to enhance this guidance and ensure it at low densities, MSCs' behavior was examined on micropatterned films having different groove dimensions and also on aligned electrospun mats. The patterns, inclined walls with 2 µm wide grooves and perpendicular walls with 5 µm and 15 µm wide grooves, were used to study the alignment of cells. Compared to TCPS surfaces, MSCs on all the microgrooved films were located in the grooves and aligned parallel to the groove axis (Figure 3.27). However, the cells on inclined wall films were able to fit side by side within the 2 µm wide grooves in some regions, which was made possible by the inclination of the groove going from 2 µm at the bottom to 50 µm at the top (Figure 3.27.a). Thus, it was found that the narrower the grooves (like the perpendicular wall patterns) the more distinct was the cell body and nucleus alignment and elongation within the grooves (Figure 3.27). There was no

significant difference in cell alignment on the perpendical wall films wide 5 µm and 15 µm wide grooves (Figure 3.27.b-c).

Considering the preferred dimension of the final construct (3 cm in length), the micropatterned films with a groove width of 15 µm were used in the later studies. Since the dimensions of the templates used in this study were 1x1 cm^2 and it was not possible to put three films end to end without disconnecting the patterned channels. Therefore, three B1 PDMS replicas were combined and used as a mold to obtain the 3 cm long micropatterned film. Moreover, the outer film part had to be porous. It is seen in Figure 3.28 that cell guidance is preserved on this porous, micropatterned film, even though the depth of the film was slightly less than original. The cytoskeletal and nuclear orientation was clearly seen in the enlarged view of WJ MSC stained with Phalloidin for cytoskeleton and DAPI for nucleus (Figure 3.28.b).
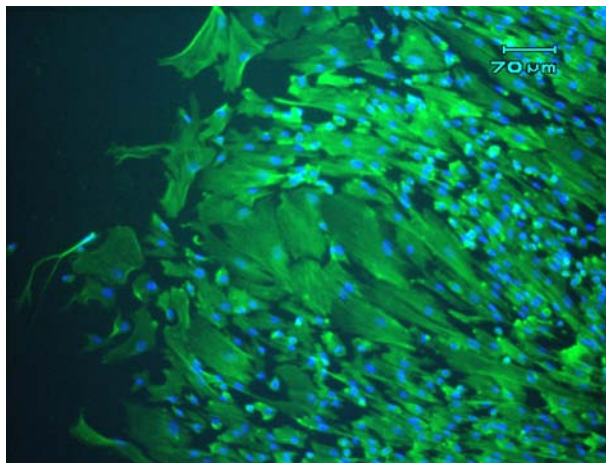
Figure 3.26. Fluorescence micrograph of Phalloidin-FITC and DAPI stained Wharton's Jelly MSCs on laminin1 coated TCPS (x100).
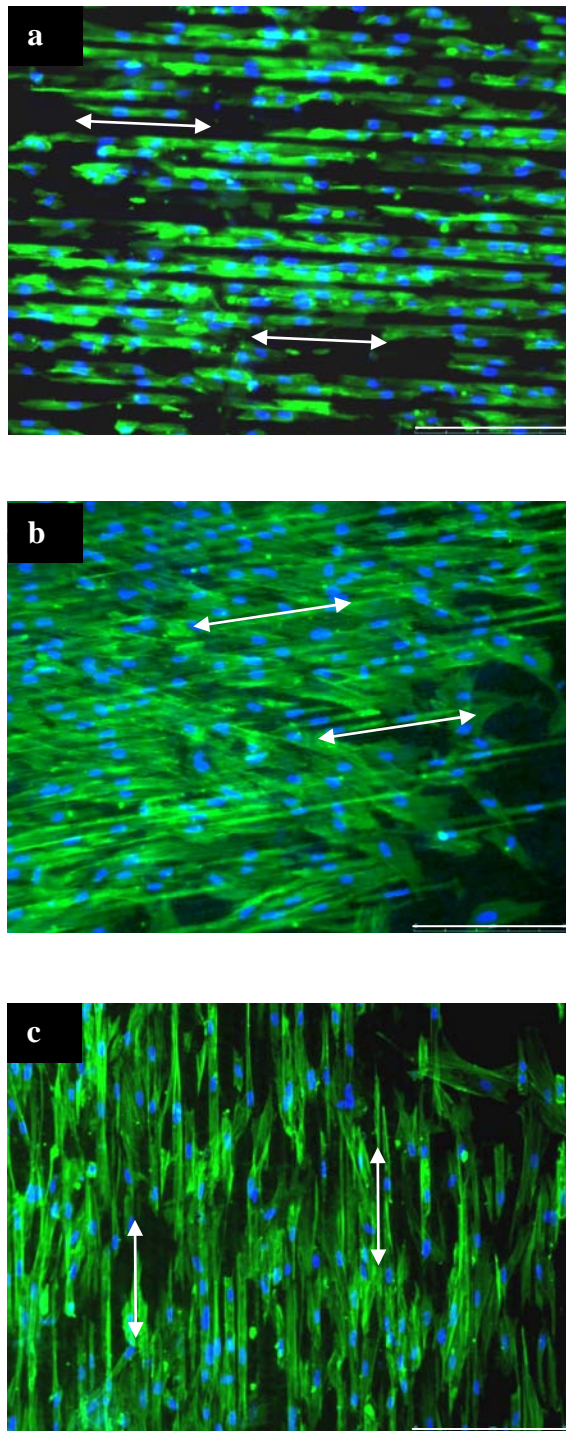
Figure 3.27. Fluorescence micrographs of Phalloidin-FITC and DAPI stained WJ MSCs on PHBV-P(L-D,L)LA micropatterned films. a) inclined-wall film, GW: 2 µm (A4), and b) 90^0-wall films, GW: 5 µm (B1), and c) 90^0-wall films, GW: 15 µm (B1 PDMS) (x100, scale bar 250 µm) (two sided arrow: direction of groove axis). After 2 days of culture.
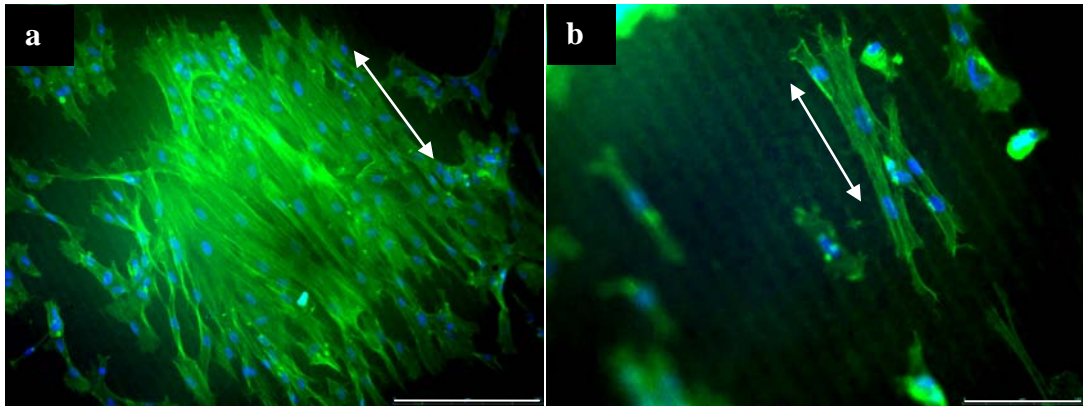
Figure 3.28. Fluorescence micrographs of Phalloidin-FITC and DAPI stained WJ MSCs on laminin1 coated, micropatterned, porous PHBV-P(L-D,L)LA-PLGA film. a) x100, scale bar: 250 µm and b) x200, scale bar: 100 µm (two sided arrow: direction of groove axis). After 4 days of culture.

Fluoresence and confocal microscopy examinations demonstrated that cytoskeleton and nucleus of WJ MSCs were aligned along the electrospun mat following the fiber axis (Figures 3.29 and 3.30). The confocal microscopy examination of Acridine Orange stained WJ MSCs on electrospun fibers gave information about the cell distribution within the mat by taking sectioning in z-direction. The cross-sectional view of the mat showed that the cells were found not just on the surface but also inside the mat. This was not an unexpected result since the cells could penetrate through fibers if the fiber density is suitable (Figure 3.30).
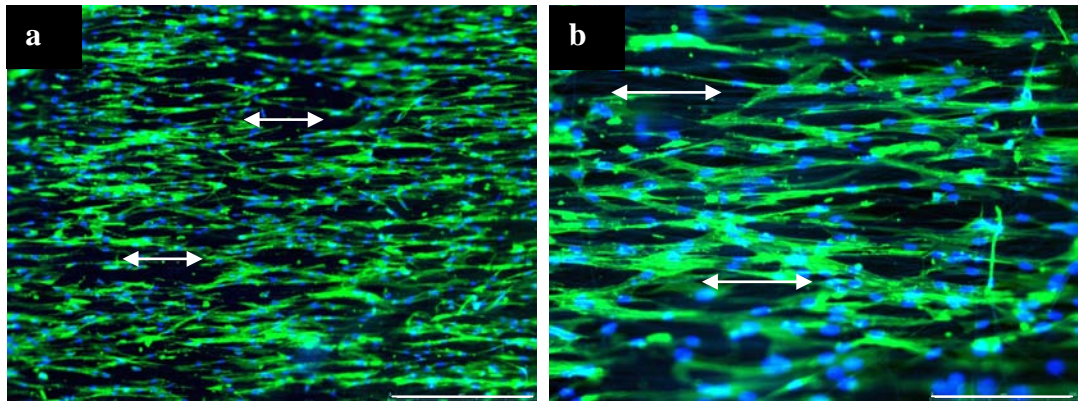
Figure 3.29. Fluorescence micrographs of Phalloidin-FITC and DAPI stained WJ MSC on laminin1 coated PHBV-PLGA electrospun mat a) x50, scale bar:500 µm and b) x100, scale bar:250 µm (two sided arrow: direction of aligned fiber axis). After 4 days of culture.
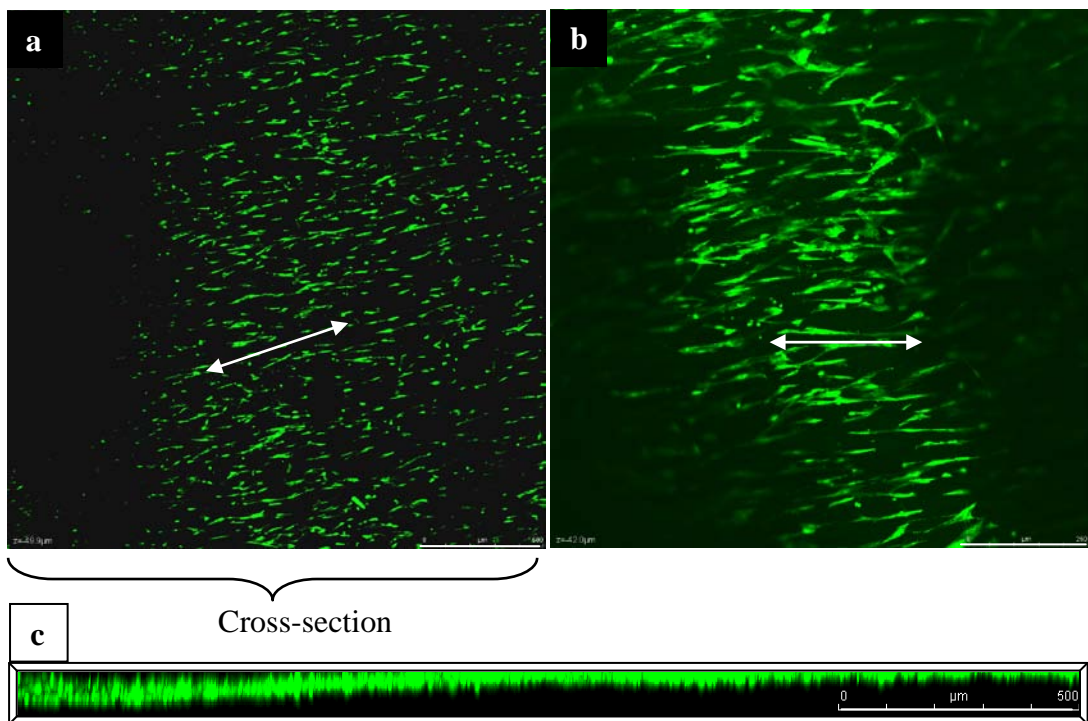
Figure 3.30. Confocal micrographs of Acridine Orange stained WJ MSCs on laminin1 coated PHBV-PLGA electrospun mat. a) x50, scale bar: 500 µm, and b) x100, scale bar: 250 µm. c) cross-section of the cells on the mat (two sided arrow: direction of aligned fiber axis). After 4 days of culture.

Normally, NSCs are loosely adherent cells and require fibronectin to attach even on surfaces like TCPS. Therefore, both micropatterned films and electrospun mats were coated with fibronectin before seeding. NSCs did not have a natural tendency of alignment on non-guiding surfaces like TCPS, and they grew in clusters, especially in crowded regions (Figure 3.31.a). For the cell guidance studies micropatterened films were used. NSCs on inclined wall films were found in and at edges of the grooves but did not align like the ones on perpendicular wall films (data not given). Since these cells were mouse NSCs and their size was smaller compared to human cells, they could respond to patterns with narrower grooves. The single NSC adapted their body to the width of the grooves on the films with a groove width of 5-15 µm and aligned along the groove axis (Figure 3.31.b-c). The micropattern with 15 µm wide grooves (B1 PDMS) was chosen for further studies taking into consideration a certain enlargement of cell upon differentiation into astrocytes. For NSC studies stem cells would be differentiated into astrocytes to support and enhance NSCs'differentiation into neurons on the electrospun mats. Similar to WJ MSCs, NSC alignment was observed on porous micropatterned surfaces (Figure 3.32). The cytoskeleton and nucleus staining with Phalloidin-DAPI and Acridine Orange showed that these cells could align in clusters along the fiber orientation on mats (Figures 3.33 and 3.34). The penetration of NSCs into the mat could be seen from the cross-sections of the 3D images of the mats (Figure 3.34).
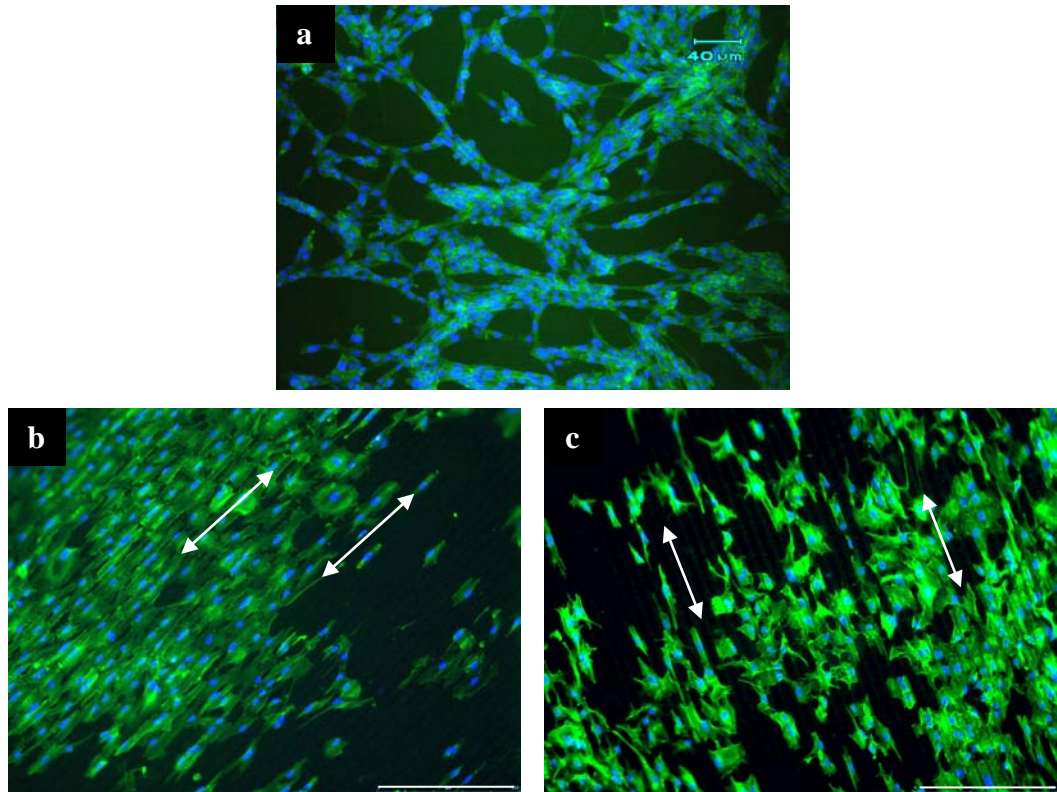
Figure 3.31. Fluorescence micrographs of Phalloidin-FITC and DAPI stained NSCs on fibronectin coated. a) TCPS (x200), PHBV-P(L-D,L)LA micropatterned films: b) GW: 5 µm, and c) GW: 15 µm (x100) (two sided arrow: direction of groove axis). After 5 days of culture in appropriate media.
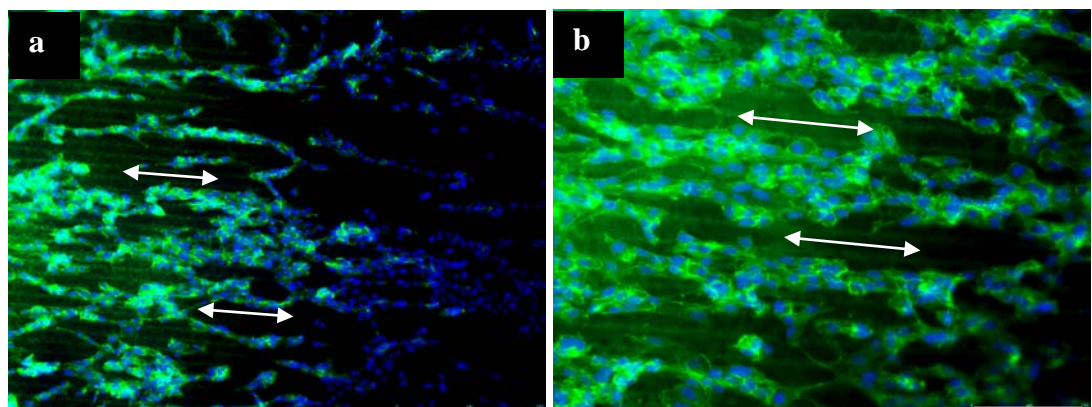

Figure 3.32. Fluorescence micrographs of Phalloidin-FITC and DAPI stained NSCs on fibronectin coated, micropatterned, porous PHBV-P(L-D,L)LA-PLGA film a) x100, scale bar: 250 µm, and b) x200, scale bar: 100 µm (two sided arrow: direction of groove axis). After 4 days of culture.
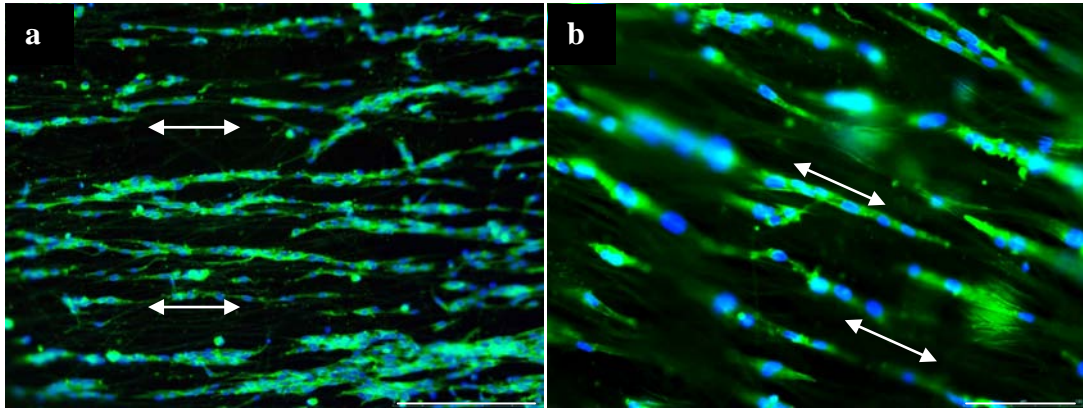
Figure 3.33. Fluorescence micrographs of Phalloidin-FITC and DAPI stained NSCs on fibronectin coated PHBV-PLGA electrospun mat. a) x50, scale bar: 500 µm, and b) x100, scale bar: 250 µm (two sided arrow: direction of aligned fiber axis). After 4 days of culture.
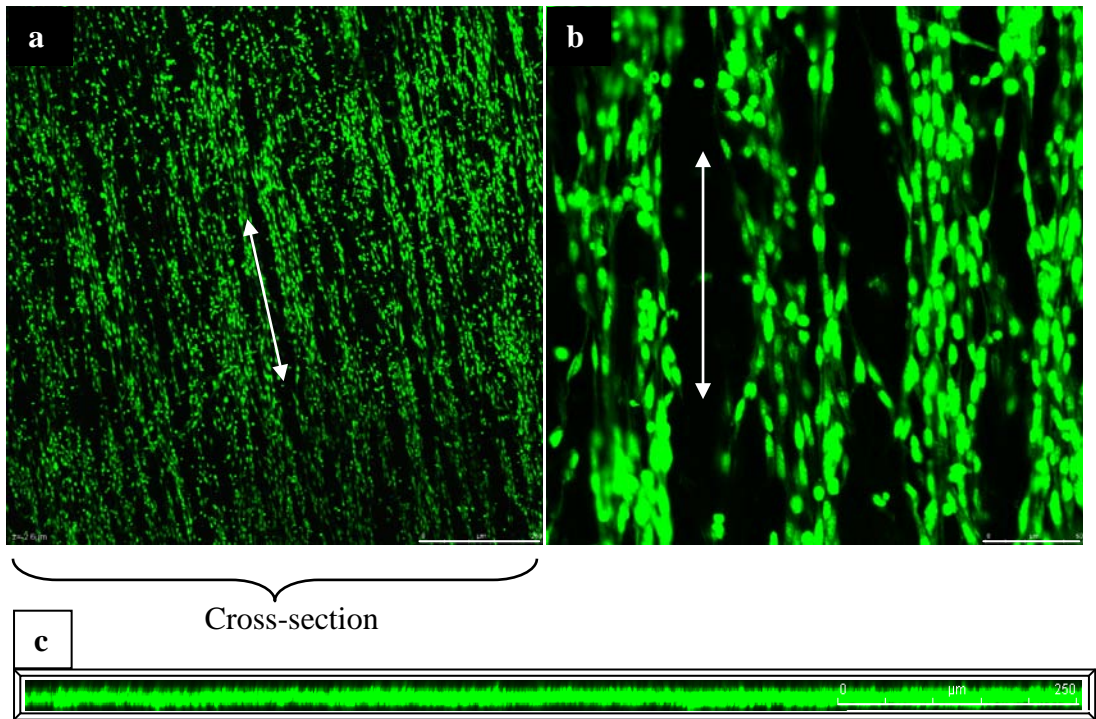

Cross-section

Figure 3.34. Confocal micrographs of Acridine Orange stained NSCs on fibronectin coated PHBV-PLGA electrospun mat. a) x100, scale bar: 250 µm, and b) x400, scale bar: 250 µm. c) cross-section of the cells on the mat. (two sided arrow: direction of aligned fiber axis). After 4 days of culture.

3.2.3.2.   Proliferation and Cell Activity of Stem Cells on Scaffolds

The cellular activity and the proliferation of stem cells on the two-component scaffold were determined with MTS assay. Absorbance values recorded from MTS assay were converted to cell number using calibration curve for each cell type and culture conditions (Appendix C). The stem cells were seeded on the films or the mats at a density of $2x\ 10^4$ cells/sample and then MTS was done after one day to determine cell density. In order to observe cell growth and proliferation rate on these surfaces MTS was done on day 7 and 14.

WJ MSCs cultured with medium #2 and medium #4 were seeded on untreated or laminin1 coated, aligned electrospun fibrous mats. MTS results obtained after a day of seeding showed that the actual seeding density was around $2x\ 10^4$ cells for all samples but with some variation especially on fibrous mats (Figures 3.35 and 3.36). This is expected considering the porosity of the mats. The fibrous mat is like a sieve and the cells leak from the mat. The remaining WJ MSCs survive and increase in number by time. It is seen that WJ MSCs could attach and grow on electrospun mats as they do on TCPS with a similar rate, especially the ones cultured in medium #4 (Figures 3.35 and 3.36). A significant increase of MSCs was determined on day 14 on electrospun mats compared to TCPS. WJ MSCs could not find a free space to proliferate on TCPS, whereas they could proliferate within electrospun mats. Even though the WJ MSCs prefer the TCPS some what more than the laminin1 coated surfaces, laminin1 coated surfaces were used in later studies after taking into consideration its positive effects on neural culture and differentiation. WJ MSCs cultured in medium #4 were seeded on laminin1 coated, porous, micropatterned films. Although WJ MSCs on micropatterned films had a lower proliferation rate than the ones on TCPS, these cells could grow and increase in number on patterned surfaces (Figure 3.37). Moreover, the small change in cell number on micropatterned surfaces from day 7 to day 14 could be due to approaching confluency around day 7.
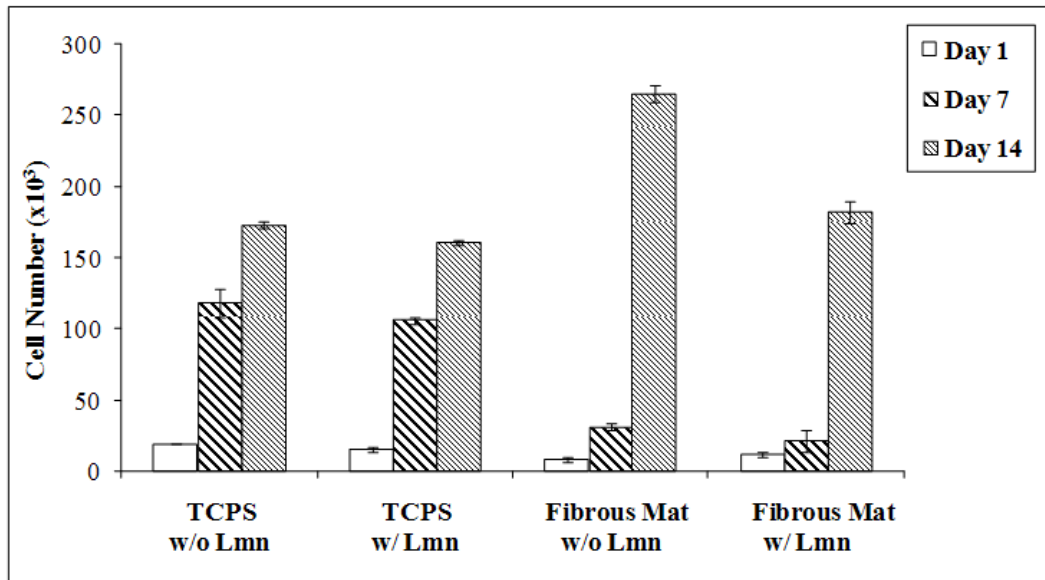
Figure 3.35. Proliferation of WJ MSCs cultured in medium #2 on PHBV5-PLGA electrospun mat compared to TCPS (w/ Lmn and w/o Lmn: surfaces coated with laminin1 and without laminin1 coating, respectively).
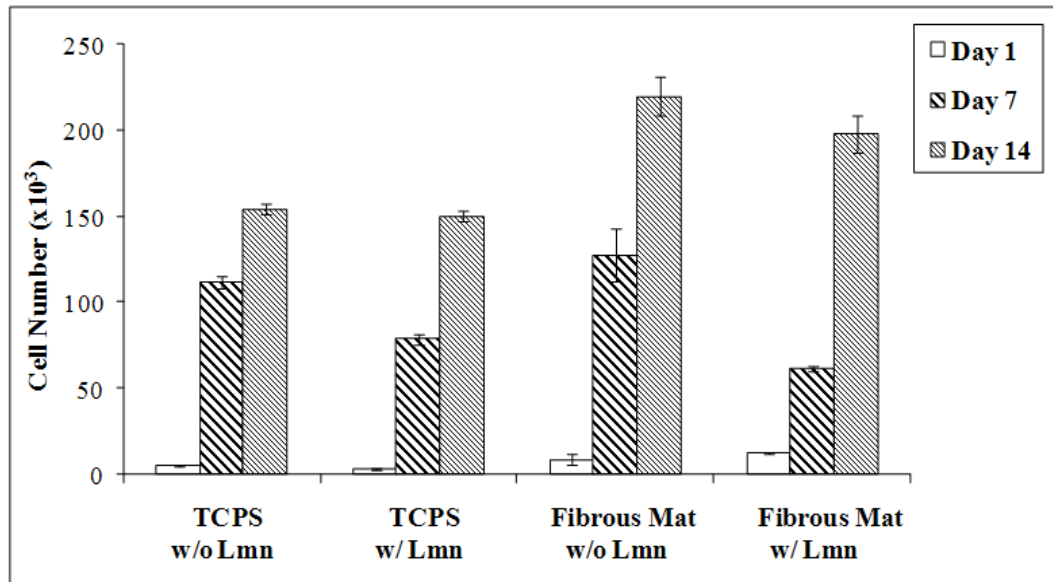
Figure 3.36. Proliferation of WJ MSCs cultured in medium #4 on PHBV5-PLGA electrospun mat compared to TCPS (w/ Lmn and w/o Lmn: surfaces coated with laminin1 and without laminin1 coating, respectively).
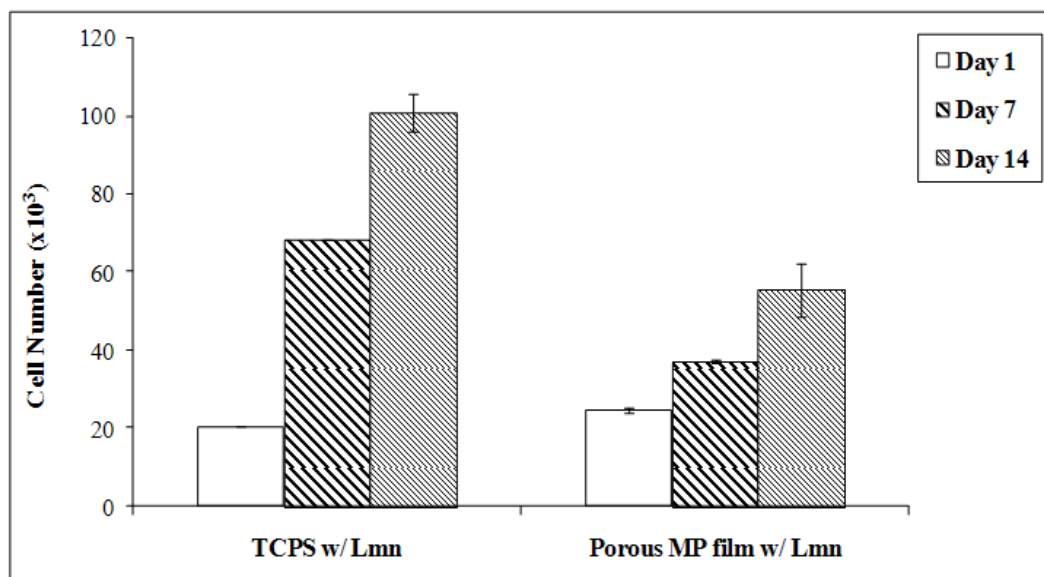
Figure 3.37. Proliferation of WJ MSCs cultured in medium #4 on porous, micropatterned (MP) PHBV-P(L-D,L)LA-PLGA film compared to TCPS (w/Lmn: surfaces coated with laminin1).

NSCs were seeded on fibronectin coated electrospun fibrous mats and porous micropatterned films to investigate their proliferation rate on the surfaces. NSCs were cultured in regular growth medium by maintaining the undifferentiated state, whereas NSCs on micropatterned surfaces and their relative TCPS samples were cultured in regular growth medium for 4 days and then cultured in astrocyte induction medium for the following days. Unlike MSCs results, the undifferentiated NSCs increased in number more on TCPS than on the mats (Figure 3.38). This could be due to that NSCs could grow in clusters on TCPS exceeding monolayer. The other reason might be that these loosely adherent cells attached weakly on the mats due to the insufficient fibronectin coating of the mats, which resulted in a less cell number on the mats. It was observed that differentiation of NSCs into astrocytes arrested the cell growth on both TCPS and the patterned films compared to undifferentiated NSCs (Figures 3.38 and 3.39). The number of astrocytes on micropatterned film was almost same on days 7 and 14 (Figure 3.39). This implied

the confluency reached after day 7 and also the decrease in proliferation rate upon astrocyte differentiation. The arrest in growth by astrocyte induction was also indicated on the cell supplier page (ATCC). According to Figure 3.39, the micropatterning had a positive effect on proliferation even though the cells were differentiated into astrocytes.

MTS results revealed that the undifferentiated WJ MSCs and the undifferentiated and the differentiated NSCs were grown and increase in number on both parts of the final construct.
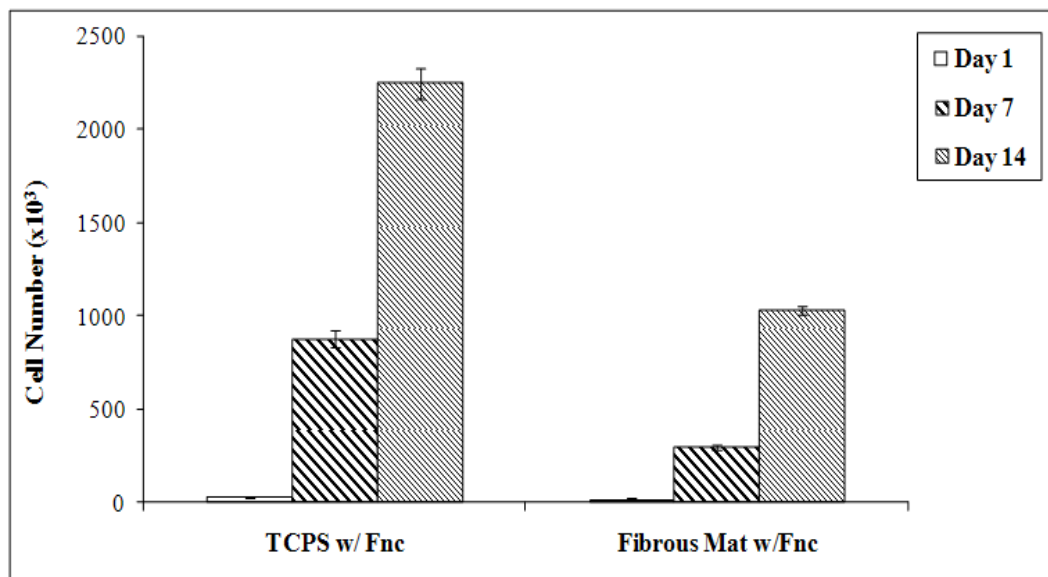
Figure 3.38. Proliferation of NSCs on PHBV5-PLGA electrospun mat compared to TCPS (w/Fnc: surfaces coated with fibronectin).
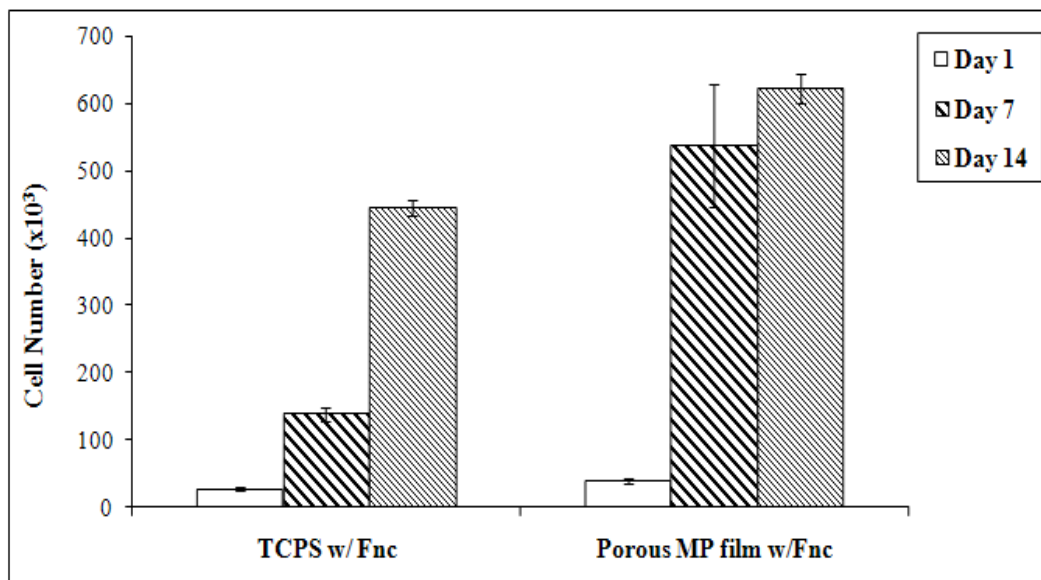
Figure 3.39. Proliferation of NSCs on porous micropatterned (MP) film compared to TCPS (w/Fnc: surfaces coated with fibronectin).

3.2.4. Formation of the Tubular Construct and Stem Cell Behavior in 3D Scaffold

The two components of the 3D structure were the porous micropatterned film and the aligned electrospun fibrous mat. The mat was placed on the patterned film, and then the final tubular structure was constructed by rolling the micropatterned film over the eletrospun mat with the micropatterns facing inside (Figure 3.40). The tubular form was maintained by the aid of elastic bands, glue and/or by suturing. The cross-section of the construct in Figure 3.40 demonstrates the bundle of fibers placed inside the tube and covered with the porous micropatterened film (Figure 3.40). SEM images show that the direction of the aligned fibers was parallel to the groove axis of the micropatterned film without any distruption as desired. This is critical because the cells on each surfaces has to be aligned in the same (axis) direction (the direction indicated with two sided arrows in Figure 3.40).

In the study the final tubular construct was formed after culturing cells separately on the individual parts of the scaffold (Figure 3.41). Isolated human WJ MSCs were seeded at P3 on the laminin1 coated porous micropatterned films (1x3 cm^2) at a density of 7 x 10^4 cells. They were also seeded at P4 on the laminin1 coated electrospun mats (1x3 cm^2) at a density of 10^5 cells. WJ MSCs on the patterned film were cultured in the normal growth medium, while the cells on the mat were induced by the established neural differentiation protocol (Section 3.2.1.3). After taking the cell death upon differentiation into consideration the seeding density for the mats was increased. The cells on each carrier were cultured separately in their indicated media for 7 days, and the tubular construct was prepared by rolling the patterned film over the fibrous mat. The tubular structure was stabilized with elastic bands and glue besides suturing (Figure 3.41). Following the tube construction, the cells were cultured in the differentiation medium for three more days. At the end of the culture, the construct was cut into three pieces (each 1 cm long), and the two components of the construct were separated and the number of cells on them were determined by MTS, and also the cells on each components were analyzed with confocal microscopy for cellular behavior, with RT-PCR for gene expression and with immunocytochemistry for protein expression.
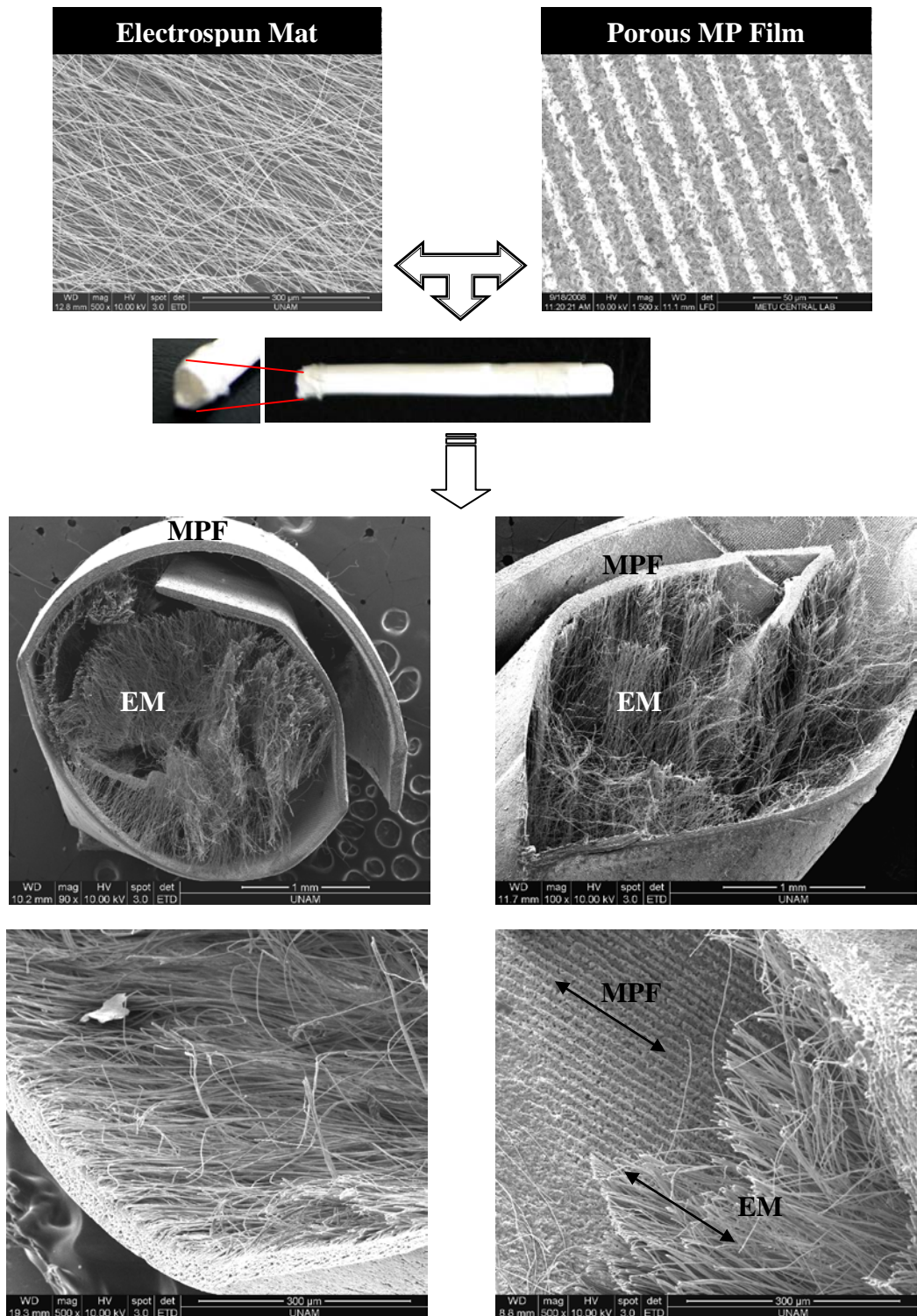
Figure 3.40. Formation of 3D construct and various cross-sectional views of the construct by SEM (EM: electrospun mat, MPF: porous micropatterned film)
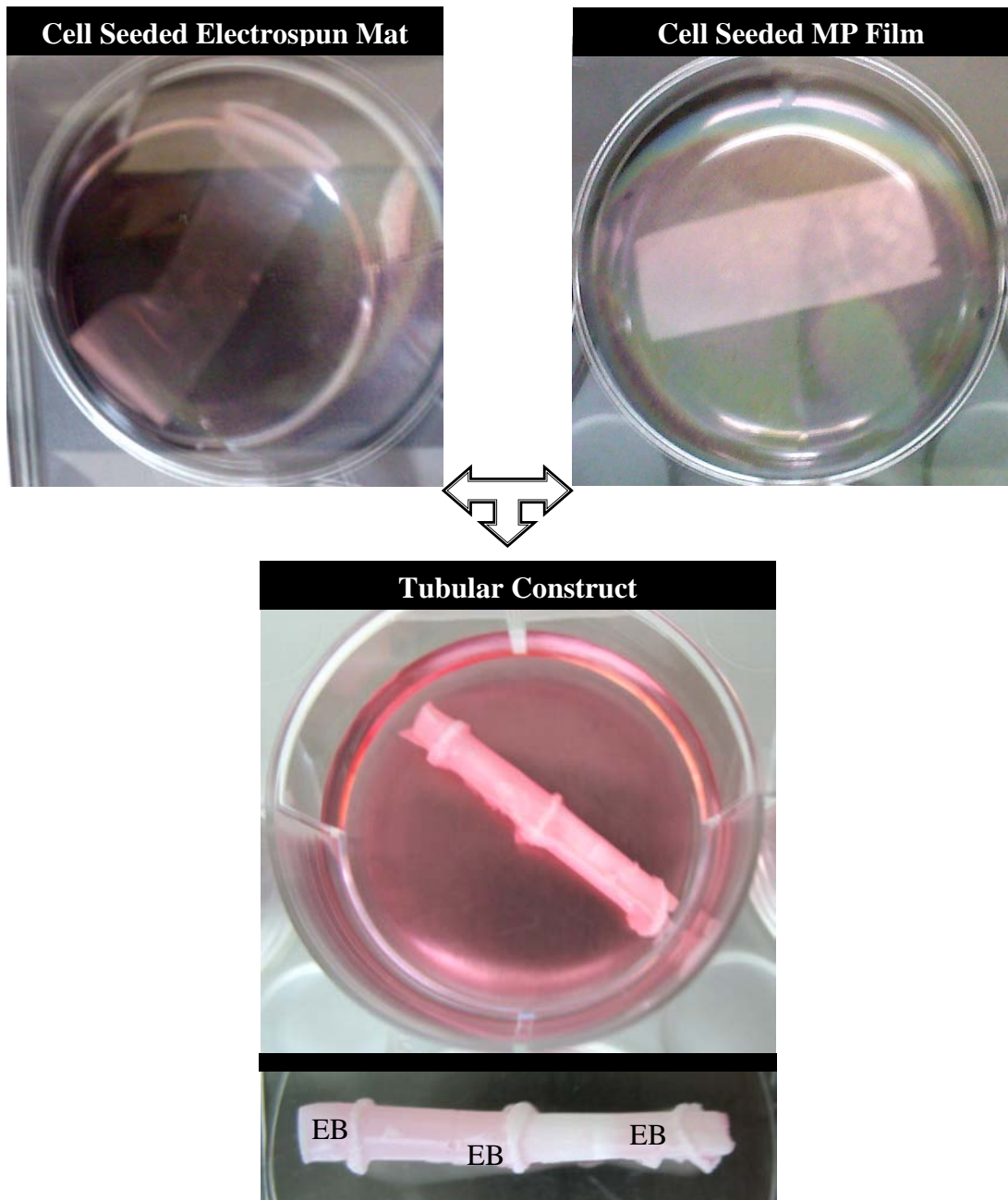
Figure 3.41. The cells were cultured separately on the micropatterned film and the fibrous mat. Then 3D tubular construct was formed by the rolling micropatterned film over the fibrous mat and the tube form was stabilized with elastic bands (EB) and a glue.

The viability of MSCs at each step of tube formation was quantified by MTS assay. The cell numbers given in Table 3.6 belong to one third of the original construct. According to MTS results, rolling the carriers into tubes did not affect the cell viability; however, the cell culturing in the tubular construct in the diffentiation medium for three more days led to a substantial decrease in cell viability (by 50%) on both micropatterned films and electrospun mats. These results showed that the over culturing in the differentiation medium led to cell death, which was expected because it was mentioned that differentiation protocol kills the cells, only some of them can survive like on TCPS. It would be better to implant these constructs just after tube formation. The cell viability after culturing cell in the tubular construct for 3 days was qualitatively shown by confocal microscopy of Acridine Orange stained cells (Figures 3.42 and 3.43). It was observed that the cells could still be found on electrospun mats and patterned films without any change in their alignment. Moreover, the cross-sectional view of electrospun mat proved the continued presence of cells within the fibrous mat (Figure 3.42.c).

RT-PCR and immunocytochemistry studies were carried out to investigate the differentiation of WJ MSCs into neural cells on the electrospun mat while on the micropatterned films the cell would be retained in undifferentiated state. The appearance of nestin and Nurr1 expression like the ones in differentiated cells in section 3.2.1.3.2 would be an indicator of neural differentiation (Figure 3.44). On the other hand, the cells on the patterned film showed similar expression with undifferentiated MSCs as expected. To support the RT-PCR results the expression of neural protein β-Tubulin III was examined by fluorescence microscopy. It was observed that the neural induced MSCs on the fibers intensively expressed this neural marker, while it was slightly expressed by the MSCs on the patterned films (Figures 3.45 and 3.46). Moreover, the neural morphology with thin bipolar extensions was clearly seen in Figures 3.45. c-d.

Table 3.6. Number of WJ MSCs on the micropatterned film and the fibrous mat before and after tube formation and after culturing in tubular form for 3 days (n=2)

WJ MSCs	Micropatterned Film	Electrospun Mat
Before tube formation	35 898 ± 3 740	19 765 ± 1 002
After tube formation	34 262 ± 1 908	31 677 ± 1 645
Cultured in tube for 3 days	16 234 ± 88	15 717 ± 117
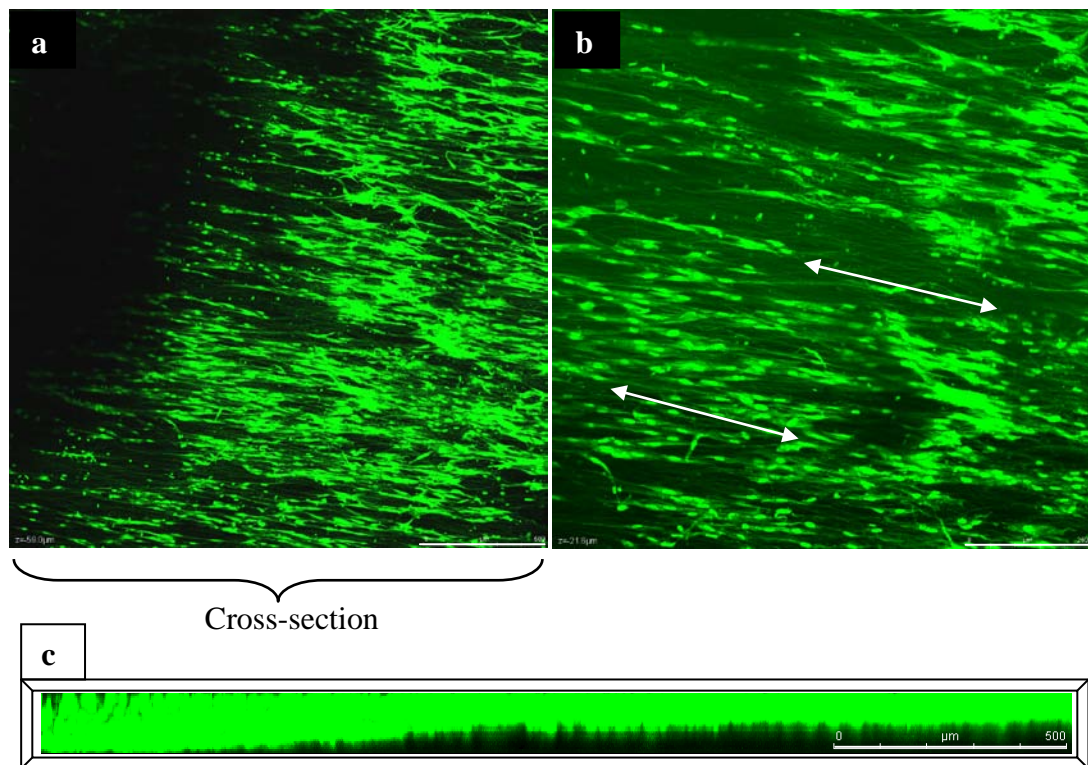
Cross-section

Figure 3.42. Confocal micrographs of Acridine Orange stained WJ MSCs on the electrospun mat cultured for 3 days following tube formation. a) x500, scale bar: 500 µm, and b) x100, scale bar: 250 µm, and c) is the cross-section of (a) (two sided arrow: direction of aligned fiber axis).
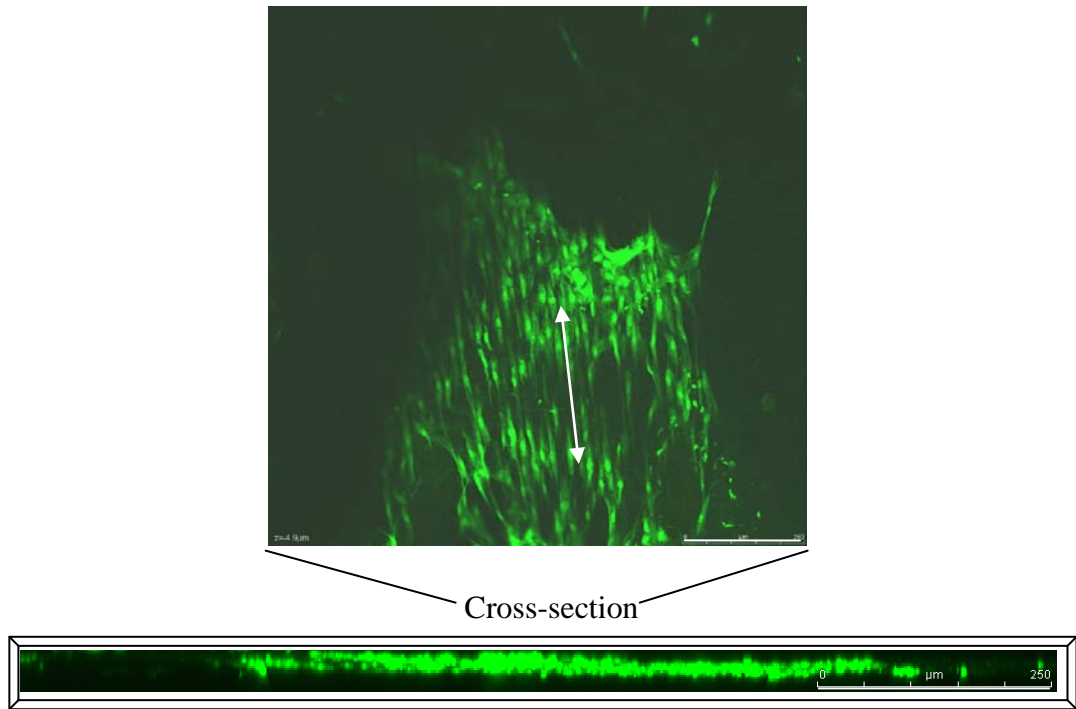
Figure 3.43. Top and side view confocal micrographs of Acridine Orange stained WJ MSCs on the porous micropatterned film cultured for 3 days following tube formation (x100, scale bar: 250 µm) (two sided arrow: direction of groove axis).

Figure 3.44. RT-PCR results for neural cell specific gene expression by the WJ MSCs on the components of the construct (30 cycles).

123
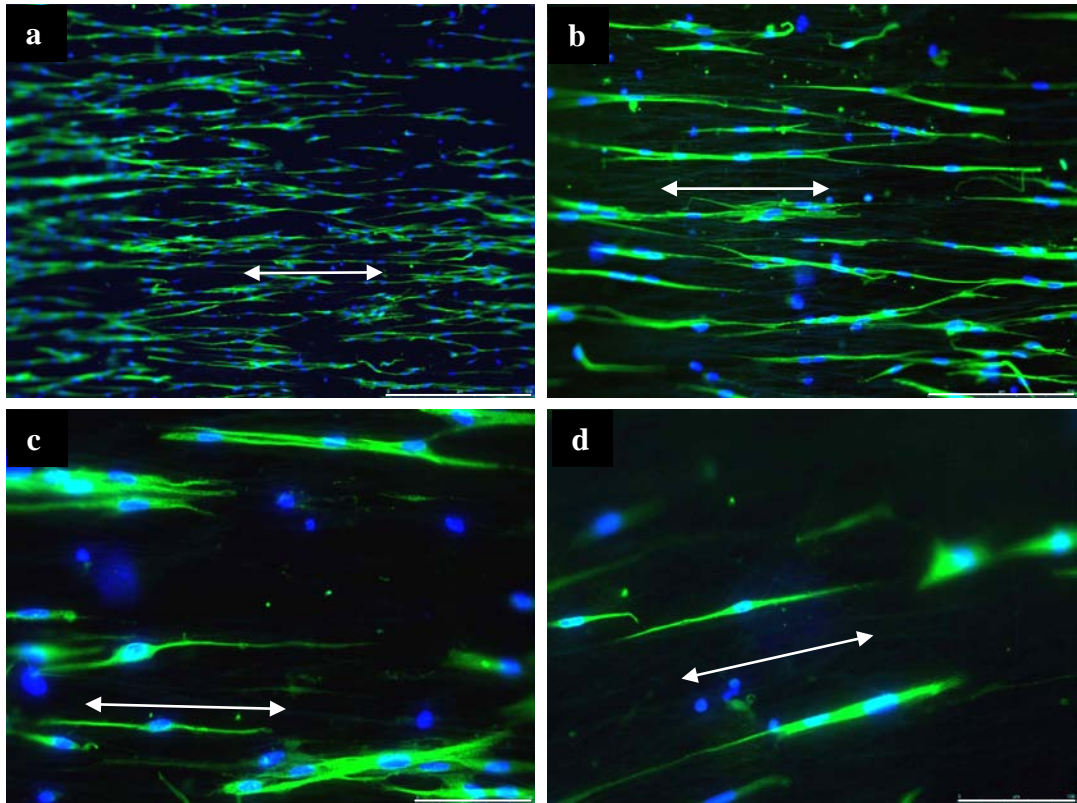
Figure 3.45. Immunofluorescence analysis of β-Tubulin III expression of WJ MSCs on the electrospun mat at the end of 10 day of culture: a) x50, scale bar: 500 µm, b) x100, scale bar: 250 µm, and c and d) x200, scale bar: 100 µm (two sided arrow: direction of aligned fiber axis).
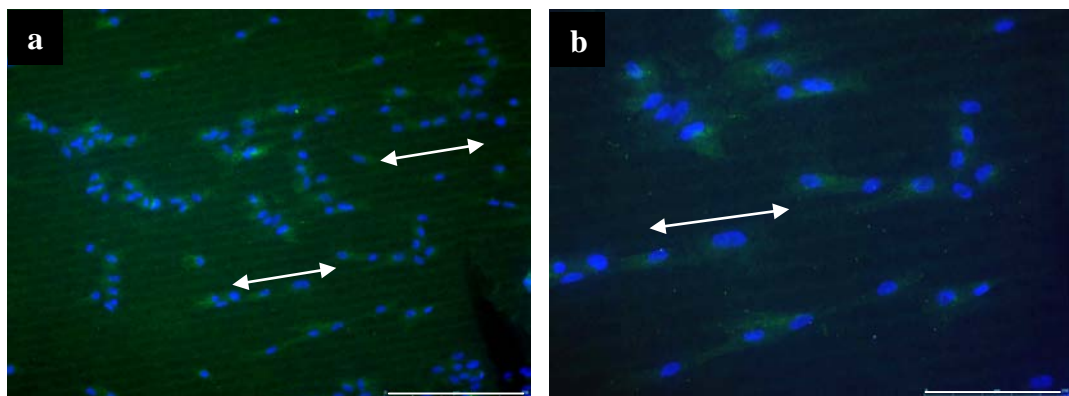
Figure 3.46. Immunofluorescence analysis of β-Tubulin III expression of WJ MSCs on the porous micropatterned film at the end of 10 day of culture: a) x50, scale bar: 500 µm, b) x100, scale bar: 250 µm, and c and d) x200, scale bar: 100 µm (two sided arrow: direction of groove axis).

This construct was designed with MSCs considering that the undifferentiated MSCs on the outer part would support the survival and enhance the differentiation of neural induced MSCs on the mats. Thus, all results showed that the cells could survive and retain alignment in the tubular construct, and the MSCs were found on the micropatterned films while the neural induced MSCs were found on the electrospun mats as desired.

Mouse NSCs were seeded on the fibronectin coated porous micropatterned films ($1 \times 3 \text{ cm}^2$) at a density of 10^5 cells, whereas they were seeded on the fibronectin coated electrospun mat ($1 \times 3 \text{ cm}^2$) at a density of 6×10^4 cells. NSCs on the film were cultured with normal expansion medium for 4 days and then with astrocyte induction medium for 5 days. Meanwhile NSCs on the mat were cultured in expansion medium for 9 days. The seeding density for the films was higher than films considering the decrease in proliferation rate upon differentiation into astrocytes. The cells on each surface were cultured separately in the indicated media, and the tubular construct was formed by rolling patterned film over fibrous mat. The tubular structure was maintained with the use of elastic bands and suturing (Figure 3.41). After the tube construction NSCs were cultured in the neural induction medium for two more days. At the end of the co-culture, the construct was cut into three pieces (each 1 cm long). The electrospun mat and the micropatterned film were separated for analysis of cell proliferation with MTS, confocal microscopy for cellular behavior, and immunocytochemistry for protein expression.

The viability of the cells on each components of the scaffold was determined quantitatively by MTS assay and also demonstrated with confocal microscopy of these cells. It was observed that the cell number on both the interior and exterior of the scaffold decreased significantly upon tubular construction (Table 3.7). However, the increase in cell number on the micropatterned film at the end of co-culture in tube demonstrated that the cells were able to survive and grow in the 3D constructs. The decrease in cell number on the electrospun mat upon co-culture might be due to cell death in the neural induction medium which was also observed on TCPS. The cell viability and guidance was shown in confocal micrographs of cells on patterned film and mats after co-culture (Figures 3.47 and 3.48). The

guided NSCs on the rolled electrospun mat were found throughout the mat (cross-section view in Figure 3.47). Astrocyte induced cells on micropatterned film were able to preserve their alignment (Figure 3.48). It was thought in the design that the alignment of astrocytes on the micropatterned films would enhance the guidance of NSCs on electrospun mat, and also provide some growth factors to support NSC differentiation and survival. The β-Tubulin III expression of NSCs on the electrospun mat demonstrated that the undifferentiated cells were not affected from co-culturing with astrocyte-induced cells in a negative manner (Figure 3.49). The astrocyte induced NSCs expressed GFAP on micropatterned films, which proved their retention of astrocytic character (Figure 3.50). Thus, as was planned the undifferentiated NSCs inside tube on aligned fibers were covered with the astrocytes on the micropatterned films, and could be co-cultured for a few days.

Table 3.7. Number of NSCs on the micropatterned film and the fibrous mat before and after tube formation and after culturing in tubular form for 2 days (n=2)

NSCs	Micropatterned Film	Electrospun Mat
Before tube formation	478 529 ± 8 735	1 090 221 ± 34 627
After tube formation	104 853 ± 9 775	631 985 ± 1 352
Cultured in tube for 2 days	184 706 ± 15 806	118 235 ± 6 655
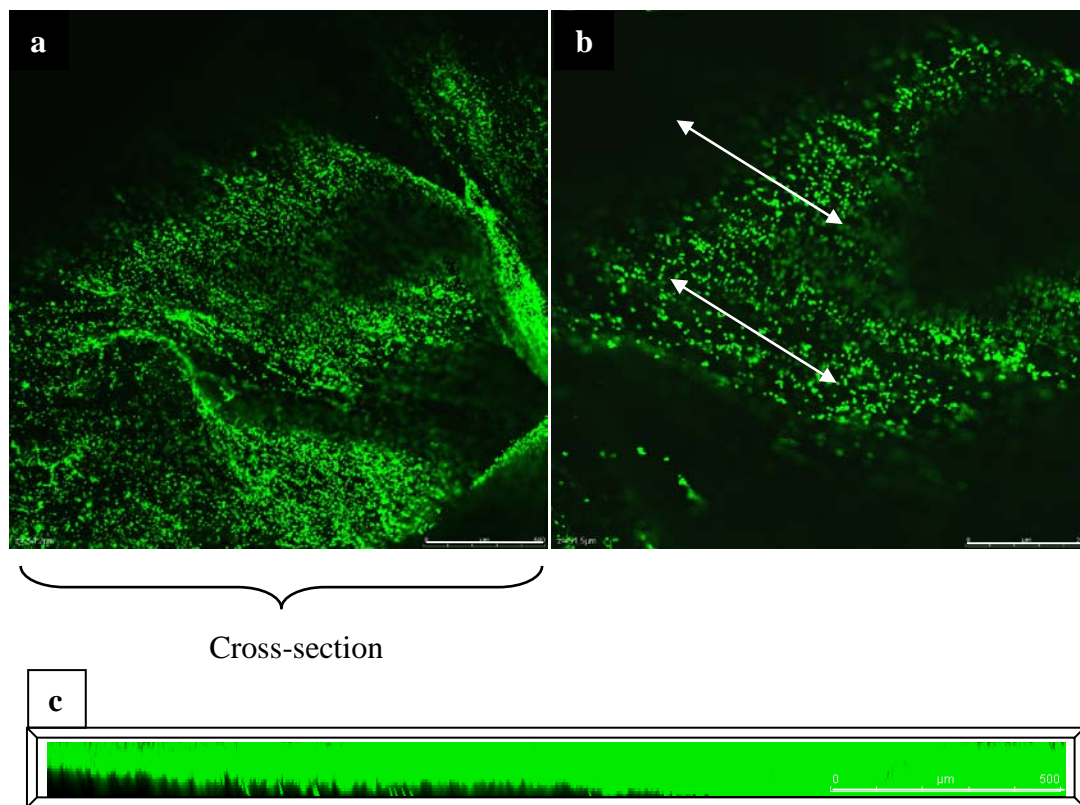
Figure 3.47. Confocal micrographs of Acridine Orange stained NSCs on the electrospun mats cultured for 2 days following tube formation. a) x500, scale bar: 500 µm, b) x100, scale bar: 250 µm, and c) is the cross-section of (a) (two sided arrow: direction of aligned fiber axis).

Cross-section
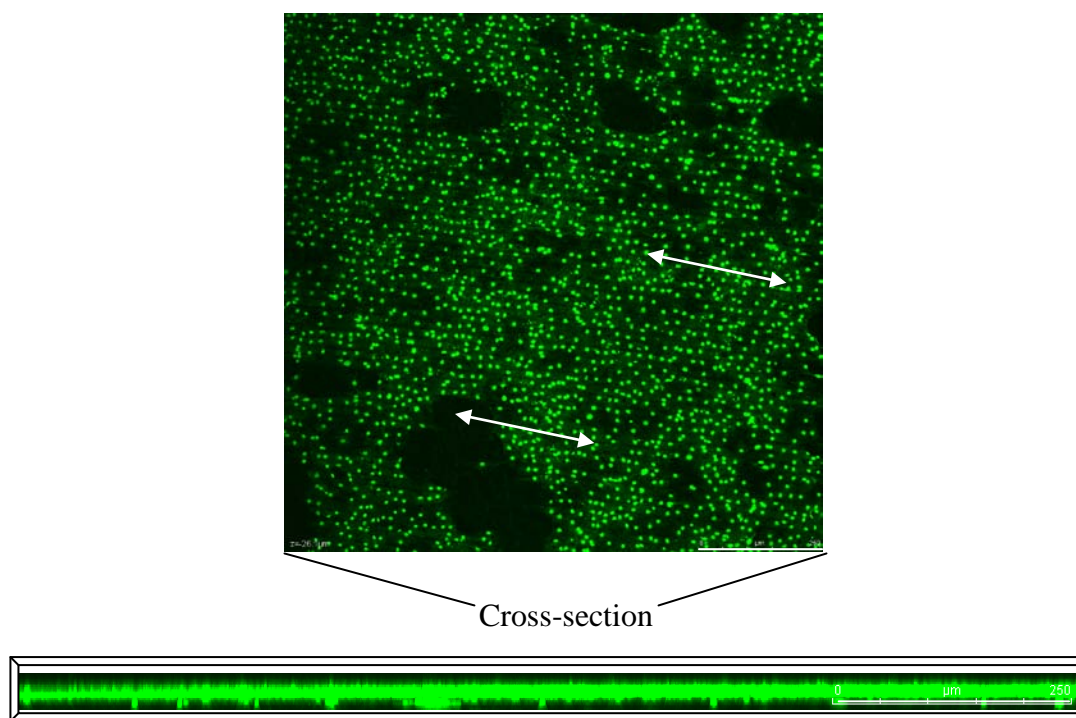
Figure 3.48. Confocal micrographs of Acridine Orange stained NSCs on the porous micropatterned film cultured for 2 days following tube formation. a) x500, scale bar: 500 µm, and b) x100, scale bar: 250 µm (two sided arrow: direction of groove axis).
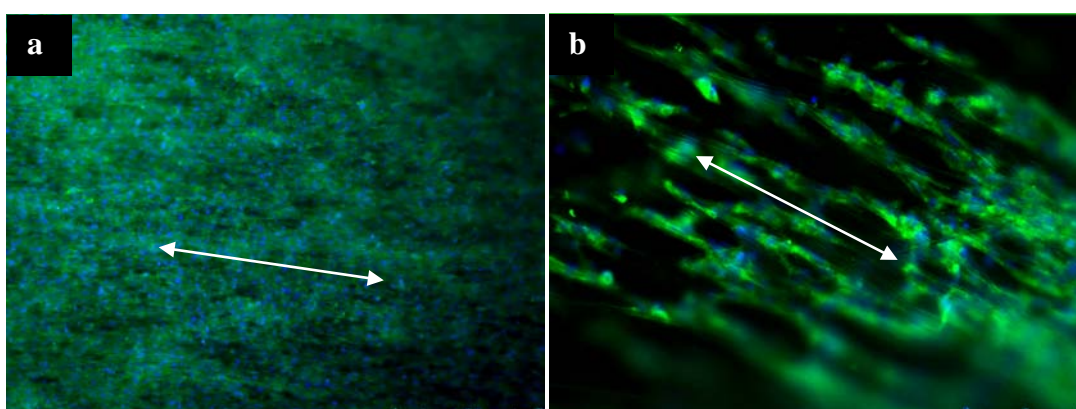
Figure 3.49. Immunofluorescence analysis of β-Tubulin III expression of NSCs on the electrospun mat at the end of 11 days culture: a) x100, scale bar: 250 µm, and b) x200, scale bar: 100 µm (two sided arrow: direction of aligned fiber axis).
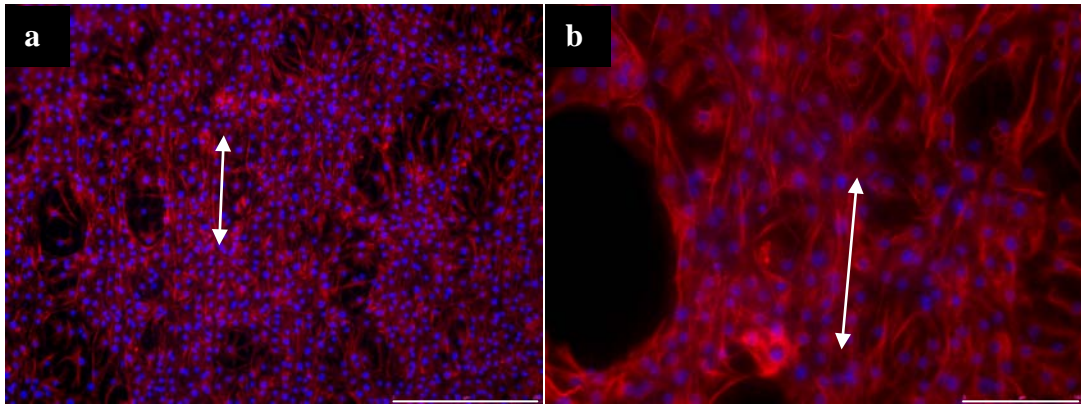
Figure 3.50. Immunofluorescence analysis of GFAP expression of NSCs differentiated into astrocytes on the porous micropatterned film at the end of 11 days culture: a) x100, scale bar: 250 µm, and b) x200, scale bar: 100 µm (two sided arrow: direction of groove axis).

Considering WJ MSCs results the reason for cell death by over culture in tubular structure might seem to be the insufficient nutrient diffusion into the construct. However, the same study carried out with NSCs showed that the cells existed following culturing in the tube. Thus, the decrease in the cell number of WJ MSCs in tubular structure was most probably because of the cell death upon co-culture in neural induction medium. The cells in the tube were cultured in static conditions. To improve and support the results the tubular construct need to be cultured in dynamic conditions or investigated in *in vivo* studies to check its performance.

The studies of the tubular construct formation to mimic nerve tissue using cell sources human MSCs and mouse NSCs revealed that the cells in the appropriate state (undifferentiated or differentiated form) were able to survive in 3D construct. In addition, the cells, which would be neurons, on the electrospun mat were able to retain their alignment following culturing in the tube for a few days. The cell guidance on the other component was also important since they would enhance alignment of the cells on mat as well as support them.

Various 3D nerve tubes were designed by many groups, like porous hollow tubes or tubes with intraluminal channels or nerve guide conduits with internal polymer filaments (Yu and Shoichet, 2005, Zhang et al., 2005b, Lietz et al., 2006, Wang et al., 2006). Besides topographical cues, chemical cues such as laminin derived oligopeptides (Yu and Shoichet, 2005) and biological cues such as support cells (Lietz et al., 2006) were used to obtain an improved nerve tube. However, the nerve tube designs found in the literature possessed only some of the properties that are essential in an ideal scaffold. In the present study, a combination of topographical, chemical and biological cues were brought together to achieve optimum *in vivo* performance. In most of the nerve tube constructs support cells were used to enhance the neurite outgrowth. As a unique approach, besides the presence of support cells, we seeded stem cells on aligned electrospun fibers inside the tubular construct to speed up the healing process.

In the use of 3D scaffolds some key points such as uniform cell seeding over the scaffold and the maintenance of cell viability within the 3D structure should be considered. Schwann cells were extensively used as support cells in 3D scaffolds for nerve tissue engineering. It was revealed in one of the studies that these cells are able to survive for at least 48 h in multiple-channel, biodegradable scaffolds in *in vitro* conditions (Moore et al., 2006). In the present study stem cells derived from both sources (mouse NSCs and humanWJ MSCs) were seeded uniformly and in a specific manner (stem cells on the fibers would be differentiated by chemical compounds and by the help of support cells on the exterior part of the tube). The promising results of the cell viability and cell behavior tests obtained with the designed 3D constructs make it a potential tissue engineered nerve tube for further testing *in vivo*.

CHAPTER 4

CONCLUSIONS

A 3D, biodegradable, polymeric nerve guide was constructed to restore the function of truncated nerve tissue. The construct was composed of two parts: the porous, micropatterned film as the exterior part and the aligned electrospun fibrous mat as the interior part. The final nerve tube was 30 mm in length and 3 mm in diameter.

The patterned film with microgrooves was successfully obtained by solvent casting technique, and the porosity was achieved by leaching out of PEG in distilled water.

Two different cell sources, human MSCs and mouse NSCs, were used in this study. Moreover, human MSCs derived from bone marrow and umbilical cord matrix Wharton's Jelly were characterized at MGH and Tufts U. (USA) and the results obtained by flow cytometry and mesodermal lineage differentiation studies confirmed that these cells had characteristics of MSCs. Their neural gene expression analysis showed that MSCs derived from both cell sources had a potential to differentiate into neural cells.

The behavior of human MSCs and mouse NSCs on the oriented electrospun fibrous mat and on the porous micropatterned films was investigated by examining cellular organization and alignment of cells and determining their proliferation on these surfaces. The cytoskeleton and nuclei of human MSCs and NSCs were aligned along the axis of the grooves on the porous micropatterned films, and also aligned on the electrospun mat along the axis of the fibers. Moreover, the cells were able to penetrate into the mat, and were found to populate the whole mat. The proliferation results showed that both MSCs and NSCs were

able to grow and increase in number on the patterned films and on the electrospun mats.

In order to be used in nerve tissue engineering a 3D nerve tube was needed. This was constructed using human MSCs and mouse NSCs. The results showed that the cells in the appropriate state (undifferentiated or differentiated form) were able to survive within the nerve tube. To mimic nerve tissue with oriented nerve bundles, the cells, which would become neurons, on the electrospun mat had to be well aligned. The cell guidance on the exterior part of the nerve tube was also important since they would enhance alignment of the cells on mat as well as support them. The stem cell behavior in 3D studies demonstrated that the cells on each component of the scaffold were able to retain their alignment after 3D tube formation and following the culturing in this tube for several days.

This approach offers a promise for regeneration of large defects in nerves using stem cells derived from patient's own tissue. Thus, the complications faced in nerve autografts and artificial conduits like immune rejections, donor site morbidity, and limited availability of nerve grafts could be avoided by using the presented stem cell-based tissue engineered guided nerve tubes.

CHAPTER 5

FUTURE PROSPECTS

In the current study, a tissue engineered 3D nerve tube composed of an aligned electrospun fibrous mat and a porous micropatterned polymeric film was constructed using stem cells. The cell viability and guidance in the tubular structure was demonstrated. Preferentially, the differentiated neurons are functional to use in an implant. As a short term improvement, further evaluation of functionality and synaptic reconnections are necessary to confirm the feasibility of the current design. Calcium imaging experiments need to be performed with confocal microscopy to follow calcium flux inside the neurons. Cells within a degradable nerve tube will be loaded with the calcium indicator such as Fluo-3, and the changes in $[Ca^{2+}]$ will be monitored as changes in the relative fluorescence of Fluo-3.

The present studies were carried out under *in vitro* conditions. In order to be used as a tissue engineered product the construct, as a midterm goal, will be tested *in vivo* and its functionality and tissue response will be investigated. Thus, experiments in rats or rabbits will be of interest for future studies.The presence and location of neurons and support cells in the construct will be shown by histological examinations. The functionality will be studied by behavioral assesstment and electrophysiological experiments like action potential measurements.

REFERENCES

Ackery A, Tator C, Krassioukov A. A global perspective on spinal cord injury epidemiology. J Neurotraum. 2004; 21: 1355-70.

Anselme K. Osteoblast adhesion on biomaterials. Biomaterials. 2000; 21(7): 667-81.

Ao Q, Wang A, Cao W, Zhang L, Kong L, He Q, Gong Y, Zhang X. Manufacture of multimicrotubule chitosan nerve conduits with novel molds and characterization *in vitro*. J Biomed Mater Res. 2006; 77A: 11-8.

Bahr M and Bonhoeffer F. Perspectives on axonal regeneration in the mammalian CNS. Trends Neurosci. 1994; 17: 473-9.

Bain G, Kitchens D, Yao M, Huettner JE, Gottlieb DI. Embryonic stem cells Express neuronal properties *in vitro*. Dev Biol. 1995; 168: 342-57.

Bain G, Yao M, Huettner J, Finley M, Gottlieb D. Neuronlike cells derived in culture from P19 embryonal carcinoma and embryonic stem cells. In Culturing Nerve Cells. 2nd Ed. Eds. Banker G and Goslin K, MIT Press, Cambridge, MA; 1998: 189-212.

Bain JR. Peripheral nerve and neuromuscular allotransplantation: current status. Microsurg. 2000; 20: 384-8.

Bellamkonda RV. Peripheral nerve regeneration: an opinion on channels, scaffolds and anisotropy. Biomaterials. 2006; 27(19): 3515-8.

Bertani N, Malatesta P, Volpi G, Sonego P, Perris R. Neurogenic potential of human mesenchymal stem cells revisited: analysis by immunostaining, timelapse video and microarray. J Cell Sci. 2005; 118: 3925-36.

Bieback K, Kern S, Klüter H, Eichler H. Critical parameters for the isolation of mesenchymal stem cells from umbilical cord blood. Stem Cells. 2004; 22: 625-34.

Blondheim NR, Levy YS, Ben-Zur T, Burshtein A, Cherlow T, Kan I, Barzilai R, Bahat-Stromza M, Barhum Y, Bulvik S, Melamed E, Offen D. Human Mesenchymal Stem Cells Express Neural Genes, Suggesting a Neural Predisposition. Stem Cells Dev. 2006; 15: 141-64.

Bossolasco P, Cova L, Calzarossa C, Rimoldi SG, Borsotti C, Deliliers GL, Silani V, Soligo D, Polli E. Neuro-glial differentiation of human bone marrow stem cells *in vitro*. Exp Neurol. 2005; 193: 312-25.

Bruder SP, Jaiswal N, Haynesworth SE. Growth kinetics, self-renewal, and the osteogenic potential of purified human mesenchymal stem cells during extensive subcultivation and following cryopreservation. J Cell Biochem. 1997; 64: 278-94.

Bunge RP. The role of the Schwann cell in trophic support and regeneration. J Neurol. 1994; 242:19-21.

Burlingham WJ, Jankowska-Gan E, Van Buskirk A, Orosz CG, Lee JH, Kusaka S. Loss of tolerance to a maternal kidney transplant is selective for HLA class II: evidence from trans-vivo DTH and alloantibody analysis. Hum Immunol. 2000; 61: 1395-402.

Buzanska L, Machaj EK, Zablocka B, Pojda Z, Domanska-Janik K. Human cord blood-derived cells attain neuronal and glial features *in vitro*. J Cell Sci. 2002; 115: 2131-38.

Campione-Picardo J, Craig J, Sun JJ, McBurney MW. Commitment in a murine embryonal carcinoma cell line during differentiation induced by retinoic acid. Exp Cell Res. 1985; 156(2): 544-52.

Cao QL, Zhang YP, Howard RM, Walters WM, Tsoulfas P, Whittemore SR. Pluripotent stem cells engrafted into the normal or lesioned adult rat spinal cord are restricted to a glial lineage. Exp. Neurol. 2001; 167: 48-58.

Carlstedt T. Nerve fibre regeneration across the peripheral-central transitional zone. J Anat. 1997; 190: 51-6.

Chen G, Ushida T, Tateishi T. Scaffold Design for Tissue Engineering. Macromol Biosci. 2002; 2: 67-77.

Chen J, Altman GH, Karageorgiou V, Horan R, Collette A, Volloch V, Colabro T, Kaplan DL. Human bone marrow stromal cell and ligament fibroblast responses on RGD-modified silk fibers. J Biomed Mater Res A. 2003; 67: 559-70.

Cho KJ, Trzaska KA, Greco SJ, McArdle J, Wang FS, Ye JH, Rameshwara P. Neurons derived from human mesenchymal stem cells show synaptic transmission and can be induced to produce the neurotransmitter substance P by interleukin-1α. Stem Cells. 2005; 23: 383-91.

Chou L, Firth JD, Uitto V-J, Brunette DM. Substratum surface topography alters cell shape and regulates fibronectin mRNA level, mRNA stability, secretion and assembly in human fibroblasts. J Cell Sci. 1995; 108: 1563-73.

Choumerianou DM, Dimitriou H, Kalmanti M. Stem Cells: Promises Versus Limitations. Tissue Eng Part B Rev. 2008; 14 (1): 53-60.

Chow SY, Moul J, Tobias CA, Himes BT, Liu Y, Obrocka M, Hodge L, Tessler A, Fischer I. Characterization and intraspinal grafting of EGF/bFGFdependent neurospheres derived from embryonic rat spinal cord. Brain Res. 2000; 874: 87-106.

Clark P, Connolly P, Curtis ASG, Dow JAT, Wilkinson CDW. Topographical control of cell behaviour: II. multiple grooved substrata. Development. 1990; 108: 635-44.

Colter DJ, Sekiya I, Prockop DJ. Identification of a subpopulation of rapidly self-renewing and multipotential adult stem cells in colonies of human marrow stromal cells. Proc Natl Acad Sci USA. 2001; 98: 7841-5.

Conconi MT, Burra P, Di Liddo R, Calore C, Turetta M, Bellini S, Bo P, Nussdorfer GG, Parnigotto PP. CD105 cells from Wharton's Jelly show *in vitro* and *in vivo* myogenic differentiative potential. Int J Mol Med. 2006; 18: 1089-96.

Denker HW. Potentiality of embryonic stem cells: an ethical problem even with alternative stem cell sources. J Med Ethics. 2006; 32: 665-71.

Devine SM and Hoffman R. Role of mesenchymal stem cell in hematopoietic stem cell transplantation. Curr Opin Hematol. 2000; 7: 358-63.

Dezawa M, Kanno H, Hoshino M, Cho H, Matsumoto N, Itokazu Y, Tajima N, Yamada H, Sawada H, Ishikawa H, Mimura T, Kitada M, Suzuki Y, Ide C. Specific induction of neuronal cells from bone marrow stromal cells and application for autologous transplantation. J Clin Invest. 2004; 113: 1701-10.

Doetsch F. A niche for adult neural stem cells. Curr Opin Genet Dev. 2003; 13, 543-50.

Eguchi Y, Ogiue-Ikeda M, Ueno S. Control of orientation of rat Schwann cells using an 8-T static magnetic field. Neurosci Lett. 2003; 351: 130-2.

Enchanted Learning, Biology, Human Anatomy, The Brain, Brain Cells, http://www.enchantedlearning.com/subjects/anatomy/brain/Neuron, last access date: 06.01.2009.

Ferreira BMP, Zavaglia CAC, Duek EAR. Films of poly(L-lactic acid)/poly(hydroxybutyrate-co-hydroxyvalerate) blends: *in vitro* degradation. Mater Res. 2001; 4 (1): 34-42.

Filippis DL, Lamorte G, Snyder EY, Malgaroli A, Vescovi AL. A novel, immortal, and multipotent human neural stem cell line generating functional neurons and oligodendrocytes. Stem Cells. 2007; 25(9): 2312-21.

Finley MF, Kulkarni N, Huettner J.E. Synapse formation and establishment of neuronal polarity by P19 embryonic carcinoma cells and embryonic stem cells. J Neurosci. 1996; 16: 1056-65.

Flemming RG, Murphy CJ, Abrams GA, Goodman SL, Nealey PF. Effects of synthetic micro- and nano-structured surfaces on cell behavior. Biomaterials. 1999; 20(6): 573-88.

Formhals, A. U. S. Patent 1,975,504 (1934).

Formhals, A. U. S. Patent 2,160,962 (1939).

Formhals, A. U. S. Patent 2,187,306 (1940).

Formhals, A. U. S. Patent 2,323,025 (1943).

Formhals, A. U. S. Patent 2,349,950 (1944).

Fu Y-S, Cheng Y-C, B Lin M-Y, Cheng H, Chu PM, Chou SC, Shih YH, Ko MH, Sung MS. Conversion of Human Umbilical Cord Mesenchymal Stem Cells in Wharton's Jelly to Dopaminergic Neurons *In vitro*: Potential Therapeutic Application for Parkinsonism. Stem Cells. 2006; 24: 115-24.

Gage FH, Ray J, Fisher LJ. Isolation, characterization, and use of stem cells from the CNS. Annu Rev Neurosci. 1995; 18: 159-92.

Gage FH. Mammalian neural stem cells. Science. 2000; 287: 1433-8.

Geiger B, Bershadsky A, Pankov R, Yamada K. Transmembrane crosstalk between the extracellular matrix-cytoskelton crosstalk. Nat Rev Mol Cell Biol. 2001; 2: 793-805.

Geller HM and Fawcett JW. Building a bridge: engineering spinal cord repair. Exp Neurol. 2002; 174: 125-36.

Goldner JS, Bruder JM, Li G, Gazzola D, Hoffman-Kim D. Neurite bridging across micropatterned grooves. Biomaterials. 2006; 27(3): 460-72.

Gomez TM and Letourneau PC. Filopodia initiate choices made by sensory neuron growth cones at laminin/fibronectin borders *in vitro*. J Neurosci. 1994; 14(10): 5959-72.

Gottlieb D and Huettner JE. An *in vitro* pathway from embryonic stem cells to neurons and glia. Cells Tissues Organs. 1999; 165: 165-72.

Griffith LG. Emerging design principles in biomaterials and scaffolds for tissue engineering. Ann NY Acad Sci. 2002; 961: 83-95.

Habich A, Jurga M, Markiewicz I, Lukomska B, Bany-Laszewicz U, Domanska-Janik K. Early appearance of stem/progenitor cells with neural-like characteristics in human cord blood mononuclear fraction cultured *in vitro*. Exp Hematology. 2006; 34: 914-25.

Hadlock T, Sundback C, Hunter D, Cheney M, Vacanti JP. A Polymer Foam Conduit Seeded with Schwann Cells Promotes Guided Peripheral Nerve Regeneration. Tissue Eng. 2000; 6 (2): 119-27.

Hasirci V and Kenar H. Novel surface patterning approaches for tissue engineering and their effect on cell behavior. Nanomed. 2006; 1 (1): 73-90.

Hasirci V and Yucel D. Polymers Used in Tissue Engineering, Encyclopedia of Biomaterials and Biomedical Engineering. 2007; 1(1): 1-17.

Hay ED. Cell biology of extracellular matrix. 2nd Ed., Eds. Hay ED, New York: Plenum Press, 1991: 305-41.

Hermann A, Gastl R, Liebau S, Popa MO, Fiedler J, Boehm BO, Maisel M, Lerche H, Schwarz J, Brenner R, Storch A. Efficient generation of neural stem cell-like cells from adult human bone marrow stromal cells. J Cell Sci. 2004; 117: 4411-22.

Hermann A, Liebau S, Gastl R, Fickert S, Habisch HJ, Fiedler J, Schwarz J, Brenner R, Storch A. Comparative Analysis of Neuroectodermal Differentiation Capacity of Human Bone Marrow Stromal Cells Using Various Conversion Protocols. J Neurosci Res. 2006; 83:1502-14.

Hsu S, Chen C-Y, Lu PS, Lai C-S, Chen C-J. Oriented Schwann Cell Growth on Microgrooved Surfaces. Biotech Bioeng. 2005; 92 (5): 579-88.

Huang YC and Huang YY. Biomaterials and strategies for nerve regeneration. Artif Organs. 2006; 30(7): 514-22.

Hudson TW, Evans GR, Schmidt C.E. Engineering strategies for peripheral nerve repair. Clin Plast Surg. 1999; 26: 617-28.

Hynes RO. Integrins: bidirectional, allosteric signaling machines. Cell. 2002; 110 (6): 673-87.

Im GI, Shin YW, Lee KB. Do adipose tissue-derived mesenchymal stem cells have the same osteogenic and chondrogenic potential as bone marrow-derived cells? Osteoarthr Cartilage. 2005; 13: 845-53.

Jacobsen S and Guth L. An electrophysiological study of the early stages of peripheral nerve regeneration. Exp Neurol. 1965; 11: 48-60.

Jeong JA, Gang EJ, Hong SH, Hwang SH, Kim SW, Yang IH, Ahn C, Han H, Kim H. Rapid neural differentiation of human cord blood-derived mesenchymal stem cells. NeuroReport. 2004; 15: 1731-34.

Jones LL, Oudega M, Bunge MB, Tuszynski MH. Neurotrophic factors, cellular bridges and gene therapy for spinal cord injury. J Physiol. 2001; 533: 83-9.

Jori FP, Napolitano MA, Melone MAB, Cipollaro M, Cascino A, Altucci L, Peluso G, Giordano A, Galderisi U. Molecular Pathways Involved in Neural *In vitro* Differentiation of Marrow Stromal Stem Cells. J Cell Biochem. 2005; 94: 645-55.

Kang X-Q, Zang W-J, Bao L-J, Li DL, Xu XL, Yu XJ. Differentiating characterization of human umbilical cord blood-derived mesenchymal stem cells *in vitro*. Cell Biol Int. 2006; 30: 569-75.

Karahuseyinoglu S, Cinar O, Kilic E, Kara F, Akay GG, Demiralp DO, Tukun A, Uckan D, Can A. Biology of stem cells in human umbilical cord stroma: In situ and *in vitro* surveys. Stem Cells. 2007; 25: 319 -31.

Kay SPJ. Obstetrical brachial palsy. J Plastic Surg. 1998; 51: 43-50.

Kim B-S and Mooney DJ. Development of biocompatible synthetic extracellular matrices for tissue engineering. TIBTECH. 1998; 16: 224-30.

Kim B, Seo JH, Bubien JK, Oh YS. Differentiation of adult bone marrow stem cells into neuroprogenitor cells *in vitro*. NeuroReport. 2002; 13: 1185-88.

Kim Y, Haftel VK, Kumar S, Bellamkonda RV. The role of aligned polymer fiber-based constructs in the bridging of long peripheral nerve gaps. Biomaterials. 2008; 29: 3117-27.

Kocsis JD, Akiyama Y, Lankford KL, Radtke C. Cell transplantation of peripheral-myelin-forming cells to repair the injured spinal cord. J Rehabil Res Dev. 2002; 39: 287-98.

Kohyama J, Abe H, Shimazaki T, Koizumi A, Nakashima K, Gojo S, Taga T, Okano H, Hata J, Umezawa A. Brain from bone: efficient ''meta-differentiation'' of marrow stroma derived mature osteoblasts to neurons with Noggin or a demethylating agent. Differentiation. 2001; 68: 235-44.

Kokai LE, Rubin JP, Marra KG. The potential of adipose-derived adult stem cells as a source of neuronal progenitor cells. Plast Reconstr Surg. 2005; 116: 1453-60.

Kondo T, Johnson SA, Yoder MC, Romand R, Hashino E. Sonic hedgehog and retinoic acid synergistically promote sensory fate specification from bone marrow-derived pluripotent stem cells. PNAS. 2005; 102: 4789-94.

Kopen GC, Prockop DJ, Phinney DG. Marrow stromal cells migrate throughout forebrain and cerebellum, and they differentiated into astrocytes after injection into neonatal mouse brains. Proc Natl Acad Sci. 1999; 96: 10711-16.

Krampera M, Marconi S, Pasini A, Galiè M, Rigotti G, Mosna F, Tinelli M, Lovato L, Anghileri E, Andreini A, Pizzolo G, Sbarbati A, Bonetti B. Induction of neural-like differentiation in human mesenchymal stem cells derived from bone marrow, fat, spleen and thymus. Bone. 2007; 40: 382-90.

Langer R and Vacanti JP. Tissue engineering. Science. 1993, 260 (5110): 920-6.

Li WJ, Laurencin CT, Caterson EJ, Tuan RS, Ko FK. Electrospun nanofibrous structure: a novel scaffold for tissue engineering. J Biomed Mater Res. 2002; 60: 613-21.

Li D and Xia Y. Electrospinning of nanofibers reinventing the wheel? Adv Mater. 2004; 16: 1151-70.

Lietz M, Dreesmann L, Hoss M, Oberhoffner S, Schlosshauer B. Neuro tissue engineering of glial nerve guides and the impact of different cell types. Biomaterials. 2006; 27: 1425-36.

Lim JY and Donahue HJ. Cell sensing and response to micro- and nanostructured surfaces produced by chemical and topographic patterning. Tissue Eng. 2007; 13(8): 1879-91.

Liu S, Qu Y, Stewart T, Howard M, Chakrabortty S, Holekamp TF, McDonald JW. Embryonic stem cells differentiate into oligodendrocytes and myelinate in culture and after spinal cord transplantation. Proc Natl Acad Sci. 2000; 97: 6126-31.

Lu L, Peter SJ, Lyman MD, Lai HL, Leite SM, Tamada JA, Uyama S, Vacanti JP, Langer R, Mikos AG. *In vitro* and *in vivo* degradation of porous poly(DL-lactic-co-glycolic acid) foams. Biomaterials. 2000; 21 (18): 1837-45.

Lu P, Blesch A, Tuszynski MH. Induction of bone marrow stromal cells to neurons: Differentiation, trans-differentiation, or artifact? J Neurosci Res. 2004; 77: 174-91.

Lund RD, Wang S, Lu B, Girman S, Holmes T, Sauvé Y, Messina DJ, Harris IR, Kihm AJ, Harmon AM, Chin FY, Gosiewska A, Mistry SK. Cells isolated from umbilical cord tissue rescue photoreceptors and visual functions in a rodent model of retinal disease. Stem Cells. 2007; 25: 602-11.

Lundborg G, Dahlin L, Dohi D, Kanje M, Terada N. A new type of "bioartificial" nerve graft for bridging extended defects in nerves. J Hand Surg. 1997; 22: 299-303.

Ma W, Fitzgerald W, Liu QY, O'Shaughnessy TJ, Maric D, Lin HJ, Alkon DL, Barker JL. CNS stem and progenitor cell differentiation into functional neuronal circuits in three-dimensional collagen gels. Exp Neurol. 2004; 190: 276-88.

Ma Z, Kotaki M, Inai R, Ramakrishna S. Potential of nanofiber matrix as tissue-engineering scaffolds. Tissue Eng. 2005a; 11(1-2): 101-9.

Ma L, Feng XY, Cui BL, Law F, Jiang XW, Yang LY, Xie QD, Huang TH. Human umbilical cord Wharton's Jelly-derived mesenchymal stem cells differentiation into nerve-like cells. Chin Med J (Engl). 2005b; 118: 1987-93.

Mahoney MJ, Chen RR, Tan J, Saltzman WM. The influence of microchannels on neurite growth and architecture. Biomaterials. 2005; 26: 771-8.

Mareschi K, Novara M, Rustichelli D, Ferrero I, Guido D, Carbone E, Medico E, Madon E, Vercelli A, Fagioli F. Neural differentiation of human mesenchymal stem cells: evidence for expression of neural markers and eag K+ channel types. Exp Hematol. 2006; 34: 1563-72.

Marolt D, Augst A, Freed LE, Vepari C, Fajardo R, Patel N, Gray M, Farley M, Kaplan D, Vunjak-Novakovic G. Bone and cartilage tissue constructs grown using human bone marrow stromal cells, silk scaffolds and rotating bioreactors. Biomaterials. 2006; 27: 6138-49.

Martini R. Expression and functional roles of neural cell surface molecules and extracellular matrix components during development and regeneration of peripheral nevre. J Neurocytol. 1994; 23: 1-28.

Mauney JR, Volloch V, Kaplan DL. Matrix-mediated retention of adipogenic differentiation potential by human adult bone marrow-derived mesenchymal stem cells during ex vivo expansion. Biomaterials. 2005; 26: 6167-75.

McCaig CD. Nerve branching is induced and oriented by a small applied electric field. J Cell Sci. 1990; 95: 605-15.

Meek MF, Varejao AS, Geuna S. Muscle grafts and alternatives for nerve repair. J Oral Maxillofac Surg. 2002; 60: 1095-96.

Mercier F, Kitasako JT, Hatton GI. Anatomy of the brain neurogenic zones revisited: fractones and the fibroblast/macrophage network. J Comp Neurol. 2002; 451: 170-188.

Millesi H. Indications and techniques of nerve grafting, In: Gelbertman RH, Ed. Operative Nerve Repair and Reconstruction. Philadelphia, PA: Lippincott JB, 1991: 525-44.

Mitchell KE, Weiss ML, Mitchell BM, Martin P, Davis D, Morales L, Helwig B, Beerenstrauch M, Abou-Easa K, Hildreth T, Troyera D. Matrix cells from Wharton's Jelly form neurons and glia. Stem Cells. 2003; 21: 50-60.

Mrksich M, Chen CS, Xia Y, Dike LE, Ingber DE. Controlling cell attachment on contoured surfaces with self-assembled monolayers of alkanethiolates on gold. Proc Natl Acad Sci. 1996; 93: 10 775-8.

Murugan R and Ramakrishna S. Design Strategies of Tissue Engineering Scaffolds with Controlled Fiber Orientation. Tissue Eng. 2007; 13(8): 1845-66.

Muscular Dystrophy Association, From Clear-Cut Endings to Complex Beginnings: Researchers probe the Origins of Charcot-Marie-Tooth Disease, Quest 8 (1), Feb 2001, .mda.org/publications/quest/q81cmtds.html, Last access date: 06.01.2009.

Nam Y, Brewer GJ, Wheeler BC. Development of astroglial cells in patterned neuronal cultures. J Biomater Sci Polymer Edn. 2007; 18 (8); 1091-100.

National Center for Health Statistics 1995, Center for Disease Control and Prevention, www.cdc.gov/nchs, Last access date: 01.01.2009.

National Spinal Cord Injury Statistical Center, Spinal Cord Injury Facts and Figures at a Glance 2008, www.spinal cord.uab.edu, Last access date: 01.01.2009

Ndreu A, Nikkola L, Ylikauppila H, Ashammakhi N, Hasirci V. Electropsun biodegradable nanofibrous mats for tissue engineering. Nanomed. 2008; 3 (1): 45-60.

Neuhuber B, Gallo G, Howard L., Kostura L, Mackay A, Fischer I. Reevaluation of *in vitro* differentiation protocols for bone marrow stromal cells: Disruption of actin cytoskeleton induces rapid morphological changes and mimics neuronal phenotype. J Neurosci Res. 2004; 77: 192-204.

Novikova LN, Pettersson J, Brohlin M, Wiberg M, Novikov LN. Biodegradable poly(β-hydroxybutyrate) scaffold seeded with Schwann cells to promote spinal cord repair. Biomaterials. 2008; 29: 1198-206.

Oakley C and Brunette DM. The sequence of alignment of microtubules, focal contacts and actin filaments in fibroblasts spreading on smooth and grooved titanium substrata. J Cell Sci. 1993, 106, 343-54.

Oakley C and Brunette DM. Response of single, pairs, and clusters of epithelial cells to substratum topography. Biochem Cell Biol. 1995; 73: 473-89.

O'Shea KS. Embryonic stem cell models of development. Anat Rec. 1999; 257: 32-41.

Owensboro Community & Technical College, Anatomy & Physiology1 Notes, Neurons,http://www.octc.kctcs.edu/gcaplan/anat/Notes/API%20Notes%20K%20%20Neurons.htm, Last access date: 06.01.2009.

Park KS, Lee YS, Kang KS. *In vitro* neuronal and osteogenic differentiation of mesenchymal stem cells from human umbilical cord blood. J Vet Sci. 2006; 7: 343-8.

Patel N, Padera R, Sanders GHW, Cannizzaro SM, Davies MC, Langer R, Roberts CJ, Tendler SJ, Williams PM, Shakesheff KM. Spatially controlled cell engineering on biodegradable polymer surfaces. FASEB J. 1998; 12(14): 1447-54.

Phinney DG and Prockop DJ. Concise Review: Mesenchymal Stem/Multipotent Stromal Cells: The State of Transdifferentiation and Modes of Tissue Repair-Current Views. Stem Cells. 2007; 25: 2896-902.

Pittenger MF, Mackay AM, Beck SC, Jaiswal RK, Douglas R, Mosca JD, Moorman MA, Simoneti DW, Craig S, Marshak DR. Multilineage potential of adult human mesenchymal stem cells. Science. 1999; 284: 143-7.

Pittenger MF and Martin BJ. Mesenchymal stem cells and their potential as cardiac therapeutics. Circ Res. 2004; 95: 9-20.

Rajnicek AM, Britland S, McCaig CD. Contact guidance of CNS neurites on grooved quartz: influence of groove dimensions, neuronal age and cell type. J Cell Sci. 1997; 110: 2905-13.

Recknor JB, Recknor JC, Sakaguchi DS, Mallapragada SK. Oriented astroglial cell growth on micropatterned polystyrene substrates. Biomaterials. 2004; 25: 2753-67.

Recknor JB, Sakaguchi DS, Mallapragada SK. Growth and Differentiation of Astrocytes and Neural Progenitor Cells on Micropatterned Polymer Films. Ann NY Acad Sci. 2005; 1049: 24-7.

Recknor JB, Sakaguchi DS, Mallapragada SK. Directed growth and selective differentiation of neural progenitor cells on micropatterned polymer substrates. Biomaterials. 2006; 27: 4098-108.

Reyes M, Lund T, Lenvik T, Aguiar D, Koodie L, Verfaillie CM. Purification and ex vivo expansion of postnatal human marrow mesodermal progenitor cells. Blood. 2001; 98: 2615-25.

Romanov YA, Svintsitskaya VA, Smirnov VN. Searching for alternative sources of postnatal human mesenchymal stem cells: candidate MSC-like cells from umbilical cord. Stem Cells. 2003; 21: 105-10.

Ruoslahti E and Pierschbacher MD. New perspectives in cell adhesion: RGD and integrins. Science. 1987; 238 (4826): 491-7.

Rutkowski GE, Miller CA, Jeftinija S, Mallapragada SK. Synergistic effects of micropatterned biodegradable conduits and Schwann cells on sciatic nerve regeneration. J Neural Eng. 2004; 1: 151-7.

Sakurada K, Ohshima-Sakurada M, Palmer TD, Gage FH. Nurr1, an orphan nuclear receptor, is a transcriptional activator of endogenous tyrosine hydroxylase in neural progenitor cells derived from the adult brain. Development. 1999; 126: 4017-26.

Samadikuchaksaraei A. An overview of tissue engineering approaches for management of spinal cord injuries. J Neuro Eng Rehab. 2007; 4: 15.

Sanchez-Ramos J, Song S, Kamath SG, Zigova T, Willing A, Cardozo-Pelaez F, Stedeford T, Chopp M, Sanberg PR. Expression of neural markers in human umbilical cord blood. Exp Neurol. 2001; 171: 109-15.

Sanghvi A B, Archit B, Murray JL, Schmidt CE. Tissue Engineering of Peripheral Nerve. Encyclopedia of Biomaterials and Biomedical Engineering. 2004; 1(1): 1613 -21.

Sarugaser R, Lickorish D, Baksh D, Hosseini MM, Davies JE. Human umbilical cord perivascular (HUCPV) cells: A source of mesenchymal progenitors. Stem Cells. 2005; 23: 220-9.

Schmalenberg KE and Uhrich KE. Micropatterned polymer substrates control alignment of proliferating Schwann cells to direct neuronal regeneration. Biomaterials. 2005; 26: 1423–30.

Schmidt CE and Leach JB. Neural Tissue Engineering: Strategies for Repair and Regeneration. Annu Rev Biomed Eng. 2003; 5: 293-347.

Schnell E, Klinkhammer K, Balzer S, Brook G, Klee D, Daltonb P, Meya J. Guidance of glial cell migration and axonal growth on electrospun nanofibers of poly-caprolactone and a collagen/poly-caprolactone blend. Biomaterials. 2007; 28: 3012-25.

Scintu F, Reali C, Pillai R, Badiali M, Sanna MA, Argiolu F, Ristaldi MS, Sogos V. Differentiation of human bone marrow stem cells into cells with a neural phenotype: diverse effects of two specific treatments. BMC Neuroscience. 2006; 7: 14-25.

Serafini M and Verfaillie CM. Pluripotency in adult stem cells: state of the art, Semin Reprod Med. 2006; 24: 379-88.

Son YJ, Trachtenberg JT, Thompson WJ. Schwann cells induce and guide sprouting and reinnervation of neuromuscular junctions. Trends Neurosci. 1996; 19: 280-5.

Song H, Stevens C, Gage F. Astroglia induce neurogenesis from adult neural stem cells. Nature. 2002; 417: 39-44.

Song M and Uhrich KE. Optimal Micropattern Dimensions Enhance Neurite Outgrowth Rates, Lengths, and Orientations. Ann Biomed Eng. 2007; 35 (10): 1812-20.

Soprano DR, Teets BW, Soprano KJ. Role of retinoic acid in the differentiation of embryonal carcinoma and embryonic stem cells. Vitam Horm. 2007; 75: 69-95.

Stewart WC, Baugh Jr JE, Floyd ZE, Stephens JM. STAT 5 activators can replace the requirement of FCS in the adipogenesis of 3T3-L1 cells. Biochem Biophys Res Commun. 2004; 324: 355-9.

Tao H, Rao R, Ma DDF. Cytokine-induced stable neuronal differentiation of human bone marrow mesenchymal stem cells in a serum/feeder cell free condition. Develop Growth Differ. 2005; 47: 423-33.

Tarleton State University, Anatomy & Physiology, Nerve Anatomy, www.tarleton.edu/~anatomy/nervepix4.html, Last access date: 06.01.2009.

Taylor GI. Electrically driven jets. Proc R Soc London. Math Phys Sci. 1969; A313; 453-475.

Terzis JK, Sun DD, Thanos PK. History and basic science review: past, present, and future of nerve repair. J Reconstr Microsurg. 1997; 13: 215-25.

Thompson DM and Buettner HM. Schwann Cell Response to Micropatterned Laminin Surfaces. Tissue Eng. 2001; 7 (3): 247-65.

Thompson DM and Buettner HM. Oriented Schwann Cell Monolayers for Directed Neurite Outgrowth .Ann Biomed Eng. 2004; 32 (8): 1120-30.

Tondreau T, Lagneaux L, Dejeneffe M, Massy M, Mortier C, Delforge A, Bron D. Bone marrow–derived mesenchymal stem cells already express specific neural proteins before any differentiation. Differentiation. 2004; 72: 319-26.

Tonge DA and Golding JP. Regeneration and repair of the peripheralnervous system. Semin Neurosci. 1993; 5: 385-90.

Tropel P, Noel D, Platet N, Legrand P, Benabid AL, Berger F. Isolation and characterization of mesenchymal stem cells from adult mouse bone marrow. Exp Cell Res. 2004; 295: 395-406.

Tropel P, Platet N, Platel JC, Noël D, Albrieux M, Benabid AL, Berger F. Functional neuronal differentiation of bone marrow-derived mesenchymal stem cells. Stem Cells. 2006; 24: 2868-76.

UCSF School of Medicine, Prologue Histology Resource, Nerves and Muscles, ://missinglink.ucsf.edu/lm/IDS_101_histo_resource, Last Access date: 06.01.2009.

Valmikinathan CM, Tian J, Wang J, Yu X. Novel nanofibrous spiral scaffolds for neural tissue engineerin. J Neural Eng. 2008; 5: 422-32.

Van Dijk J, Pondaag W, Malessy M. Obstetric lesions of the brachial plexus. Muscle Nerve. 2001; 24: 1451-61.

Vleggeert-Lankamp CLAM, Pego AP, Lakke EAJF, Deenen M, Marani E, Thomeer RTWM. Adhesion and proliferation of human Schwann cells on adhesive coatings. Biomaterials. 2004; 25: 2741-51.

Wang JCY, Doedens M, Dick JE. Primitive human hematopoietic cells are enriched in cord blood compared with adult bone marrow or mobilized peripheral blood as measured by the quantitative *in vivo* SCID-repopulating cell assay. Blood. 1997; 89: 3919-24.

Wang HS, Hung SC, Peng ST, Huang CC, Wei HM, Guo YJ, Fu YS, Lai MC, Chen CC. Mesenchymal stem cells in the Wharton's Jelly of the human umbilical cord. Stem Cells. 2004; 22: 1330-7.

Wang A, Ao Q, Cao W, Yu M, He Q, Kong L, Zhang L, Gong Y, Zhang X. Porous chitosan tubular scaffolds with knitted outer wall and controllable inner structure for nerve tissue engineering. J Biomed Mater Res. 2006; 79A: 36-46.

Wang HB, Mullins ME, Cregg JM, Hurtado A, Oudega M, Trombley MT, Gilbert RJ. Creation of highly aligned electrospun poly-L-lactic acid fibers for nerve regeneration applications. J Neural Eng. 2009; 6 (1): 16001.

Wei YT, Tian WM, Yu X, Cuı FZ, Hou SP, Xu QY, Lee IS. Hyaluronic acid hydrogels with IKVAV peptides for tissue repair and axonal regeneration in an injured rat brain. Biomed Mater. 2007; 2 (3): S142-6.

Weiss ML, Medicetty S, Bledsoe AR, Rachakatla RS, Choi M, Merchav S, Luo Y, Rao MS, Velagaleti G, Troyera D. Human umbilical cord matrix stem cells: preliminary characterization and effect of transplantation in a rodent model of Parkinson's disease. Stem Cells. 2006; 24: 781-92.

Wexler SA, Donaldson C, Denning-Kendall P, Rice C, Bradley B, Hows JM. Adult bone marrow is a rich source of human mesenchymal stem cells but umbilical cord and mobilized adult blood are not. Br J Haematol. 2003; 121: 368-74.

Winn SR, Aebischer P, Galletti PM. Brain tissue reaction to permselective polymer capsules. J Biomed Mater Res.1989; 23: 31-44.

Wislet-Gendebien S, Hans G, Leprince P, Rigo JM, Moonen G, Rogister B. Plasticity of Cultured Mesenchymal Stem Cells: Switch from Nestin-Positive to Excitable Neuron-Like Phenotype. Stem Cells. 2005; 23: 392-402.

Woodbury D, Schwarz EJ, Prockop DJ, Black IB. Adult rat and human bone marrow stromal cells differentiate into neurons. J Neurosci Res. 2000; 61: 364-70.

Wulf GG, Viereck V, Hemmerlein B, Haase D, Vehmeyer K, Pukrop T, Glass B, Emons G, Trümper L. Mesengenic progenitor cells derived from human placenta. Tissue Eng. 2004; 10: 1136-47.

Yang SE, Ha CW, Jung MH, Jin HJ, Lee M, Song H, Choi S, Oh W, Yang YS. Mesenchymal stem/progenitor cells developed in cultures from UC blood. Cytotherapy. 2004; 6: 476-86.

Yang F, Murugan R, Wang S, Ramakrishna S. Electrospinning of nano/micro scale poly(L-lactic acid) aligned fibers and their potential in neural tissue engineering. Biomaterials. 2005; 26: 2603-10.

Yarin AL, Koombhongse S, Reneker DH. On bending instability in electrospinning of nanofibers. J Appl Phy. 2001; 89: 3018-26.

Yu TT and Shoichet MS. Guided cell adhesion and outgrowth in peptide-modified channels for neural tissue engineering. Biomaterials. 2005; 26: 1507-14.

Zalewski AA and Gulati AK. Rejection of nerve allografts after cessation of immunosuppression with cyclosporine A. Transplantation.1981; 31: 88-90.

Zetterstrom RH, Williams R, Perlmann T, Olson L. Cellular expression of the immediate early transcription factors Nurr1 and NGFI-B suggests a gene regulatory role in several brain regions including the nigrostriatal dopamine system. Mol Brain Res. 1996; 41: 111-20.

Zhang N, Yan H, Wen X. Tissue-engineering approaches for axonal guidance. Brain Res Rev. 2005a; 49: 48-64.

Zhang N, Zhang C, Wen X. Fabrication of semipermeable hollow fiber membranes with highly aligned texture for nerve guidance. J Biomed Mater Res. 2005b; 75A: 941-9.

Zuk PA, Zhu M, Ashjian P, De Ugarte DA, Huang JI, Mizuno H, Alfonso ZC, Fraser JK, Benhaim P, Hedrick MH. Human adipose tissue is a source of multipotent stem cells. Mol Biol Cell. 2002; 13: 4279-95.

APPENDIX A

MATERNAL CONSENTS

Figure A.1. Maternal consent of 28 years old donor

MATERNAL CONSENT

I am willing to consent to:

1. The collection and storage of umbilical cord after delivery of my baby.

2. Use the umbilical cord for research projects at Middle East Technical University, Department of Biological Sciences, Biotechnology Research Unit.

Mother's Name: Özlem Beyter   Mother's Signature:

Witness Name: Halime Kenar   Witness Signature:

Date: 24 / 8 / 2008

Figure A.2. Maternal consent of 32 years old donor

APPENDIX B

# CALIBRATION CURVES FOR ALP ACTIVITY
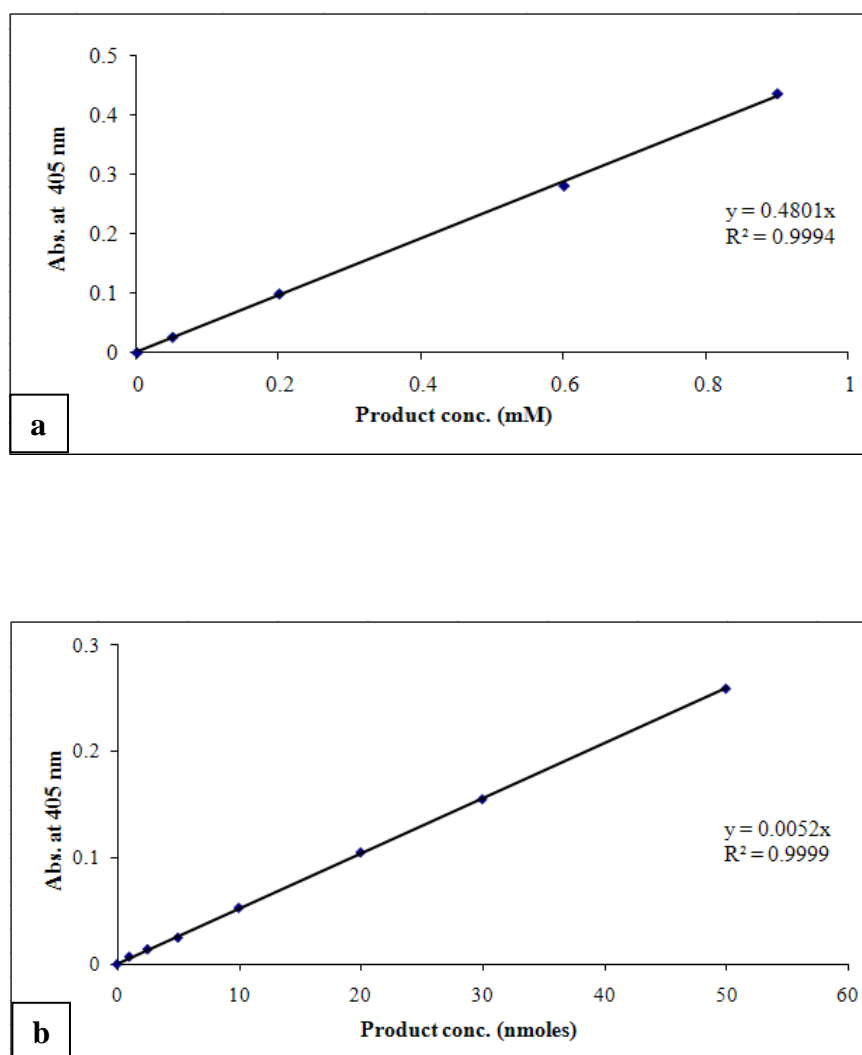
Figure B.1. The calibration curve for ALP activity, prepared by using p-nitrophenol at different concentrations. The graph obtained from the studies carried out in a) MGH and Tufts Univ. (Boston, USA) and b) at METU.

APPENDIX C

# CALIBRATION CURVES FOR CELL NUMBER DETERMINATION

The plotted trendline equation reads:

$$y = 0.017662x$$
$$R^2 = 0.989376$$

with the y-axis labeled "Abs at 490 nm" and the x-axis labeled "Cell Number ($\times10^3$)".
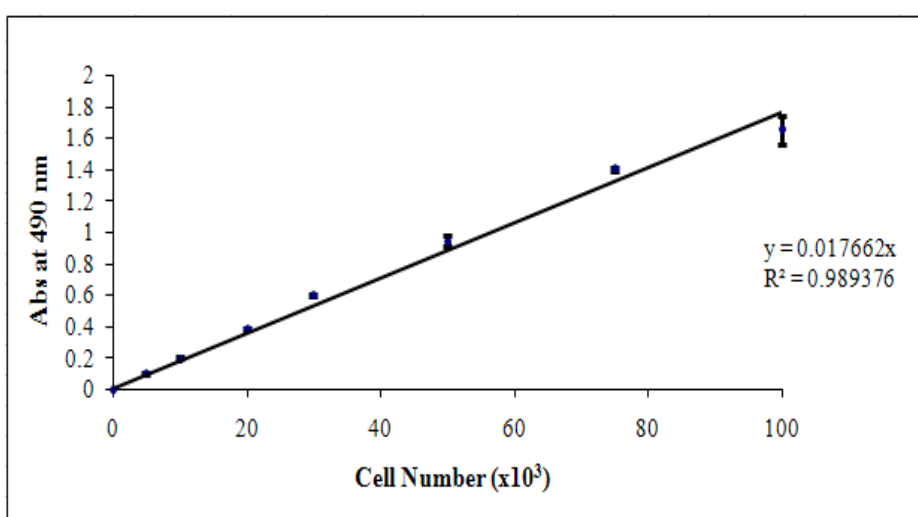
Figure C.1. The calibration curve obtained by MTS assay using WJ MSCs cultured in medium #2.
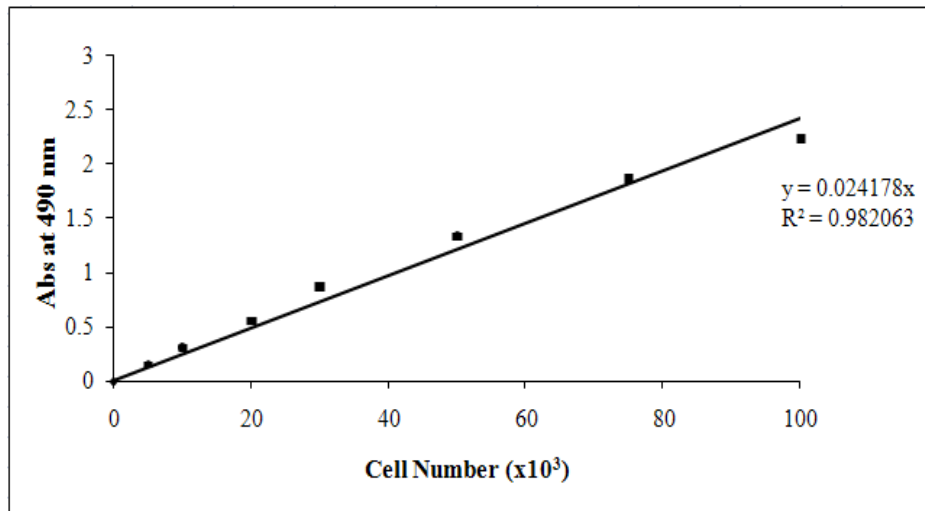
Figure C.2. The calibration curve obtained by MTS assay using WJ MSCs cultured in medium #4.
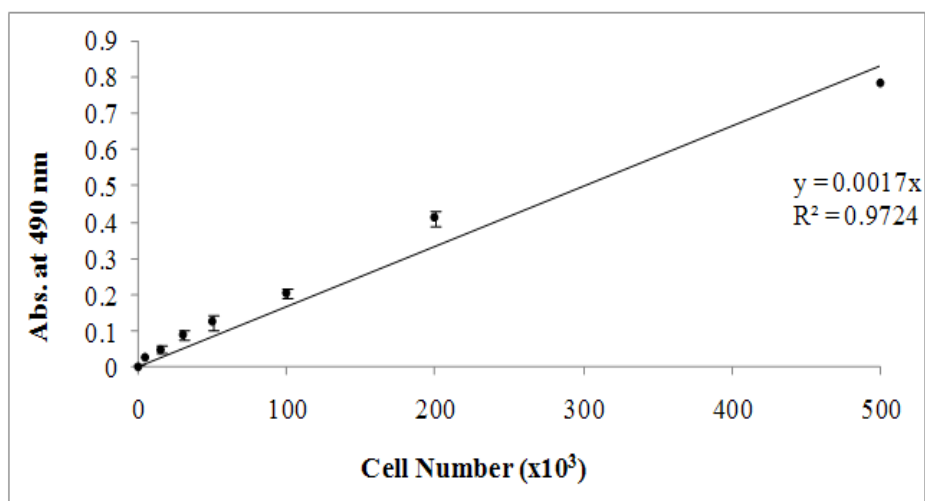

Figure C.3. The calibration curve obtained by MTS assay using mouse NSCs.

CURRICULUM VITAE

PERSONAL INFORMATION

Surname, Name: Yücel, Deniz

Nationality: Turkish (T.C.)

Date and Place of Birth: 6 May 1979, Ankara, Turkey

Marital Status: Single

Phone: +90 312 210 53 41

Fax: +90 312 210 15 42

E-mail: dyucel@metu.edu.tr, denyucel@gmail.com

EDUCATION

Degree	Institution	Year of Graduation
MS	METU, Dept. of Biotechnology	2003
BS	METU, Dept. of Biological Sciences	2001
High School	TED Ankara College	1996

ACADEMIC EXPERIENCE

Year	Place	Enrollment
2001- 2008	METU, Dept. of Biological Sciences (Bioanaly. Chem. & Biochem. Lab.)	Research Assistant
2005-2006	Massachusetts. General Hospital	Visiting Researcher
June-Sep 2007	Shriners Burn Hospital	
	Harvard Medical School	
	Tufts University	

FOREIGN LANGUAGES: Advanced English

PUBLICATIONS

1. Hasirci V and Yucel D. Polymers Used in Tissue Engineering. Encyclopedia of Biomaterials and Biomedical Engineering. 2007; 1(1): 1-17.

2. Yucel D, Ozer N, Hasirci V. Construction of a choline biosensor through enzyme immobilization on a poly(2-hydroxyethyl methacrylate) grafted Teflon film. J Applied Polymer Science. 2007; 1004: 3469-3477.

3. Yılgor P, Yucel D, Kenar H, Hasirci V. Polyhydroxyalkanonates: A Versatile Class of Biolpolymers and their Biomedical Potential. Book Chapter in Brazilian Network on Green Chemistry Ed. Carioca JOB, 2008, Chapter 20: 415-433.